GAMMA-RAY CROSS SECTIONS FROM

121 keV TO 10.8 MeV

TOTAL AND PARTIAL CROSS SECTIONS FOR THE INTERACTIONS OF ELECTROMAGNETIC RADIATION WITH MATTER

by

LAWRENCE CAMERON HENRY, B.Sc.

A Thesis

Submitted to the Faculty of Graduate Studies

in Partial Fulfilment of the Requirements

for the Degree

Doctor of Philosophy

McMaster University

August, 1971

DOCTOR OF PHILOSOPHY (1971) McMASTER UNIVERSITY
(Physics) Hamilton, Ontario

TITLE: Total and Partial Cross Sections for the Interactions of Electromagnetic Radiation with Matter

AUTHOR: Lawrence Cameron Henry, B.Sc. (McMaster University)

SUPERVISOR: Dr. T. J. Kennett

NUMBER OF PAGES: x, 173

SCOPE AND CONTENTS:

A measurement of the cross section for the interaction of electromagnetic radiation with matter has been undertaken. Total cross sections for 29 photon energies from 121 keV to 10.8 MeV in 9 target elements from carbon to uranium have been realized and pair production cross sections, for energies above 2 MeV, deduced from the results. A direct measurement of the partial pair cross section for photons with energies from 1120 to 2754 keV in 6 target elements from titanium to lead has also been included.

ACKNOWLEDGMENTS

I wish to express my deepest appreciation to my Research Director, Dr. T. J. Kennett for his ready and valuable assistance and encouragement throughout the period of this study. Thanks are due also to Dr. W. V. Prestwich for his assistance, much in the form of a critical appraisal of proposed experimentation. This proved invaluable in the optimization of experimental techniques.

I am indeed grateful to the many other people who assisted in the various areas of this study: Mr. A. H. Colenbrander and Mr. G. R. Norman for their assistance in computer programming; Mr. L. W. Nichol for his efforts in the fabrication of the solid state detector used in this study as well as for his effort along with those of Mr. A. Robertson and Mr. A. M. Lopez in the development of the internal irradiation facility at the McMaster reactor; the reactor staff for their ready and capable assistance; and finally, Mrs. Susan Anderson for her assistance in preparing and typing this manuscript.

I am particularly indebted to my wife Lise for her faithful support throughout the duration of this research.

TABLE OF CONTENTS

LIST OF ILLUSTRATIONS

LIST OF TABLES

CHAPTER I

INTRODUCTION

1.1 Introduction

The quantum theory of radiation was conceived through the concerted efforts of such notable scientists as Dirac, Heisenberg, and Pauli. Unlike most good physical theories which after an initial period of success are superseded by improved theories, quantum electrodynamics has matured, under intensive investigation, into what is believed to be an excellent approximation with an accuracy that leaves little to be desired[1]. Although it has become obvious that the theory fails to yield exact results it does yield, to a very good first approximation, results on the probability for the interaction of electromagnetic radiation with matter if the interaction between the electron and the radiation can be treated as weak. The theory has been extended to include higher order, radiative correction terms and experimental verification of the anomalous electron magnetic moment[2], the Lamb shift[3], and the existence of a real part of the Delbrück scattering amplitude[4] substantiate the excellence of the theory.

The success attained in determining the function of a sub-microscopic system weighs heavily on the combined efforts of the theoretical and experimental scientists. The theoretician's task involves the formulation of a mathematical model which at least approximates the physical experience. The responsibility then lies with the experimen-

talist to examine the model in a comprehensive, systematic manner. Only then can the successes and failures of the model be determined and subsequent adjustments and improvements made. The importance of such an examination is particularly significant when the theory involves such fundamental and consequential concepts as the properties of electromagnetic radiation and the physical states of matter with which this radiation interacts.

Motivation for the measurement of the photon cross section undertaken in this research was not limited simply to a confirmation or evaluation of the proposed theories. The increasing use of electromagnetic radiation in the field of nuclear medicine has broadened the requirement for a more complete understanding of the interaction processes. Further, the advances being made in the development of nuclear power has led to an increased requirement for the application of radiation shielding techniques which, clearly, require a detailed knowledge of the interaction processes. Another modern development, the exploration of space, has led to a greater awareness of the biological effects of gamma radiation. Penetration of space has resulted in man being exposed to higher energy radiation which is normally attenuated by the earth's atmosphere. Since the pair production interaction begins to dominate at higher energies, a full understanding of this process becomes of particular interest.

The quantum theory of radiation, however effective, has not been properly tested in the intermediate energy region (3-15 MeV). A shortage of measured data in the energy region above 3 MeV is due, primarily, to the difficulty in obtaining photon sources of substantial intensity

that will provide a good distribution of energies for study. In the intermediate energy region, the pair production process is of particular interest since the reliability of the Klein-Nishina formula for inelastic scattering is not expected to deteriorate with energy and since the elastic scattering and photoelectric absorption cross sections are barely competitive at these energies. At energies below 3 MeV, the total cross section has been measured in detail and the elastic and inelastic scattering cross sections as well as the photoelectric absorption process have been well investigated. In the energy region of 1-3 MeV, where long lived β-decay, gamma-ray sources are available, agreement between theoretical and experimental results on the interaction cross sections have, in general, been very good.

In the preceding paragraph, the importance of understanding the pair production process for photons in the intermediate energy region has been suggested. In the pair production process, an electron in the negative energy state absorbs a photon with energy $E_\gamma > 2\ mc^2$ (m is the rest mass of the electron) and is subsequently transferred to a positive energy state, thus leaving a "hole" or positron in the negative energy region. This interaction necessarily takes place in the Coulomb field of another particle (usually the nucleus) in order that momentum can be conserved, the necessary momentum transfer to the nucleus being accomplished through the Coulomb interaction between the created positron-electron pair and the nuclear charge. If this Coulomb interaction is small compared to the energies E_+ and E_- imparted to the created positron and electron respectively, then the first order (Born) approximation[5] will be valid and the final state eigenfunctions describing

the electron and positron will differ very little from plane waves. The Born approximation is valid only when the positron and electron velocities v_+ and v_- are such that the conditions

$$Ze^2/hv_+,\ Ze^2/hv_- << 1 \qquad 1.1$$

are met. Consequently, from equation 1.1 it is evident that the conditions of the Born approximation, particularly for higher Z target elements, cannot be satisfied for all incident photon energies. With the exception of the very low atomic number results, the Bethe-Heitler pair cross section[6] (obtained using the Born approximation) in the region of a few MeV is found, in general, to be too low. As the incident photon energy E_γ approaches the threshold energy $2\ mc^2$, the Bethe-Heitler cross section becomes quite inadequate in describing the interaction. Further, in using the Born approximation, the electrostatic potential energy between the nucleus and the created positive and negative electrons occurs squared in the cross section; thus, the sign of the charge dissappears. Consequently, the theory fails to provide for the asymmetries in the positron and electron energy distributions as a result of the Coulomb repulsion and attraction experienced by the pair of oppositely charged electrons. A Coulomb correction factor[7] is normally applied in order to account for these asymmetries.

A third complication relating to atomic electron screening must also be considered. As the velocities of the newly produced pairs increase (with increasing incident photon energy), the mean pair production interaction radius moves outward from the nucleus with the

result that atomic electrons begin to be more effective in shielding the created electron and positron from the nuclear charge. Consequently, the correct result can only be obtained by modifying the Z term in the electrostatic potential. The Thomas-Fermi model [8] for the atom is frequently used in determining the screening effect. At energies near threshold, pair production necessarily occurs in close proximity of the nucleus thus screening effects are negligible. At sufficiently high energies, the mean interaction radius extends beyond the mean atomic radius and a maximum screening effect is experienced.

From the above discussion, it is clear that the Born approximation to the pair production cross section in the energy region from 1 to 15 MeV is rather inadequate. At low positron and electron energies, the Coulomb interaction cannot be correctly treated as a perturbation and therefore, using unperturbed plane wave solutions for the final wave functions is unsatisfactory. Further, an energy dependent Coulomb correction factor, accounting for the asymmetries in the energy distributions of the positron-electron pair, must be considered. Finally, with the departure of the incident photon energy from the threshold energy $2\ mc^2$, the necessity for screening corrections increases.

Motz [9] in a recent detailed review of studies made of the pair production processes has stressed the requirement for (i) more experimental data with good accuracy on the total cross section in the intermediate energy region where only interpolation procedures and semi-empirical formulas exist and, (ii) studies of the total pair cross section for targets with low atomic number in order to determine the relative contributions of the elastic and inelastic processes. Clearly then, if a definite understanding of the pair process in the

intermediate energy region is to be realized and an adequate theory proposed, a need exists for a comprehensive measurement of the gamma-ray cross section as a function of energy and atomic number.

1.2 Nomenclature - The Cross Section

Photons are generally classified according to their mode of origin, not their energy. Gamma-rays are electromagnetic radiations associated with nuclear transitions. Bremsstrahlung photons are the result of the acceleration of free electrons or other charged particles. Characteristic X-rays are emitted in atomic transitions of bound electrons between the K, L, M, --- shells. Annihilation radiation is emitted when a positron and an electron combine. The interactions of photons with matter are dependent only on the quantum energy $h\nu$ of the radiation and not on their mode of origin.

During cross section measurements where the attenuation of a photon beam by some target material is being observed, the removal of a photon from the beam is accomplished by a single event assuming that conditions of "good geometry" exist. Therefore, under these conditions, beam attenuation shows an exponential dependence on target thickness. Although one frequently considers the interaction of photons with matter in terms of the three or four principal interactions a number of processes of varying strengths are possible. These are conveniently catalogued by Fano[10] in the following manner:

Kinds of Interaction	Effects of Interaction
1. with atomic electrons	a) Complete absorption
2. with nucleons	b) Elastic scattering (coherent)
3. with the electric field surrounding nuclei or electrons	c) Inelastic scattering (incoherent)
4. with the Meson field surrounding nucleons	

Since this particular research will be limited to the gamma-ray variety of photon, only four of the twelve possible combinations taken from the table will have any significance to the measurement. These are: 1(c) Compton (inelastic) scattering, 1(a) photoelectric absorption, 1(b) Rayleigh (elastic) scattering, and 3(a) pair production. The total photon interaction is given simply by the sum of these four processes.

The concept of "cross section" is used in a wide variety of interactions and when it is encountered in the literature the exact meaning of the term may have to be deduced from context or even by dimensional analysis[11]. There are, however, two quite distinct interpretations of the term depending upon whether a wave or corpuscular model is to be visualized. In the development of theories describing electromagnetic interactions with matter it is often convenient to utilize the wave or field model. The experimentalist, however, having the corpuscular model in mind may feel more comfortable in speaking of the probability of removing a photon from the beam. This poses little difficulty since a straight forward transfer from one view point to the other can be made.

Consider the interaction of a plane-polarized electromagnetic wave with a free electron. The dimensions of the plane wave normal to the direction of propogation are assumed infinite compared with the wavelength of the radiation and the physical dimensions of the scattering body. The energy transmitted in such an infinite medium must be expressed in terms of the energy flux, I_0 [energy/unit Area/unit time]. The total power eQ removed from such a collimated beam through interaction

with an electron is proportional to the incident intensity, thus,

$$\frac{eQ}{t} = e^{\sigma} I_0 \text{ ergs/sec-electron.} \qquad 1.2$$

Since the proportionality constant e^{σ} has units of cm^2 it is conveniently called the "cross section" for interaction. It may then be visualized as an area in the incident wave front through which flows the amount of power which is removed by the target electron. Mathematically, of course, it is the ratio between the rate of energy removal and the incident intensity per target particle.

When a number of distinguishable types of interaction may take place in competition with one another, we speak of the "partial cross section" for each particular process. The "differential cross section refers to the cross section for the interaction which removes an amount of power dQ/t from the incident collimated beam and scatters this power into the solid angle $d\Omega$ at mean angle θ, thus

$$\frac{d(eQ)}{t} = d(e^{\sigma})I_0 \text{ ergs/sec-electron.} \qquad 1.3$$

A statistical or probability-law interpretation of cross section can be easily developed through a transition to a corpuscular view point. The incident electromagnetic radiation is quantized, that is, it is divided into photons, each containing the energy $h\nu$. Therefore, the total number of photons incident on an area S of target in unit time is given by

$$n = \frac{I_0 S}{h\nu} \quad \text{photons/second,} \qquad 1.4$$

and the number of incident photons removed from the collimated beam per second is

$$dn = \frac{Q/t}{h\nu} \quad \text{photons/second.} \qquad 1.5$$

Consequently,

$$Q/t = e^{\sigma} I_0 SNZ\ dx \quad \text{ergs/sec,} \qquad 1.6$$

(which is similar to equation 1.2 only extended to include the total number of electrons encountered in the volume Sdx) can be written

$$h\nu\ dn = e^{\sigma} nh\nu NZ\ dx \quad \text{ergs/sec,} \qquad 1.7$$

or

$$\frac{dn}{n} = e^{\sigma} NZ\ dx \quad \text{(dimensionless)} \qquad 1.8$$

Clearly, N is the density of target atoms and Z the atomic number.

It is seen that the fraction (dn/n) of the incident particles removed from the beam by some interaction is independent of time and area of either the incident beam or the target. Since

$$e^{\sigma} = \frac{dn/n}{NZ\ dx} \quad \text{cm}^2 , \qquad 1.9$$

the cross section can be interpreted as the probability that one incident particle will undergo the specific interaction while passing through a foil containing just one target centre per cm^2. It may,

therefore, be visualized as a hypothetical area associated with each target particle and through which must pass those incident quanta which undergo the specific reaction. A similar argument is extended to the differential cross section.

The differential cross section is not limited to describing spacial distributions but may involve as is the case of Bremsstrahlung a description of the energy distribution of the scattered radiation. After integration over all angles but prior to integration over the energy spectrum one finds the quantity

$$d\sigma_{rad} = \sigma_{rad}(E)dE \quad cm^2. \tag{1.10}$$

If confusion is to be avoided, it is essential that the differential cross section has the units of cm^2 and therefore it must be expressed as the product of two terms, namely $\sigma(E)dE$.

CHAPTER II

APPROXIMATION THEORY ON THE INTERACTION OF ELECTROMAGNETIC RADIATION WITH MATTER

2.1 Introduction

Past theoretical studies of the interaction of photons with matter [12] have frequently used perturbation theory in which the Hamiltonian of the pure radiation field H_{RAD} and the Hamiltonian of the electron (or nucleus) H_{EL} (or H_{NUCL}) in the absence of the radiation field are used to obtain the unperturbed wave function from the wave equation

$$i\hbar \dot{\Psi} = (H_{RAD} + H_{EL})\ \Psi \ . \qquad 2.1$$

(The dot denotes differentiation with respect to time.)
The interaction energy H_{INT} must then be added to the unperturbed Hamiltonian and a solution for the wave equation

$$i\hbar \dot{\Psi}' = (H_{RAD} + H_{EL} + H_{INT})\ \Psi' \qquad 2.2$$

obtained by expanding Ψ' in terms of the solutions Ψ_n of equation 2.1

Since the interaction involves a charged particle in an electromagnetic field, the force $\underline{K}$ acting on the particle is given by the Lorentz equation

$$\underline{K} = q(\underline{E} + \frac{1}{c}\,\underline{v} \times \underline{H}), \qquad 2.3$$

where $\underline{E}$ and $\underline{H}$ are the electric and magnetic fields associated with the radiation. From equation 2.3 it is seen that the interaction energy H_{INT} is a function of the charge q (actually the electronic charge e). Equation 2.3, however, is only a first order approximation of the force since it assumes that the presence of the charge will not modify the total radiation field. A more correct expression would include terms of higher order in q. These higher order terms represent radiative corrections which have, at most, a small effect on interactions involving photons of energy at or below those experienced in nuclear transitions. Higher order effects can be generalized under two categories, self-mass and self-charge effects. Heitler[13] offers an excellent evaluation of these effects.

In general, the solution Ψ' of equation 2.2 can be expanded in a power series of the electronic charge (or more conveniently, in a power series of the dimensionless fine structure constant $\alpha = e^2/\hbar c = 1/137$) and an approximate solution obtained by keeping only the first non-vanishing term.

The purpose of this chapter is simply to provide the reader with the basic tools used in obtaining approximations of the various interaction cross sections using the concepts of perturbation theory. Because of the vast quantities of detail that would be required, the various cross sections will not be developed; however, in the interest of providing an example for the application of the perturbation techniques outlined, the inelastic scattering process will be considered

in reasonable detail. For any reader interested in an in-depth approach to the various cross section theories, Heitler's "Quantum Theory of Radiation" is exceptionally good and has, in fact, been used as the principal reference throughout this study.

2.2 Electromagnetic Field Equations

Given a charge density ρ and current density $\underline{j} = \rho\underline{v}$ (both functions of time), the electronic state of matter is classically described in terms of the associated electromagnetic fields $\underline{E}$ and $\underline{H}$ by

$$\nabla \times E + \frac{1}{c}\dot{\underline{H}} = 0 \qquad 2.5\ (a)$$

$$\nabla \cdot \underline{H} = 0 \qquad 2.5\ (b)$$

$$\nabla \times \underline{H} - \frac{1}{c}\dot{E} = \frac{4\pi}{c}\rho\underline{v} \qquad 2.5\ (c)$$

$$\nabla \cdot \underline{E} = 4\pi\rho \qquad 2.5\ (d)$$

commonly known as Maxwell's equations.

Using the vector identity $\nabla \cdot \nabla \times A \equiv 0$ it is clear from equation 2.5 (b) that the magnetic field is satisfied by $\underline{H} = \nabla \times \underline{A}$, where $\underline{A}$ is defined as the vector potential. Substitution of $\underline{H} = \nabla \times \underline{A}$ into 2.5 (a) yields

$$\nabla \times (\underline{E} + \frac{1}{c}\dot{\underline{A}}) = 0. \qquad 2.6$$

Using a second vector identity $\nabla \times \nabla\phi \equiv 0$ it is seen from equation 2.6 that

$$\underline{E} + \frac{1}{c}\dot{\underline{A}} = -\nabla\phi, \qquad 2.7$$

where ϕ is defined as the scalar potential. The electric and magnetic fields may, therefore, be expressed in terms of a vector potential $\underline{A}$ and the scaler potential ϕ. Maxwell's four equations may then be written:

$$\underline{E} + \frac{1}{c}\dot{\underline{A}} = -\nabla\phi, \qquad 2.8\ (a)$$

$$\underline{H} = \nabla \times \underline{A}, \qquad 2.8\ (b)$$

$$\frac{1}{c^2}\ddot{\underline{A}} - \nabla^2\underline{A} + \nabla(\nabla\cdot\underline{A} + \frac{1}{c}\dot{\phi}) = \frac{4\pi}{c}\rho\underline{v}\ , \qquad 2.8\ (c)$$

$$-\nabla^2\phi - \frac{1}{c}\nabla\cdot\underline{A} = 4\pi\rho\ . \qquad 2.8\ (d)$$

In a pure radiation field formed by the superposition of transverse waves, where no sources exist, the equations 2.8 may be written

$$\underline{E} = -\frac{1}{c}\dot{\underline{A}}(\underline{r}\ ,\ t)\ , \qquad 2.9\ (a)$$

$$\underline{H} = \nabla \times \underline{A}(\underline{r}\ ,\ t)\ , \qquad 2.9\ (b)$$

$$\nabla^2\underline{A}\ (\underline{r}\ ,\ t) - \frac{1}{c^2}\ddot{\underline{A}}(\underline{r}\ ,\ t) = 0\ , \qquad 2.9\ (c)$$

$$\nabla\cdot\underline{A}\ (\underline{r}\ ,\ t) = 0\ . \qquad 2.9\ (d)$$

The significant feature of equations 2.9 is that the electromagnetic fields are defined by the vector potential only. Consequently, a pure radiation field in free space formed by the superposition of transverse waves can be described in terms of a single quantity, the vector potential.

2.3 Quantization of a Pure Radiation Field

The vector potential $\underline{A}$ can, in general, be represented by a series of plane waves,

$$\underline{A}(\underline{r},t) = \sum_{\lambda} \left| q_{\lambda}(t)\, \underline{A}_{\lambda}(\underline{r}) + q_{\lambda}^{*}(t)\, \underline{A}_{\lambda}^{*}(\underline{r}) \right| , \qquad 2.10$$

where λ represents the quantum state of a particular oscillator. Consider the particular solution

$$\underline{A}_{\lambda}(\underline{r},t) = q_{\lambda}(t)\underline{A}_{\lambda}(\underline{r}) , \qquad 2.11$$

for the field equations 2.9. The separation of variables method leads to the time and spacial dependent differential equations

$$\ddot{q}_{\lambda}(t) + c^{2}\kappa_{\lambda}^{2} q_{\lambda}(t) = 0 , \qquad 2.12$$

$$\nabla^{2}\underline{A}_{\lambda}(r) + \kappa_{\lambda}^{2}\underline{A}_{\lambda}(\underline{r}) = 0 , \qquad 2.13$$

and

$$\nabla \cdot \underline{A}_{\lambda}(\underline{r}) = 0 , \qquad 2.14$$

where $\underline{\kappa}$ is the propagation vector ($|\kappa_{\lambda}| = \omega_{\lambda}/c$) for the plane wave defined by the quantum number λ.

Equations 2.12 - 2.14 are satisfied by the normalized solutions

$$q_{\lambda}(t) = (\hbar/2\omega_{\lambda})^{1/2}\, e^{i\omega_{\lambda} t} , \qquad 2.15$$

and

$$\underline{A}_{\lambda}(\underline{r}) = (4\pi c^{2})^{1/2}\, \underline{e}_{\lambda}\, e^{i\underline{\kappa}_{\lambda}\cdot\underline{r}} , \qquad 2.16$$

where $\underline{e}_\lambda$ is the unit polarization vector for the particular wave. It should be noted that the volume enclosing the field has been normalized to unity, otherwise a factor of $L^{-3/2}$ must be included in the expansion of $\underline{A}$ if $\underline{A}_\lambda$ is to be normalized to $4\pi c^2$. Making use of the familiar energy equation for an electromagnetic field

$$H_{RAD} = \frac{1}{8\pi} \int (E^2 + H^2)\, dV = \sum_\lambda H_{RAD_\lambda} , \qquad 2.17$$

the energy of a single wave may be written

$$H_{RAD_\lambda} = 2\omega_\lambda^2 \, q_\lambda^* q_\lambda . \qquad 2.18$$

Since the functions q are orthonormal, no cross terms exist in the total energy equation $\sum_\lambda H_{RAD_\lambda}$. And therefore, from equations 2.15, 2.17, and 2.18

$$H_{RAD} = \sum_\lambda n_\lambda \hbar\omega_\lambda \qquad 2.19$$

where n_λ is the number of oscillators that have the quantum of energy $\hbar\omega_\lambda$. Similarly, the momentum of the field is given by

$$\underline{G} = \frac{1}{4\pi} \int (\underline{E} \times \underline{H}) dV = \sum_\lambda G_\lambda , \qquad 2.20$$

and the momentum of a single wave by

$$\underline{G}_\lambda = 2\omega_\lambda c\underline{\kappa}_\lambda q_\lambda^* q_\lambda \ , \qquad 2.21$$

where $(|\underline{\kappa}_\lambda| = \omega_\lambda/c)$,

and therefore, the total momentum in the direction of wave propagation is given by

$$\underline{G}_\lambda = \sum_\lambda n_\lambda \hbar\omega_\lambda \ . \qquad 2.22$$

Equations 2.19 and 2.22 are consistent with the argument that a plane wave behaves exactly as a beam of n free particles with energy $\hbar\omega$ and momentum $\hbar\omega/c$. Thus the concept of field quantization.

Following quantization, the field quantity $\underline{A}$ and therefore $\underline{E}$ and $\underline{H}$ become operators which will act on the state vector Ψ which satisfies the wave equation $i\hbar\dot{\Psi} = H_{RAD}\,\Psi$.

Since H_{RAD} is the Hamiltonian for a pure radiation field where no interaction between the radiation oscillators exist, an eigenstate of H_{RAD} must be the product $\psi^{(1)}\psi^{(2)}---\psi^{(\lambda)}---$ where $\psi^{(\lambda)}$ is a normalized Eigen state of H_{RAD}. Further, since the eigenvalues of H_{RAD} are $E_\lambda = n_\lambda\hbar\omega_\lambda$, the states $\psi^{(\lambda)}$ can be characterized by the number of photons n_λ and therefore $\psi^{(\lambda)} = \psi_{n\lambda}$

where $n = 0, 1, 2, ---$

and $$H_\lambda\psi_{n\lambda} = n_\lambda\hbar\omega_\lambda\psi_{n\lambda} \ . \qquad 2.23$$

If one is familiar with the standard treatment of the simple harmonic oscillator problem (covered in most Quantum texts), he will

realize that the role of q_λ and q^*_λ are precisely that of the SHO "ladder" operators. It turns out, that q(t) and q*(t) are the absorption and emission operators respectively which form their respective matrix elements

$$q_{n/n+1} = (\Psi_n, q\,\Psi_{n+1}) = (\hbar/2\omega)^{1/2}(n+1)^{1/2}, \qquad 2.24$$

and

$$q^*_{n+1/n} = (\Psi_{n+1}, q^*\Psi_n) = (\hbar/2\omega)^{1/2}(n+1)^{1/2}. \qquad 2.25$$

Consider the simple case of spontaneous emission of a quantum λ by a system $|i, 0_\lambda>$ which goes over to $|f, 1\lambda>$ in the transition. If it is assumed that the time dependence of the initial state vector can be written $|i,0_\lambda> \simeq e^{iE_i t/\hbar}$, then from equation 2.15 it is seen that

$$q^*_\lambda(t)\ |i,0_\lambda> \simeq e^{-i\omega_\lambda t}\ e^{iE_i t/\hbar} \qquad 2.26$$

$$= e^{i(E_i - \hbar\omega_\lambda)t/\hbar}$$

In the transition, the initial time dependence $e^{iE_i t/\hbar}$ corresponding to the initial energy E_i goes over to $e^{iE_f t/\hbar}$ corresponding to the final energy E_f where $E_f = E_i - \hbar\omega_\lambda$, which is consistent with spontaneous emission of a photon of energy $\hbar\omega_\lambda$. An identical treatment using the absorption operator $q_\lambda(t)$ yields a final energy state of $E_f = E_i + \hbar\omega_\lambda$.

Quantization of an electromagnetic field leads to a transformation from the concept of the superposition of plane waves to the concept of free non-interacting particles known as photons. The time and

space-dependent components $q_\lambda(t)$ and $\underline{A}_\lambda(\underline{r})$ of the electromagnetic vector potential $\underline{A}(r,t)$ become operators which operate respectively on the time and space dependent components of the total initial wave vector $|i,n_\lambda>$ bringing about a transition to some final state $|f, n \pm 1\lambda>$.

2.4 The Dirac Electron

The wave equation $H\Psi = E\Psi$ for a non-relativistic particle of mass m and momentum p in a potential V(r) is given by

$$(p^2/2m + V(r))\Psi = E\Psi. \qquad 2.27$$

making use of the momentum and energy operators

$$p = -i\hbar\nabla \quad \text{and} \quad E = i\hbar \frac{\partial}{\partial t} , \qquad 2.28$$

the equation takes the form

$$(\frac{-\hbar^2}{2m} \nabla^2 + V(r))\Psi = i\hbar\dot{\Psi} . \qquad 2.29$$

At relativistic energies, the Hamiltonian for a free particle is given by

$$H = \pm (p^2c^2 + m^2c^4)^{1/2} \qquad 2.30$$

and consequently the wave equation for a free, relativistic particle is written

$$\nabla^2\Psi(\underline{r},t) - \frac{1}{c} \ddot{\Psi}(\underline{r},t) = (\frac{mc}{\hbar})^2\Psi(\underline{r},t) , \qquad 2.31$$

and commonly referred to as the Klein-Gordon equation. Equation 2.31 satisfies the conservation equations and the correspondence principle, however, an examination of the density ρ leads to the conclusion

$$\rho = \frac{E}{mc^2} |\Psi|^2 , \qquad 2.32$$

and from equation 2.30 it is seen that the eigenvalue E of the relativistic Hamiltonian operating on the wave function can take on both positive and negative values. The existence of a physically significant, negative density was understandably disturbing.

In an effort to resolve the difficulty, Dirac[14] proposed a relativistic form of the wave equation with the following basic principles

(i) first order in $\partial/\partial t$,

(ii) symmetrical treatment of x, y, z, ct,

(iii) linear in Ψ (to retain the principle of superposition), and

(iv) must satisfy relativistic energy equation (2.30).

The relativistic wave equation for a free electron became

$$(\underline{\alpha}\cdot\underline{p} + \beta\mu)\ \Psi = i\hbar\dot{\Psi} \qquad 2.33$$

where $\underline{p}$ = c x momentum and $\mu = m_o c^2$. $\underline{\alpha}$ and β were necessarily 4 x 4 matrices satisfying the relations.

$$\alpha_x\beta + \beta\alpha_x = 0,$$

$$\alpha_x\alpha_y + \alpha_y\alpha_x = 0,$$

$$\alpha_x^2 = \alpha_y^2 = \alpha_z^2 = \beta^2 = 0. \qquad 2.34$$

The existence of two electron spin states had been established and the Pauli-Spin matrices proposed[15]. Since Dirac's α-matrix necessarily behaved in a manner similar to the Pauli-Spin matrices, $\underline{\alpha}$ and $\underline{\beta}$ could be represented in the form

$$\underline{\alpha} = \begin{vmatrix} \underline{0} & \underline{\sigma} \\ \underline{\sigma} & \underline{0} \end{vmatrix}, \qquad \beta = \begin{vmatrix} \underline{1} & \underline{0} \\ \underline{0} & \underline{-1} \end{vmatrix}, \tag{2.35}$$

where $\underline{1}$, $\underline{0}$ are 2 x 2 matrices and $\underline{\sigma}$ are the Pauli-Spin matrices defining the electron spin

$$\underline{s} = \frac{\hbar}{2}\underline{\sigma} = \frac{\hbar}{2}\begin{vmatrix} \underline{\sigma} & \underline{0} \\ \underline{0} & \underline{\sigma} \end{vmatrix}. \tag{2.36}$$

Explicitly,

$$\underline{\alpha}_x = \begin{vmatrix} 0 & 0 & 0 & 1 \\ 0 & 0 & 1 & 0 \\ 0 & 1 & 0 & 0 \\ 1 & 0 & 0 & 0 \end{vmatrix}, \quad \underline{\alpha}_y = \begin{vmatrix} 0 & 0 & 0 & -i \\ 0 & 0 & i & 0 \\ 0 & -i & 0 & 0 \\ i & 0 & 0 & 0 \end{vmatrix}, \quad \underline{\alpha}_z = \begin{vmatrix} 0 & 0 & 1 & 0 \\ 0 & 0 & 0 & -1 \\ 1 & 0 & 0 & 0 \\ 0 & -1 & 0 & 0 \end{vmatrix} \tag{2.37}$$

The wave function Ψ consists of 4 components,

$$\Psi = \begin{vmatrix} \Psi_1 \\ \Psi_2 \\ \Psi_3 \\ \Psi_4 \end{vmatrix},$$

where a typical plane-wave solution for a free electron is given by

$$\Psi = u e^{i(\underline{p}\cdot\underline{r})/\hbar c_e - iEt/\hbar}, \tag{2.38}$$

where $E^2 = p^2 + \mu^2$ and where $\underline{p}$ and E are numbers and u is a 4-component quantity called a spinor which is dependent on energy and momentum but independent of space and time[16]. The four components of u are required to describe the four possible energy-spin combinations.

Making the transformation from a free electron to one in an electromagnetic field using the substitutions

$$\underline{p} \rightarrow \underline{p} - e\underline{A}$$

$$E \rightarrow E - e\phi$$

leads to the wave equation

$$(\underline{\alpha} \cdot \underline{p} - e\underline{A} + \beta\mu + e\phi)\Psi = i\hbar\dot{\Psi} \ . \qquad 2.39$$

The wave equation for the perturbed system is given by

$$(H_{RAD} + H_{EL} + H_{INT})\Psi = i\hbar\dot{\Psi}, \qquad 2.40$$

where, making use of the previous discussion on field quantization and the Dirac electron,

$$H_{RAD} = \sum_{\lambda} n_\lambda \hbar\omega_\lambda, \qquad 2.41$$

$$H_{EL} = \sum_{k} [\underline{\alpha}_k \cdot \underline{p}_k + \beta_k \mu_k], \qquad 2.42$$

$$H_{INT} = -\sum_{k} e_k (\underline{\alpha}_k \cdot \underline{A}_\lambda(k)) + \sum_{i>k} e_i e_k / r_{ik}, \qquad 2.43$$

where i, k refer to individual electrons of the atom. Normally, the Coulomb term $e\phi = \sum_{i>k} e_i e_k / r_{ik}$ is regarded as part of the unperturbed

problem and is included in H_{EL} rather than in H_{INT}.

The interaction Hamiltonian for an electron in collision with a photon defined by the quantum number λ (using equations 2.11, 2.16, and 2.43) becomes

$$H_{INT_\lambda} = -e\alpha_e(4\pi c^2)^{1/2} \, e^{i(\underline{\kappa}_\lambda \cdot \underline{r})} \, q_\lambda(t) \qquad 2.44$$

where $q_\lambda(t)$ is the absorption operator and α_e is the component of the vector $\underline{\alpha}$ in the direction of the photon polarization vector (and therefore $\underline{\alpha}_e \perp \underline{\kappa}_\lambda$ where $\underline{\kappa}_\lambda$ is the propagation vector). From equation 2.44 it is seen that $H_{INT} = H_1(\underline{r})H_2(t)$ and therefore, the matrix element for the transition can be written as the product of two matrix elements assuming separation of the time and space dependences of the total wave equation is possible.

2.5 The Transition Rate

The interaction of electromagnetic radiation with some system involves a transition of some sort from an initial unperturbed state to some final state. Consequently, the transition probability for the particular interaction and the resulting change in total energy of the system are of particular interest.

The application of elementary perturbation theory yields the first order approximation

$$W_{F|0} = \frac{2\pi}{\hbar} \left| H_{F|0} \right|^2 \rho_F \qquad 2.45$$

where $W_{F|0}$ is the transition probability (s^{-1}) that a system in the initial state 0 will undergo transition to the final state F. For example, at time t = 0 the system is supposed to be in the definite unperturbed state 0 whereby an atomic electron exists in its ground state and a photon is present. The Coulomb interaction between the electron and the radiation field modifies the unperturbed Hamiltonian and through the action of this perturbation H_{INT} the system in the course of time may be transformed to a final state whereby the photon has been absorbed and the atom is in an excited state.

Since equation 2.45 is the product of first order perturbation theory, the matrix element $H_{F|0}$ has a non-zero value only if the number of photons in the F state differ by 1 from the number in the 0 state. It is, therefore, the correct expression for describing the probability of absorption or emission of a single photon. The scattering of a photon by an electron cannot be described by equation 2.45 since in this process two photons must be changed; the primary photon must be absorbed and the secondary or scattered photon must be emitted. Consequently, the required mathematical process must involve second order perturbation theory where two matrix elements must be considered. That is, the transition from the initial state 0 to the final state F is bridged by the intermediate states I_1, I_2,--- and the transition probability is given by

$$W_{F|0} = \frac{2\pi}{\hbar} \left| \sum_i \frac{H_{F|I_i} H_{I_i|0}}{(E_o - E_i)} \right|^2 \rho_F \qquad 2.46$$

where $\sum_i$ denotes summation over all available intermediate (virtual)

states. Since in the intermediate state only momentum (not necessarily energy) need be conserved, a number of intermediate states may exist. This may be illustrated by considering Compton scattering.

In the initial state 0 a primary quantum defined by its momentum vector $\underline{k}_o$ is incident on an electron assumed to be free and at rest and therefore its momentum is $\underline{p}_o = 0$ and its energy $E_o = \mu = m_o c^2$. $W_{F|0}$ is the transition rate per second for the transition from the 0 state to the F state where the electron has energy E and momentum $\underline{p}$ and the scattered quantum has momentum $\underline{k}$. Since only momentum need be considered in the intermediate states, the following virtual states or channels are possible:

I. The photon with momentum $\underline{k}_o$ is absorbed and the electron's momentum is $\underline{p}' = \underline{k}_o$. A photon with momentum $\underline{k}$ must then be emitted in the transition I → F.

II. A photon with momentum $\underline{k}$ is emitted and exists with $\underline{k}_o$ and the electron's momentum is $\underline{p}' = -\underline{k}$. The photon with momentum $\underline{k}_o$ must then be absorbed in the transition II → F.

The transition rate for Compton scattering is then given by

$$W_{F|0} = \frac{2\pi}{\hbar} \left| \Sigma \frac{H_{F|I} H_{I|0}}{E_0 - E_I} + \frac{H_{F|II} H_{II|0}}{E_0 - E_{II}} \right|^2 \rho_F \qquad 2.47$$

where in this case, Σ denotes summation over all four intermediate electron states (i.e. both spin directions and both signs ($\pm$) of energy).

2.6 The Cross Section

The concepts encountered earlier in this chapter may now be used in order to define the cross section. It is clear that the matrix element of equation 2.45 is of the form $H_{n|m}$ where m = a,---, n_λ---- are the quantum numbers for the initial state scattering system and the primary radiation field (n_λ being the number of λ-radiation oscillators) and n = b,---, $n_\lambda \pm 1$,--- are the quantum numbers defining the final system including the transformed scattering system and the secondary radiation field. Of particular significance is the fact that for each matrix element the number of quantum states λ increases or decreases by one.

Consider the matrix element for the absorption of one photon ($n_\lambda + 1 \rightarrow n_\lambda$) while the electron system undergoes the transition b→a,

$$H_{a,n_\lambda|b,n_\lambda+1} = (\Psi_{a,n_\lambda}, \hat{H}_{INT}\, \Psi_{b,n_\lambda+1}) \qquad 2.48$$

Assuming the $e\phi = e_i e_k / r_{ik}$ term belongs to H_{EL}, the interaction energy for a particular electron with a λ-radiation oscillator is given by

$$\hat{H}_{INT} = -e\alpha_e\, (4\pi c^2)^{1/2}\, e^{i(\underline{\kappa}_\lambda \cdot \underline{r})}\, \hat{q}_\lambda \qquad 2.49$$

where α_e is the component of the matrix vector $\underline{\alpha}$ in the direction of the polarization of the light (and perpendicular to the propagation vector $\underline{\kappa}_\lambda$).

Therefore

$$H_{a,n_\lambda|b,n_\lambda+1} = -e(4\pi c^2)^{1/2}(\Psi_{a,n_\lambda},\alpha_e\, e^{i(\underline{\kappa}_\lambda\cdot\underline{r})}\hat{q}_\lambda\,\Psi_{b,n_\lambda+1}) \ . \qquad 2.50$$

Assuming that the interaction is incoherent, it is possible to write

$$\Psi_{b,n_\lambda+1} = \Psi_b\Psi_{n_\lambda+1} \ , \qquad 2.51$$

and equation 2.50 becomes

$$H_{a,n_\lambda|b,n_\lambda+1} = -e(4\pi c^2)^{1/2}(\Psi_a,\alpha_e e^{i(\underline{\kappa}_\lambda\cdot\underline{r})}\Psi_b)(\Psi_{n_\lambda},\hat{q}_\lambda\Psi_{n_\lambda+1}) \ , \qquad 2.52$$

and therefore (using equation 2.24) becomes

$$H_{a,n_\lambda|b,n_\lambda+1} = -e\left(\frac{2\pi\hbar^2c^2}{k_\lambda}\right)^{1/2}(n_\lambda+1)^{1/2}(\Psi_a,\alpha_e e^{i(\underline{\kappa}_\lambda\cdot\underline{r})}\Psi_b) \ , \qquad 2.53$$

where $k_\lambda = \hbar\omega_\lambda$.

Similarly, the matrix element for the emission of a photon is given by

$$H_{a,n_\lambda+1|b,n_\lambda} = -e\left(\frac{2\pi\hbar c^2}{k_\lambda}\right)^{1/2}(n_\lambda+1)^{1/2}(\Psi_a,\alpha_e e^{-(\underline{\kappa}_\lambda\cdot\underline{r})}\Psi_b) \ . \qquad 2.54$$

Although the energy will not in general be conserved if either of the states in question are virtual, the energy difference for both transitions are

$$E_n - E_m = E_a - E_b \pm k_\lambda . \qquad 2.55$$

The integration limits of the matrix elements of equations 2.53 and 2.54 are over all space coordinates and summation over all possible spinors of the electron wave functions is implied.

Dirac's treatment of the free electron in a radiation field where the final and initial electron states Ψ_a and Ψ_b have momenta $\underline{p}_a$ and $\underline{p}_b$ yields

$$\Psi_a = u_a e^{i(\underline{p}_a \cdot r)/\hbar c} , \qquad 2.56$$

and

$$\Psi_b = u_b e^{i(\underline{p}_b \cdot r)/\hbar c} , \qquad 2.57$$

where the spinors u_a and u_b are 4-component vectors dependent on the electron energies and momenta E_a, E_b and $\underline{p}_a$, $\underline{p}_b$ but independent of space and time coordinates.

Finally, the matrix element for the interaction of a Dirac electron with an electromagnetic field resulting in the absorption (or emission) of a single quantum is given by

$$H_{p_a,n_\lambda|p_b,n_\lambda+1} = -e\left(\frac{2\pi\hbar c^2}{k_\lambda}\right)^{1/2} (n_\lambda+1)^{1/2} (u_a, \alpha_e u_b) \int e^{i(p_b - p_a \pm \underline{k}_\lambda \cdot \underline{r})/c\hbar} d\tau \qquad 2.58$$

$$= H_{p_a,n_\lambda+1|p_b,n_\lambda} ,$$

where the $-\underline{k}_\lambda \cdot \underline{r}$ term applies to the emission case.

Since

$$\int e^{i(\underline{p}_b - \underline{p}_a \pm \underline{k}_\lambda \cdot r)\hbar c} \, d\tau \rightarrow \delta(\underline{p}_b - \underline{p}_a \pm \underline{k}_\lambda) \ , \qquad 2.59$$

the condition for non-vanishing matrix elements is

$$\underline{p}_b - \underline{p}_a \pm \underline{k}_\lambda = 0 \qquad 2.60$$

which states that for all interaction processes involving light quanta with a free particle, the momentum is conserved. The 4 components of the Dirac spinors are required to describe the four possible energy-spin combinations.

Once the matrix element is known, the interaction cross section is obtained in a straight forward manner. Consider an incident plane wave contained in a unit volume and described by the wave function

$$\phi = e^{i(\underline{k}_o \cdot \underline{r} - \omega_{k_o} t)} \ . \qquad 2.61$$

The rate at which the plane wave and the scattering centre interact is given by the transition probability

$$W_{f|i} = \frac{2\pi}{\hbar} \left| H_{f|i} \right|^2 \rho_F \quad [s^{-1}]. \qquad 2.62$$

The differential cross section for scattering of radiation by a target centre into a solid angle $d\Omega$ is defined as

$$\begin{aligned} d\sigma_s &= \text{Transition Rate x } d\Omega/\text{Incident flux} \\ &= \frac{2\pi}{\hbar} \left| H_{f|i} \right|^2 \rho_F \, d\Omega/\text{Incident flux} \end{aligned} \qquad 2.63$$

But $$\text{Incident Flux} = |\phi|^2 v \qquad 2.64$$

$$= v$$

and therefore

$$d\sigma_s = \frac{2\pi}{\hbar} \left| H_{f|i} \right|^2 \rho_F \, d\Omega/v \; . \qquad 2.65$$

Since photons are being considered at this time, v is given by the speed of light c. In the case of Bremsstrahlung radiation, the incident particles are electrons and, therefore, v is given by $\hbar k_o/m$.

Evaluation of the differential cross section for a particular interaction requires knowledge of the density of final states ρ_F. ρ_F differs for each type of interaction; however, two particular cases occur.

(i) The final state system has a discrete energy spectrum. Compton scattering is an example since by defining the scattering angle, the secondary photon energy $\underline{k}$ and the scattered electron energy E are uniquely determined.

(ii) The final state has a continuous energy spectrum. Photo-electric absorption is an example of this situation since the final electron can have any energy up to

$$E_{max} = E_\gamma - \text{Binding Energy.} \qquad 2.66$$

In this case, ρ_F must be defined as the number of quantum states per unit volume of the electron.

The density of final states is determined using the normal mode technique. Again, this technique is covered in most texts dealing with transition probabilities.

Consider the case of inelastic scattering. The final state is

completely determined by the energy of the scattered quantum $\underline{k}$ and the scattering angle θ. Consequently,

$$\rho_F dE_F = \rho_k \, dk, \tag{2.67}$$

and therefore

$$\rho_F = \rho_k \left(\frac{dk}{dE_F}\right), \tag{2.68}$$

where ρ_k is the number of states for the scattered quantum per unit energy interval dk. Using the normal mode technique, this is established to be

$$\begin{aligned} \rho_k &= \frac{dN(k)}{dk} \\ &= \frac{k^2 d\Omega}{(2\pi\hbar c)^3} \end{aligned} \tag{2.69}$$

Since

$$\begin{aligned} E_F &= k + E \\ &= k + (p^2 + \mu^2)^{1/2} \\ &= k + (k_o^2 + k^2 - 2kk_o\cos\theta + \mu^2)^{1/2}, \end{aligned} \tag{2.70}$$

then

$$\left(\frac{\partial k}{\partial E_F}\right)_\theta = \frac{Ek}{\mu k_o} \tag{2.71}$$

and therefore, from equations 2.68, 2.69, and 2.71

$$\rho_F = \frac{Ek}{\mu k_o} \cdot \frac{k^2 d\Omega}{(2\pi\hbar c)^3} \quad . \tag{2.72}$$

The transition rate for Compton scattering was given earlier (equation 2.47) as

$$W_{F|0} = \frac{2\pi}{\hbar} \left| \Sigma \left(\frac{H_{F|I} H_{I|0}}{E_0 - E_I} + \frac{H_{F|II} H_{II|0}}{E_0 - E_{II}} \right) \right|^2 \rho_F \ , \tag{2.73}$$

where Σ denotes summation over the 4-fold intermediate states and E_0, E_I, and E_{II} represent the total energies in the initial and intermediate states. Conservation of energy requires

$$E_0 - E_I = \mu + k_o - E' \tag{2.74}$$

and

$$E_o - E_{II} = \mu - E'' - k \tag{2.75}$$

where E' and E'' are the energies of the electron in the two intermediate states. Substitution of equations 2.72, 2.74, and 2.75 into equation 2.73 and dividing by the incident photon velocity c yields the differential cross section for the inelastic process,

$$d\sigma_{(INCOH)} = \frac{e^4 Ek^2 d\Omega}{\mu k_o^2} \left| \Sigma \left| \frac{(u,\alpha u')(u',\alpha_o u_o)}{u+k_o-E'} + \frac{(u,\alpha_o u'')(u'',\alpha u_o)}{u-k-E''} \right| \right|^2 , \tag{2.76}$$

where the four matrix elements have been replaced by the appropriate forms of equation 2.58. Summation Σ is over all spin directions and both signs of the energy for the intermediate states.

Following the procedures described by Heitler[17] equation 2.76 is then reduced to the Klein-Nishina formula for unpolarized radiation,

$$d\sigma_{(INCOH)} = \frac{r_o^2}{2} d\Omega \frac{k^2}{k_o^2} \left(\frac{k_o}{k} + \frac{k}{k_o} - \sin^2\theta \right) , \qquad 2.77$$

where r_o is the classical electron radius and k is a function of θ given by the Compton formula

$$k = \frac{k_o \mu}{u + k_o (1-\cos\theta)} . \qquad 2.78$$

CHAPTER III

MEASUREMENT OF THE TOTAL PHOTON CROSS SECTION

3.1 Introduction

In the intermediate energy region from 3-15 MeV, a shortage of good accuracy experimental data on photon cross sections has left the various theoretical predictions virtually untested. The shortage of measured data in this region stems directly from the difficulty in obtaining a reasonably simple gamma-ray spectrum comprising a number of intense, well distributed photon energies. On the other hand, total cross section measurements extending from the x-ray energies to as high as the 2754 keV beta-decay line in ^{24}Na have been quite exhaustive and the present theories are in good accord with measured values. In view of these facts, a measurement of the total gamma-ray cross section was proposed whereby in a single measurement, cross sections extending across the well understood 1-3 MeV region into the untested intermediate-energy region could be realized. A comparison of the measured cross sections with previously established values in the 1-3 MeV region would then be useful in assessing the significance of the higher energy results. Since the primary purpose of the measurement would be to provide an effective evaluation of the proposed theoretical cross sections in the intermediate-energy region above 3 MeV, a considerable volume of accurately measured data would necessarily have to extend over both energy and atomic number with an

even distribution in both dimensions being ideal. As a result of this requirement, detailed experimental planning was carried out with the express purpose of realizing an optimum experimental system which would facilitate the efficient accumulation of accurate data on the total cross section.

3.2 Experimental Planning and Design

The proposed experimental method involved the standard technique of observing the energy spectrum associated with the gamma-ray beam with and without a target positioned in the beam and therefore determine the attenuation of the gamma-ray intensity in the target. The mass-attenuation coefficient for a particular photon energy and target material is then related to the measured target and no-target gamma-ray intensities R and R_o by the equation

$$\mu/\rho = \ell n(R_o/R)/x, \qquad 3.1$$

where μ/ρ has units of cm^2/g for target thickness x in units of g/cm^2. Equation 3.1 follows directly from the assumption that a photon is removed from the beam in a single interaction with a target centre, assuming the conditions of "narrow beam" geometry exist. Under these conditions, beam attenuation shows a truly exponential dependence on target thickness.

Having decided on the general experimental method and keeping the objectives of the measurement in mind, detailed planning of experimental design and procedures followed with definite emphasis being placed on all aspects of experimental optimization while remaining within the limits of available resources. Optimization procedures

necessarily involved selection of the best possible combination of available materials and instruments which would then be arranged and operated in such a manner as to facilitate the efficient accumulation of considerable quantities of statistically significant spectroscopic intensity data relating to the cross section (equation 3.1). A suitable experimental arrangement is generalized in figure 3-1(a) where it becomes clear that the problems concerning optimization may be classified into areas concerning (1) the photon source, (2) the spectrometer, (3) the target system, and (4) the control unit. Details concerning the general experimental arrangement including all aspects of beam collimation will be considered during the discussions of each of these specified areas. As is usually the case, the classification of problems into specific areas simplifies the explanation of details; however, it must be realized that some overlap does exist and frequently a decision in one area is largely determined by some condition existing beyond its boundaries.

A brief but general description of the proposed experimental technique (sketched in figure 3-1(a)) will further simplify the discussion of details associated with the specified areas. Gamma radiation from the source, with the target positioned clear of the beam, is detected, pulse height analysed, and subsequently stored in some region of the analyser memory. Following a predetermined time, pulse height analysis is temporarily suspended and the target is automatically transferred to a position where it intercepts the beam. Pulse height analysis then resumes and the observed spectrum is stored in a memory region isolated from that assigned to the open-beam spectrum. Through use of electronic timing and control, the procedure will be repeated

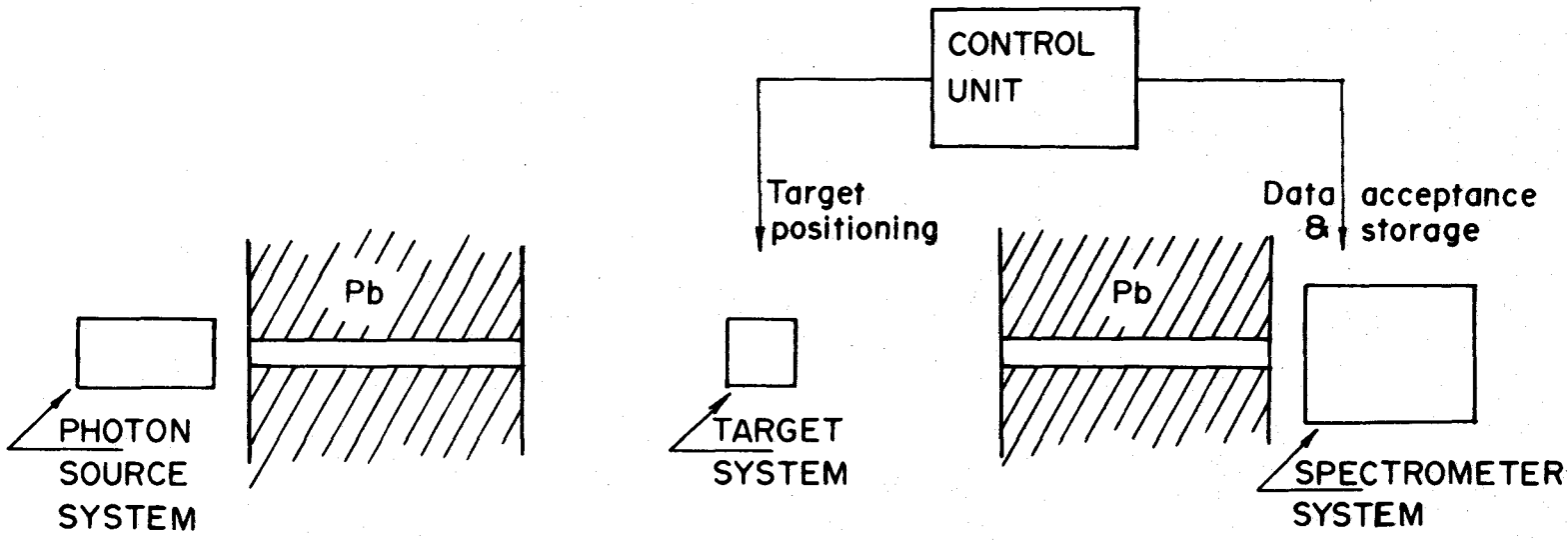

Figure 3-1(a): Basic experimental system suitable for a measurement of the total cross section.

until the statistical errors associated with the target and no target gamma-ray peak intensities have been reduced to the desired level. Measured target and no target intensities would then be evaluated and equation 3.1 applied in order to obtain the mass-attentuation coefficients.

(1) Photon Source:

Initial planning included use of the 2 MWatt swimming-pool type reactor at McMaster University. The photon beam was to be generated through the radiative capture $X(n,\gamma)Y$ reaction. Decisions were required concerning the choice of capture material X (frequently referred to as the photon source) and the choice of a geometrical arrangement between neutron source (reactor core) and capture material.

Gamma radiation following neutron capture using a reactor facility may be obtained either by delivering the neutrons to the capture material situated external to the reactor pool or by placing the capture material in a high flux region of the core and extracting the resulting photons in a collimated beam. The two arrangements, both available with the McMaster facility, are illustrated schematically in figure 3-1(b). Ignoring the effects of losses in neutron and photon intensities due to absorption in the capture material (these effects are approximately comparable in both systems), the photon flux delivered by the external target system will be reduced by a factor $\omega/\omega_1\omega_2$ over that delivered by the internal target facility. If the photon beams of both systems are to be equally collimated, the factor reduces to $1/\omega_1 \simeq 10^{-5}$. Further, an examination of the geometries of the two systems leads to the conclusion that considerably

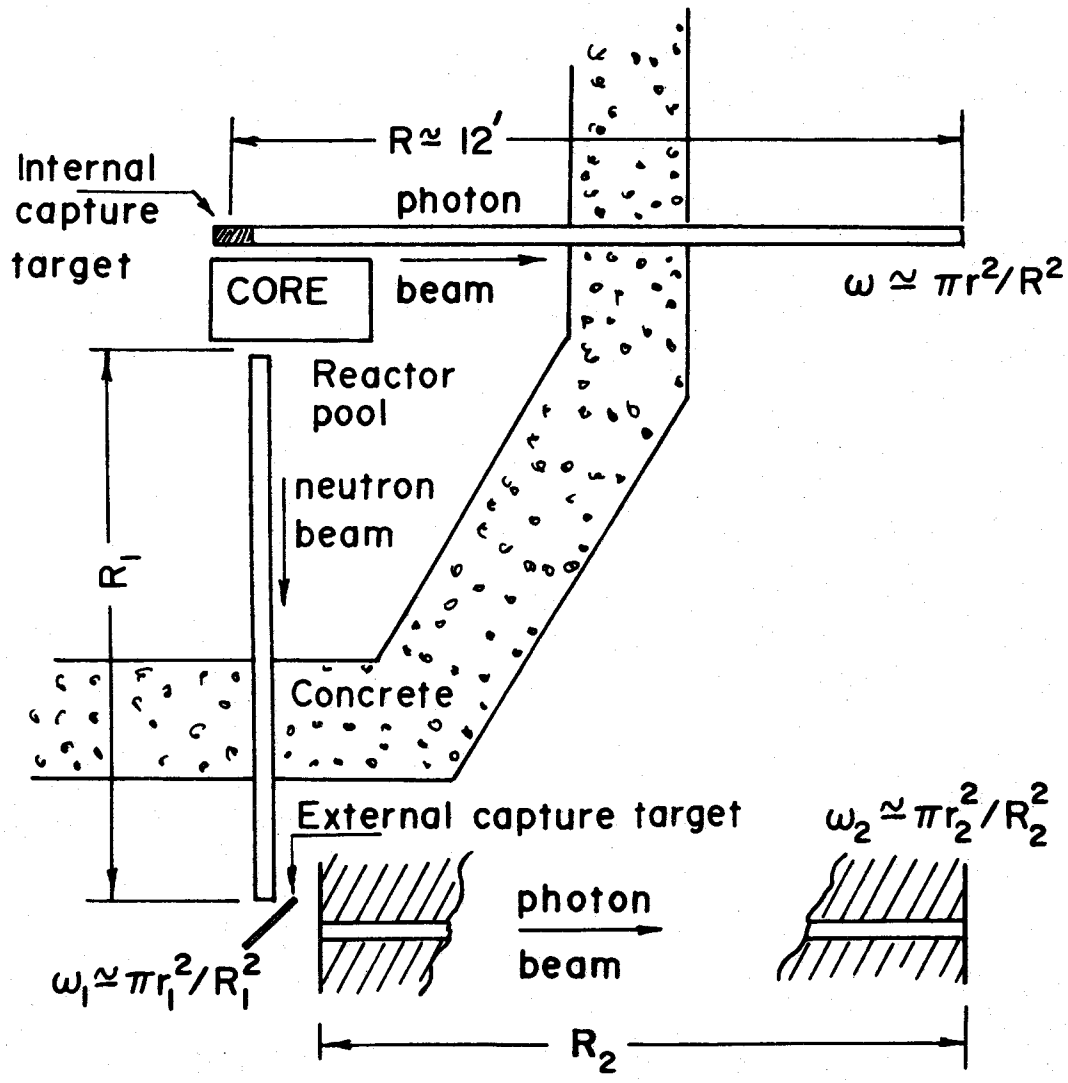

Figure 3-1(b): Two available methods for obtaining reactor produced, neutron capture gamma rays.

larger effective target volumes are possible using the internal system. Clearly, in a measurement involving the accumulation of large quantities of data using a narrow beam geometry, the internal target facility capable of delivering considerably greater photon intensities would be far superior. A detailed discription of the McMaster reactor internal source facility is given by Nichol et al[18].

The choice of capture material followed from a number of considerations including the availability of sufficiently pure materials and their cross sections for thermal neutron capture as well as details of their spectra; particularly energy range, distribution, and relative photon yields per capture reaction. Consideration was necessarily given to the possible production of long-lived radioisotopes which would create the problem of active-waste disposal. Using as a guide the catalogued (n,γ) transition energies and intensities of Rasmussen[19], it was concluded that the radiation spectrum following thermal neutron capture in ^{14}N was by far the most suitable for the proposed measurement. Although the capture cross section is not particularly high ($\sim$ 0.1 barns), the spectrum includes several relatively strong, well distributed energies ranging as high as 10.827 MeV. Solid nitrogen was found commercially available in an $H_6C_3N_6$ (Melamine) compound which could be obtained in a relatively pure powdered form. Further, the melamine would prove particularly useful as a source material since the relatively simple capture gamma-ray spectra associated with the hydrogen and carbon elements would not interfere with the nitrogen spectrum but would, in fact, provide useful energies for the cross section study. It was decided that an energy gap in the 3 MeV region of the gamma-ray spectrum following neutron capture by

the ^{1}H, ^{12}C and ^{14}N melamine nuclei could be effectively closed by the addition of a small quantity of Na powder. Further, a fifth source element could be introduced by way of an aluminum source holder purposely designed so its capture spectrum would contribute to the photon beam. Such an addition would effectively close the gap between the 7.3 and 8.3 MeV ^{15}N energies. The more prominent capture gamma-ray energies for the five proposed source elements are shown in table 3-1 as are their relative intensities. With this proposed choice of target mixture, disposal following irradiation would pose little difficulty since, with the exception of small quantities of contaminants, the resulting product nuclei would be sufficiently short lived, with 15 hour ^{24}Na being the longest lived isotope produced.

The McMaster reactor and internal target facility (including through tube and external collimator) are shown schematically in figure 3-2 while the through tube assembly including the proposed source and holder is detailed in figure 3-3. Consideration of an optimum source position using the internal irradiation facility led to the conclusion that the source be located at the corner of the reactor core farthest from the detector. This would serve the purpose of minimizing the effects of any gamma radiation from the core region being Compton scattered by the source into the collimator. The necessity for such a precaution is easily demonstrated. Since each fission reaction can be expected to yield at least the same number of gamma rays as neutrons and since the neutron capture cross sections encountered are comparable to if not smaller than the Compton scattering cross sections one can expect at least a one to one (and probably much

Table 3-1: Energies and relative intensities for the more prominent gamma rays, suitable for the total cross section measurement, obtained through the ^{1}H ^{12}C ^{14}N ^{23}Na $^{27}Al(n,\gamma)$ reaction. The relative intensities I_γ refer to the number of particular photons generated per 100 captures by a particular isotope.

Energy in MeV (E_γ)	Relative Intensities (I_γ) per 100 Captures				
	$^{1}H(n,\gamma)$	$^{12}C(n,\gamma)$	$^{14}N(n,\gamma)$	$^{23}Na(n,\gamma)$	$^{27}Al(n,\gamma)$
1.779					88
1.889			27		
2.225	100				
2.519			9		
2.754				100	
3.098				10	
3.530			10		
3.675			16		
3.982				22	
4.508			16		
4.945		67			
5.278*			44		
5.542*			27		
6.321			17		
7.299			8		
7.724					17
8.308			4		
9.151			2		
10.827			15		

*Weighted averages of the 5.267 and 5.297 MeV and the 5.532 and 5.562 MeV gamma energies were used to obtain the 5.278 and 5.542 MeV energies and intensities attributed to the nitrogen spectrum.

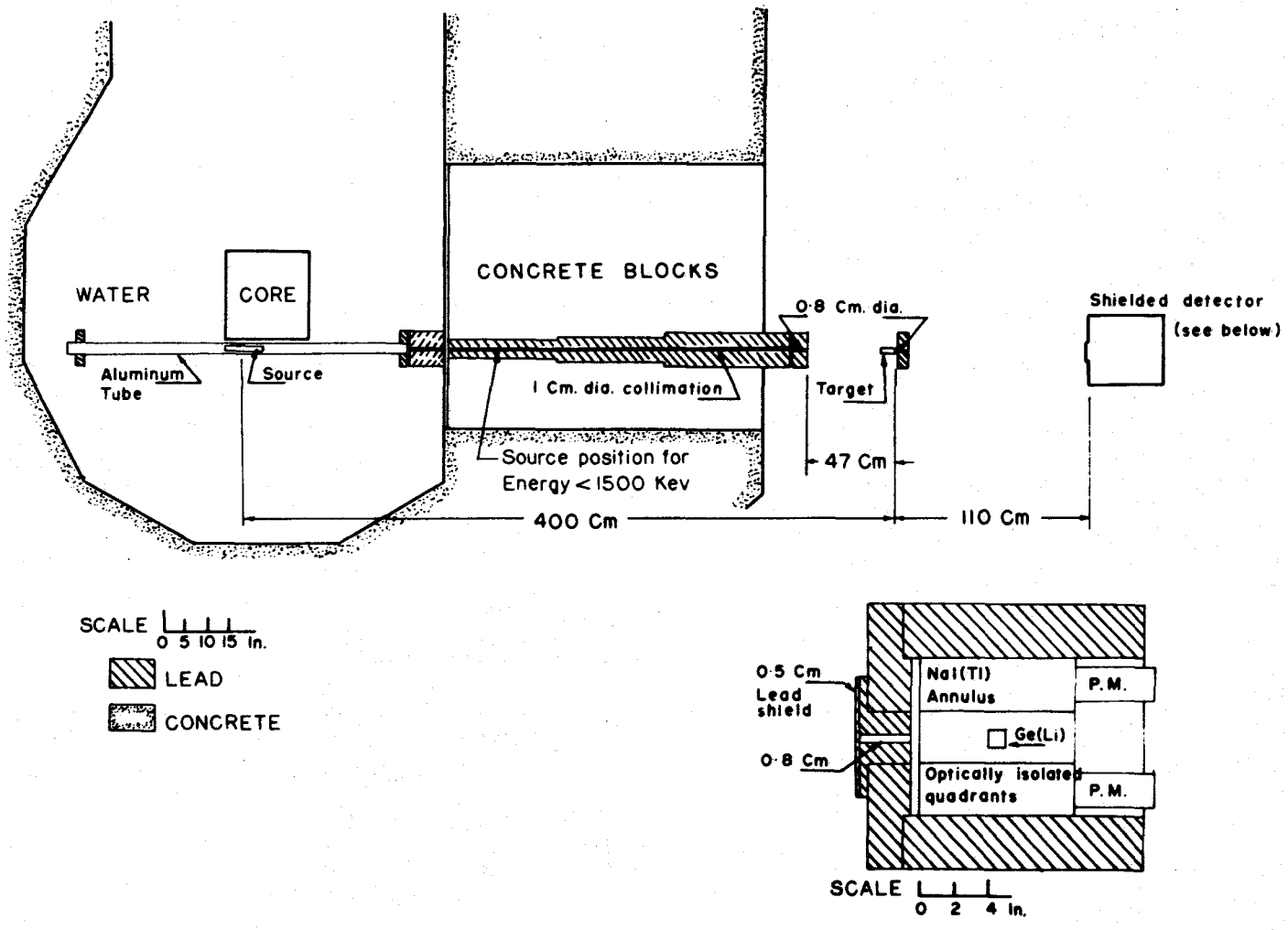

Figure 3-2: General experimental arrangement for measurement of the total gamma-ray cross section. The NaI(Tℓ) annulus (Harshaw Chemical Co.) is optically divided into quadrants and is 15.2 cm in length, 23 cm in diameter, and has a central hole 7.6 cm in diameter.

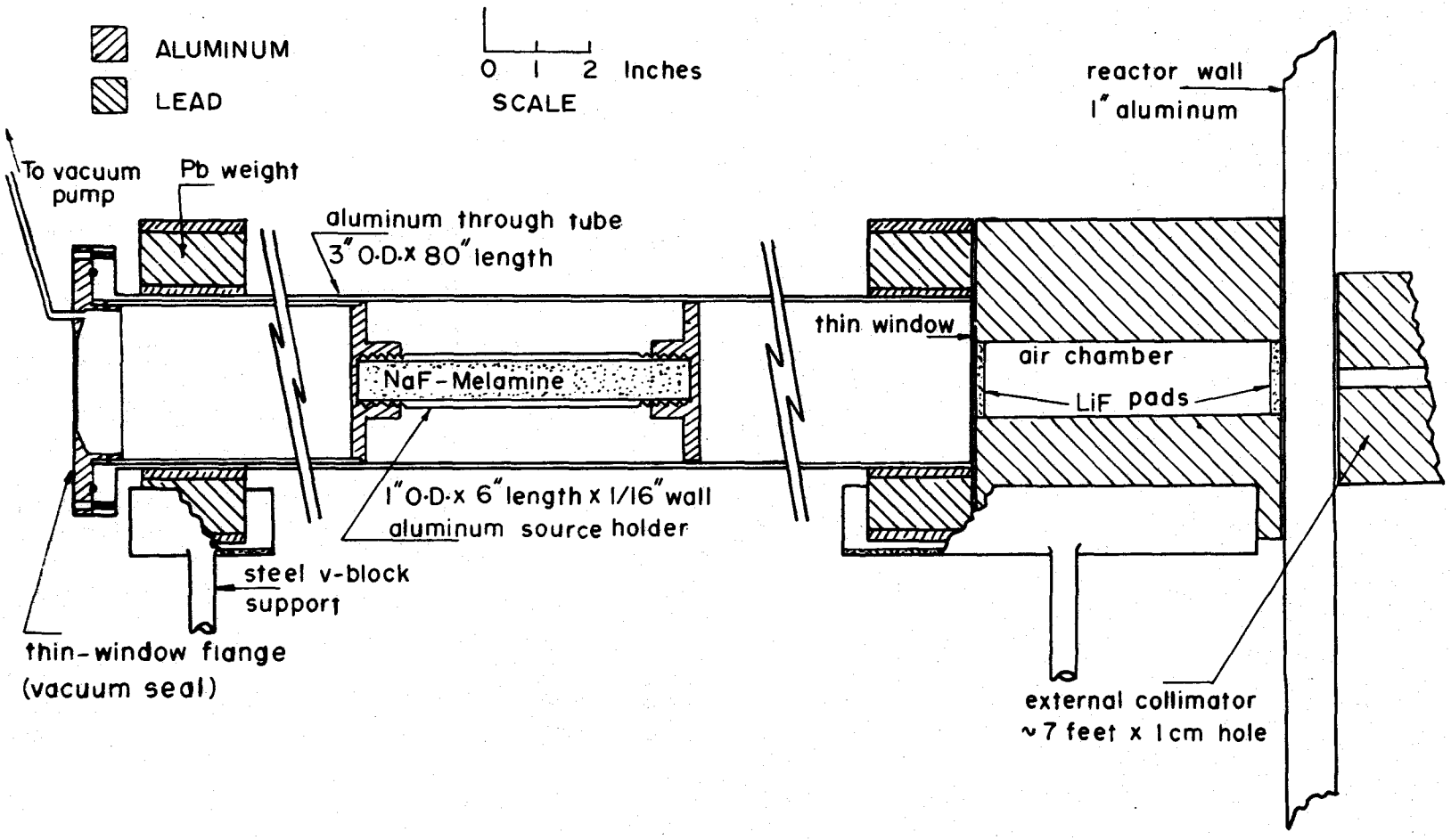

Fig 3-3: Reactor through tube and source arrangement. The source holder was secured in the through tube by three struts fixing the holder to the flange. The source consisted of 150 g of $N_6C_3H_6$ (Melamine) and 5 g of Na. The aluminium holder also served as source material. Through collimation, the effective source diameter was reduced to approximately 1.5 cm. Thermal-neutron flux in the source region was approximately 5 x 10^{12} neutrons/cm^2/s.

higher) ratio of Compton scattered photons to neutron capture events. Use of the proposed optimum source position would insure that all radiation Compton scattered into the collimator would be compressed into an energy spectrum having an upper limit of approximately 511 keV. This low energy component could then be effectively reduced by passing the beam through a relatively thin absorber. Further, the proposed source position would use to advantage the anisotropy of the Compton distribution, allowing only the reduced back-angle scattered components to see the counter. For example, the differential Compton cross section for 1 MeV gamma rays scattered at an angle of 30° is approximately 0.036 barns/electron/sr as compared to a value of .0016 barns/electron/sr for 150° scattering.

(2) Spectrometer and Related Electronics:

A block diagram of a basic system suitable for the proposed measurement is shown in figure 3-4. Available equipment included a choice of NaI(Tℓ) and Ge(Li) gamma-ray detectors as well as an NaI(Tℓ) annulus detector (figures 3.2 and 3.5) optically divided into quadrants. A ND-3300 multichannel pulse height analyser (PHA) included a gateable input, electronically stabilized analogue to digital converter (ADC) having a maximum conversion gain of 4096 channels and access to a 16K magnetic-core memory. Spectra could be stored in different regions of the memory by applying an appropriate control signal at the input of a data ROUTE facility. This facility would be used to isolate the spectra obtained with the target in different positions, generation of the appropriate control signal for data routing being one of the responsibilities of the control unit.

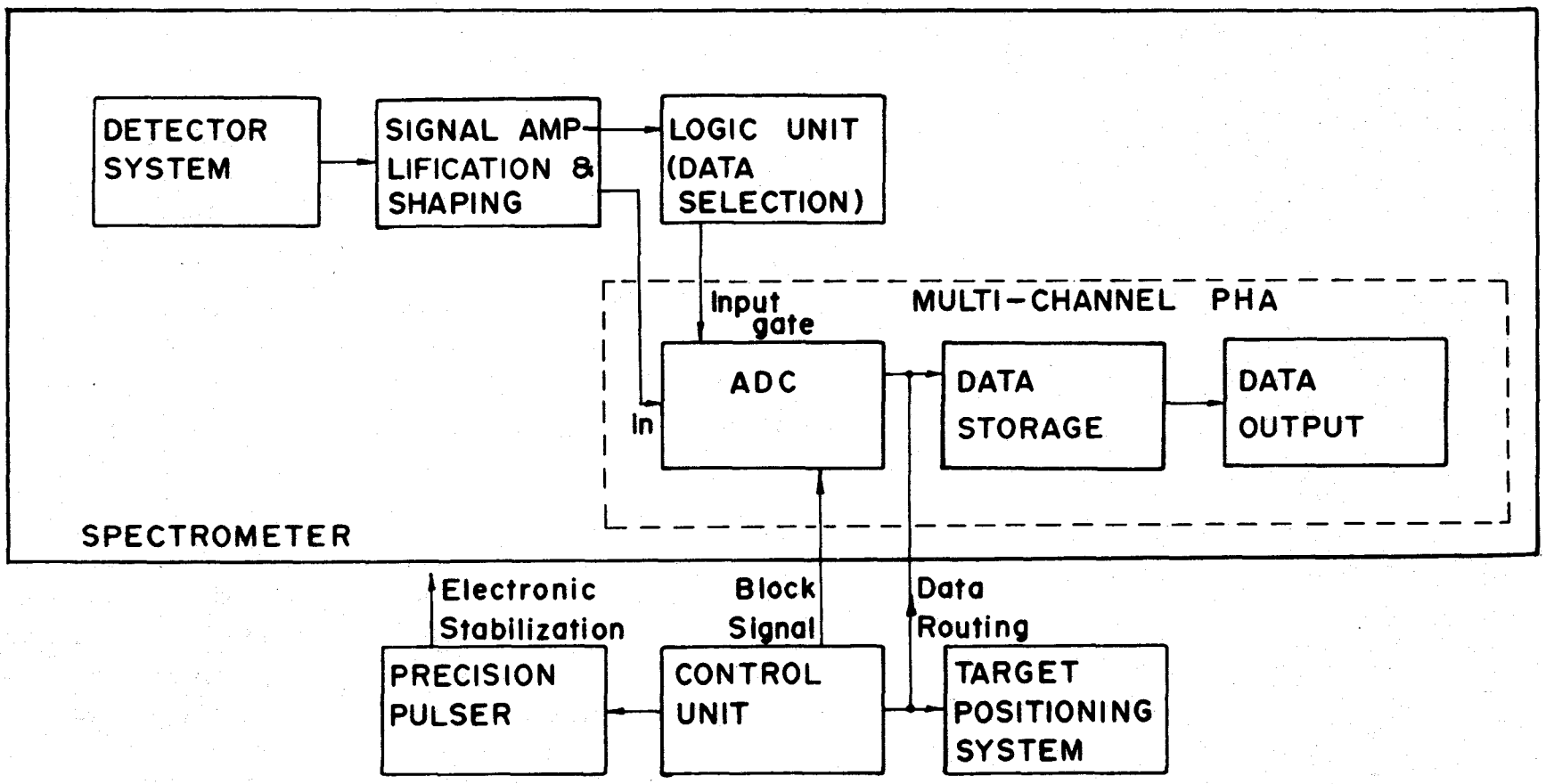

Figure 3-4: Basic system including spectrometer and related electronics suitable for total photon cross section measurements.

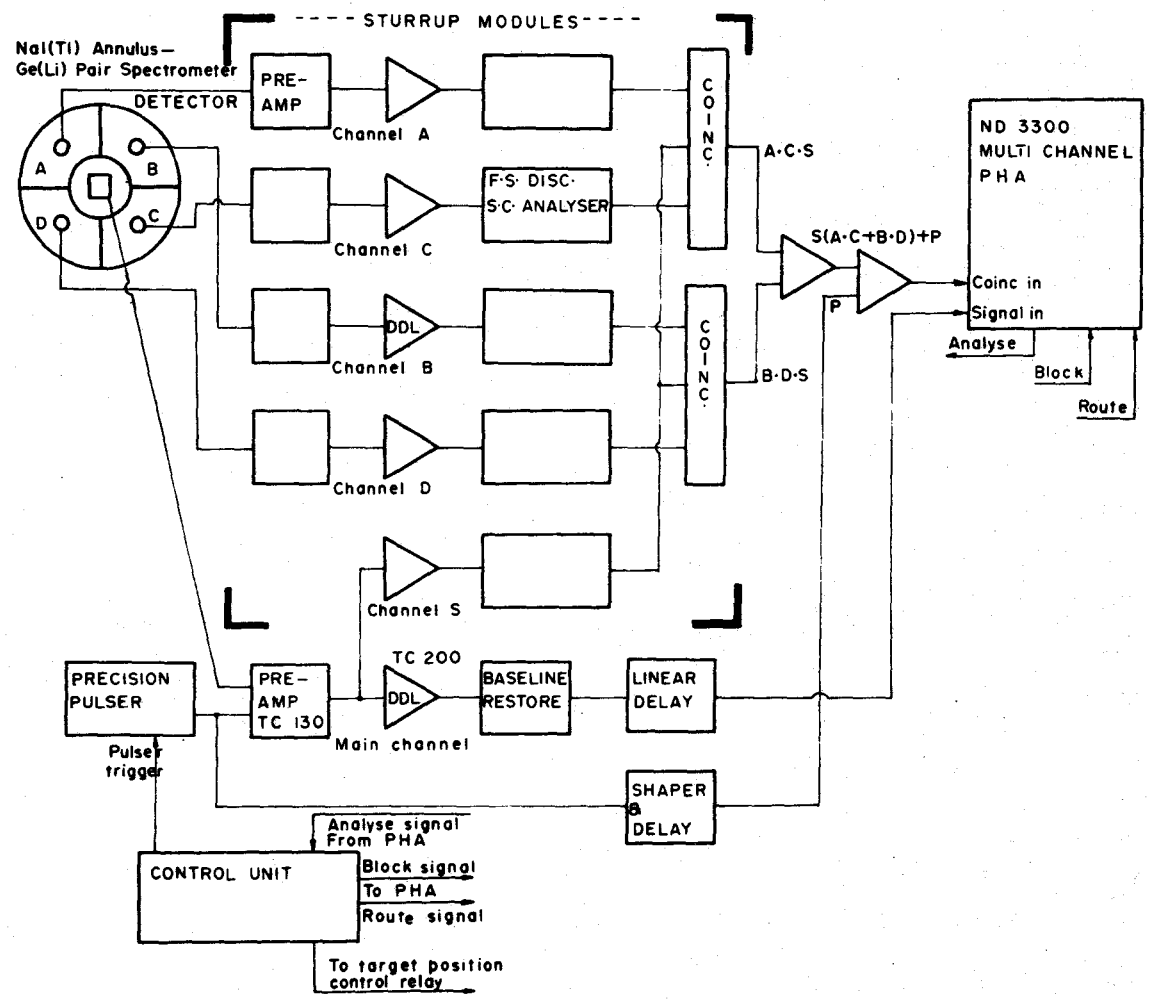

Figure 3-5: NaI(Tℓ) annulus-Ge(Li) triple-coincidence, pair spectrometer. Logic electronic modules are arranged to enable pulse-height analysis and storage of an event detected in the main (S) channel provided that the event originated at the pulser, or provided that it has been detected simultaneously with 511-keV radiation in each of two opposite NaI quadrants [S(A.C + B.D) + P].

Since the choice of a detector system would depend on the available photon beam intensity and energy distribution, a preliminary investigation using the proposed source system was undertaken in order to establish some definite facts relating source size, beam collimation, and possible count rates. The results indicated that little difficulty would be encountered in obtaining substantial count rates even under conditions of severe collimation. In view of this fact, the conclusion was reached that the solid state Ge(Li) detector would be superior to the NaI(Tℓ) scintillation detector for intensity analysis. Detector efficiency would be sacrificed for improved energy resolution. While the relatively low Ge(Li) efficiencies would necessarily extend counting times, this would prove far more acceptable than the increased uncertainty in intensity results which would arise from the reduced peak definitions should the poorer resolution NaI(Tℓ) detector be used.

As previously suggested, the effectiveness of the study would depend on the realization of a distribution of cross sections, obtained in a single measurement, extending from the 1 MeV region well into the intermediate region. The entire set of results would then have the same uncertainties relating to possible systematic experimental errors. The degree of uncertainty could then be evaluated by comparing the measured 1-3 MeV results with the already well established theoretical values for that region. The preliminary investigation clearly demonstrated that the proposed source mixture would provide the required distribution and range of energies and that the solid state detector would be the most suitable for intensity analysis. The substantial beam strengths available plus the fact that the energy region of interest was above 1 MeV allowed for a choice in methods of data acquisition.

One choice would be to operate the Ge(Li) counter as the only detector and record the resulting "singles" spectrum. Using this technique of single parameter sampling, the entire spectrum could be recorded in one measurement; however, the spectrum would be complicated by the combination of Compton continuum, single and double escape peaks associated with pair production, and full energy photo peaks. The 4096 channel spectrum shown in figure 3-6 was obtained during the preliminary investigation using single parameter sampling of the radiation spectrum following the (n,γ) reaction on melamine+ Na+Al. Signal to noise ratios (S/N) and energy resolutions (FWHM) are indicated for a few of the peaks.

A second method of data acquisition would use the solid state counter as the energy channel device operating in conjunction with the NaI(Tℓ) annulus as a pair spectrometer. The detector system is illustrated in figure 3.2 and again with the entire spectrometer in figure 3.5. An event would be recorded following the coincidental detection of radiation in the main (energy) channel and a 511 keV annihilation quantum in each of two opposite NaI quadrants. The system, therefore, would behave as a triple coincidence, pair spectrometer. This mode of operation is suitable for energies above about 1500 keV where the cross section for pair production in the counter becomes reasonably significant. The spectrum shown in figure 3-7, also recorded during the preliminary study of source strengths, was obtained using the pair spectrometer illustrated in figure 3-5.

A comparison of figures 3.6 and 3.7 clearly illustrates the improved simplicity of the pair spectrum. Further, the signal to noise ratios in the pair spectrum are shown to be approximately 3 times

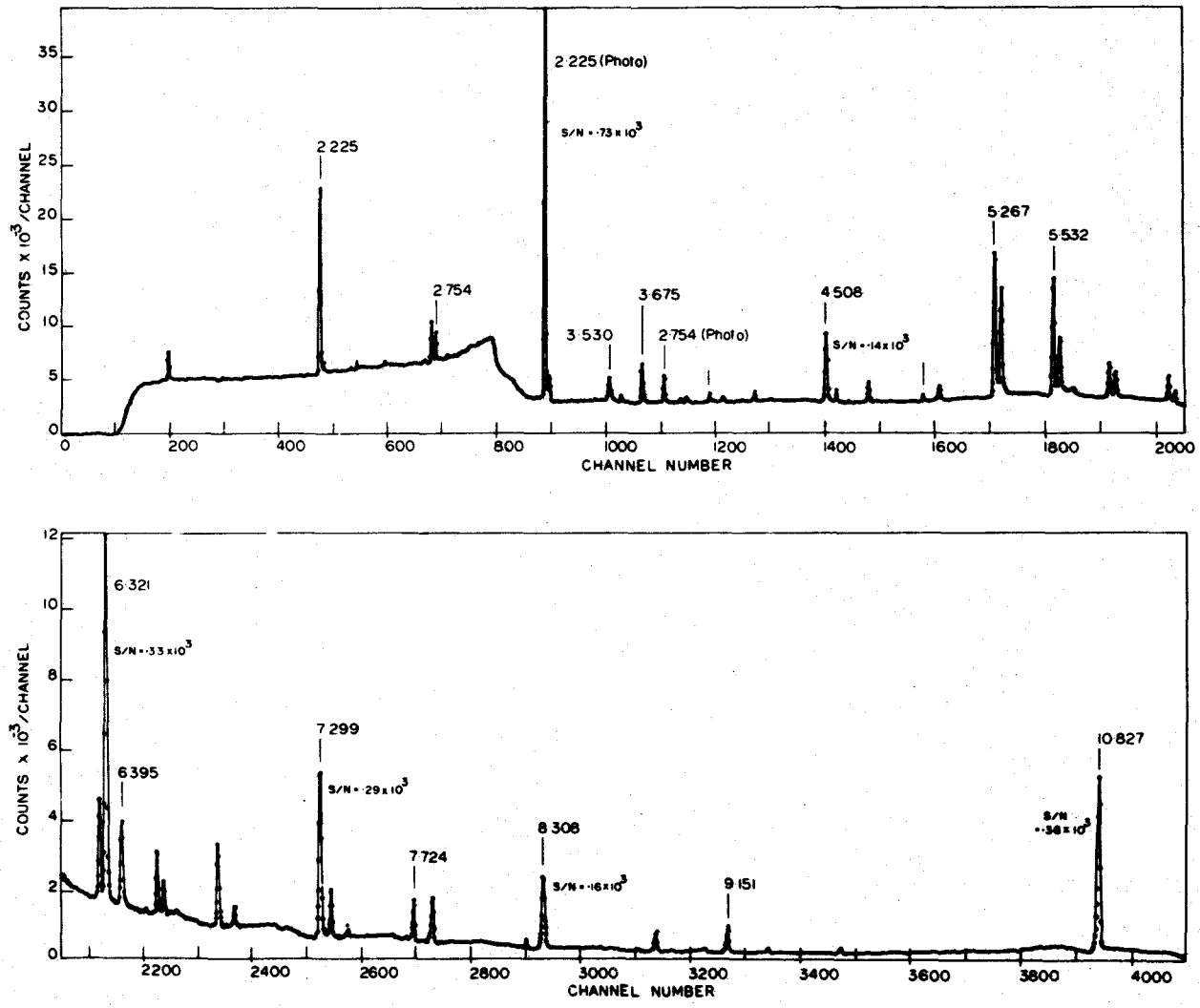

Figure 3-6: 4096-channel spectrum recorded using single parameter sampling

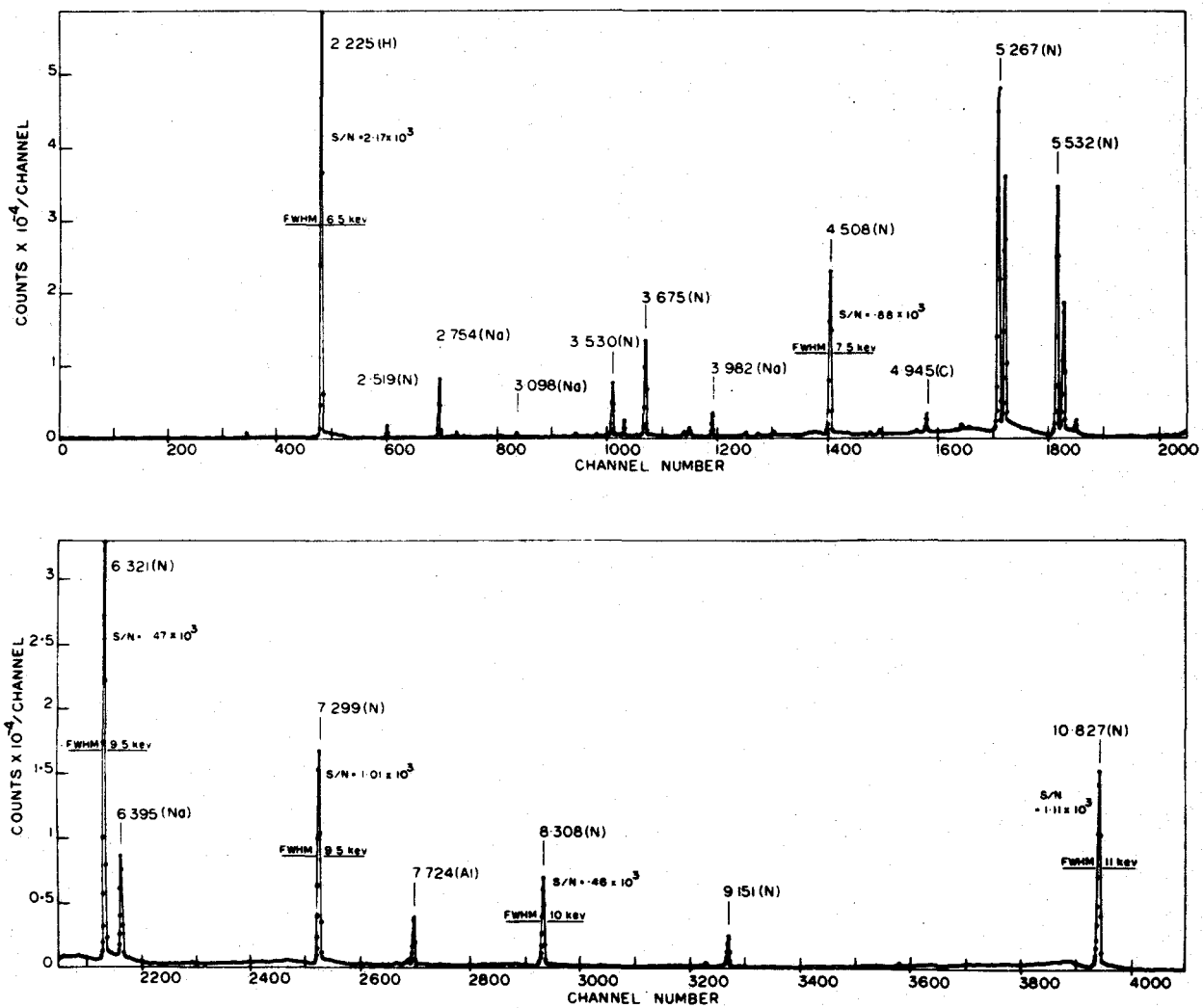

Figure 3-7: 4096-channel spectrum recorded using a triple coincidence, pair spectrometer (figure 3-5).

those obtained using single parameter sampling. Improved signal to noise ratios and greater spectral simplicity were sufficient evidence to conclude that the pair spectrometer would be the best instrument for the acquisition of data at energies above 1500 keV.

Since the accuracy of results would be of considerable importance in realizing the experimental purpose, detailed consideration was given to spectroscopic counting losses. Losses due to analyser dead time and random-summing effects were necessarily considered and a proposed method of direct compensation for these losses thoroughly evaluated. The need for stabilization to prevent the deterioration in energy resolution as a result of electronic gain shifts was established. Consider a substantial open beam pair count rate as being roughly 200 counts/s. This, in fact, was the rate proposed for the cross section measurement, as a result of the preliminary investigation. The corresponding singles rate N_s at the solid state counter would be about 10,000 counts/s. Immediate observations taken from these facts are:

(i) analyser dead-time effects, depending only on the lower pair rate, would be quite small,

(ii) random-summing effects, related to the much higher singles rate N_s, would probably be significant and,

(iii) counting times required to limit the statistical errors in observed pair-peak intensities to better than 1% would run into several days with the consequence that electronic instabilities, if left unregulated, would possibly be a factor adding to the uncertainty in results.

Once an event arrives and is accepted for pulse height analysis at the ADC input of the PHA, the input becomes electronically blocked

to any further events and it remains in this state until analysis and storage of the first event has been completed. Consequently, events arriving at the ADC during the analysis or storage cycle of a previous event will not be counted and are said to have found the analyser "dead". Clearly then, when calculating a peak intensity from its area, one must divide by the "live" time which is given by live time = (real time-dead time). Total analyser dead time depends on the rate of events arriving at the analyser as well as on the energy distribution of these events. The dependence on energy distribution follows from the fact that ADC cycle times are approximately proportional to the signal amplitudes.

The random sum rate can be described by the relationship

$$N_{RS} = 2\tau N_S^2 , \qquad 3.2$$

where N_s is the singles rate previously discussed and τ is the electronic resolving time. In simple terms, random-summing distortion occurs when two gamma-ray events are detected within a sufficiently short period of time that the following amplifiers are unable to identify them as being two different events. The energies deposited in the detector by the two photons are collected in the form of electronic charge and the resulting pulse is larger than that which either one of the events could singly produce. If the two events fall sufficiently close in time, the resulting signal, following amplification, will have an amplitude equal to the sum of the two possible amplitudes had the events been resolved. This situation has the most distinctive effect on the observed spectrum. Consider the simplified situation where a very active monoenergetic source is being analysed by a device

having a single-Gaussian response function. The resulting spectrum will not appear as a single peak corresponding to the source energy but will in fact appear as a Gaussian with a tail on its high energy side which extends out to an energy corresponding to twice the photon energy. At this point, a second much smaller peak appears. This is referred to as the random-sum peak and corresponds to the arrival of two photons in a time considerably shorter than the electronic resolving time. Under the ideal conditions of this proposed example, the correct peak intensity would be obtained by integrating over the entire spectrum. Matters are not so simple for more complex spectra under actual conditions of detector response and, clearly, the effects of random summing become increasingly difficult to determine with increasing complexity of the spectrum. A detailed examination of the problems relating to random-summing distortion has been given by Kennett et al[20]. The most significant effects of random summing, as related to the proposed cross section measurement, are the losses in peak intensity and the uncertainty in choice of integration limits arising from the peak distortion.

In a later discussion it will be shown that the best choice of target thickness for the cross section measurements will be such that positioning the target in the beam will reduce the intensity by a factor of approximately 13. According to equation 3.2, this would reduce the random-sum rate N_{Rs} by a factor of 13^2 thus reducing it to a level of near non-existence. Consequently, the ratio of no-absorber to absorber measured peak intensities R_o/R would appear low as would the resulting mass-attenuation coefficient according to equation 3.1.

The uncertainties in R_o/R as a result of random summing would be very difficult to estimate and, therefore, consideration was necessarily given to a technique whereby compensation for random-summing intensity losses could be directly obtained.

If a pulser event is introduced at the preamplifier input, the statistical probability of a random (source) event adding with a pulser event is identical to the probability of the addition of two random events. Consequently, the pulser spectrum if stored in a memory range isolated from that assigned to the source spectrum should reflect the same random-summing distortion and suffer the same peak intensity losses as the random spectrum. If one determines the areas S_o and P_o of the peaks associated with the random and pulser spectra respectively by using the same integration limits then, as a result of the cancellation of random-summing effects, the ratio S_o/P_o should reflect the corrected peak area. An investigation was undertaken to evaluate the effectiveness of such a technique (referred to in this study as the pulser technique).

Consider the situation where a nuclear-radiation spectrum is being observed, analysed, and recorded using a solid state detector and the spectrometer as illustrated in figure 3-8. The 1024-channel PHA featured a data ROUTE facility which was used to isolate the source spectrum from the pulser spectrum introduced at the preamplifier input. The control electronics, constructed primarily of logic electronic modules, functioned as follows. Upon completion of pulse-height analysis and storage of a source event, the change in state of the PHA BUSY NOT signal is detected by the Schmitt trigger and properly

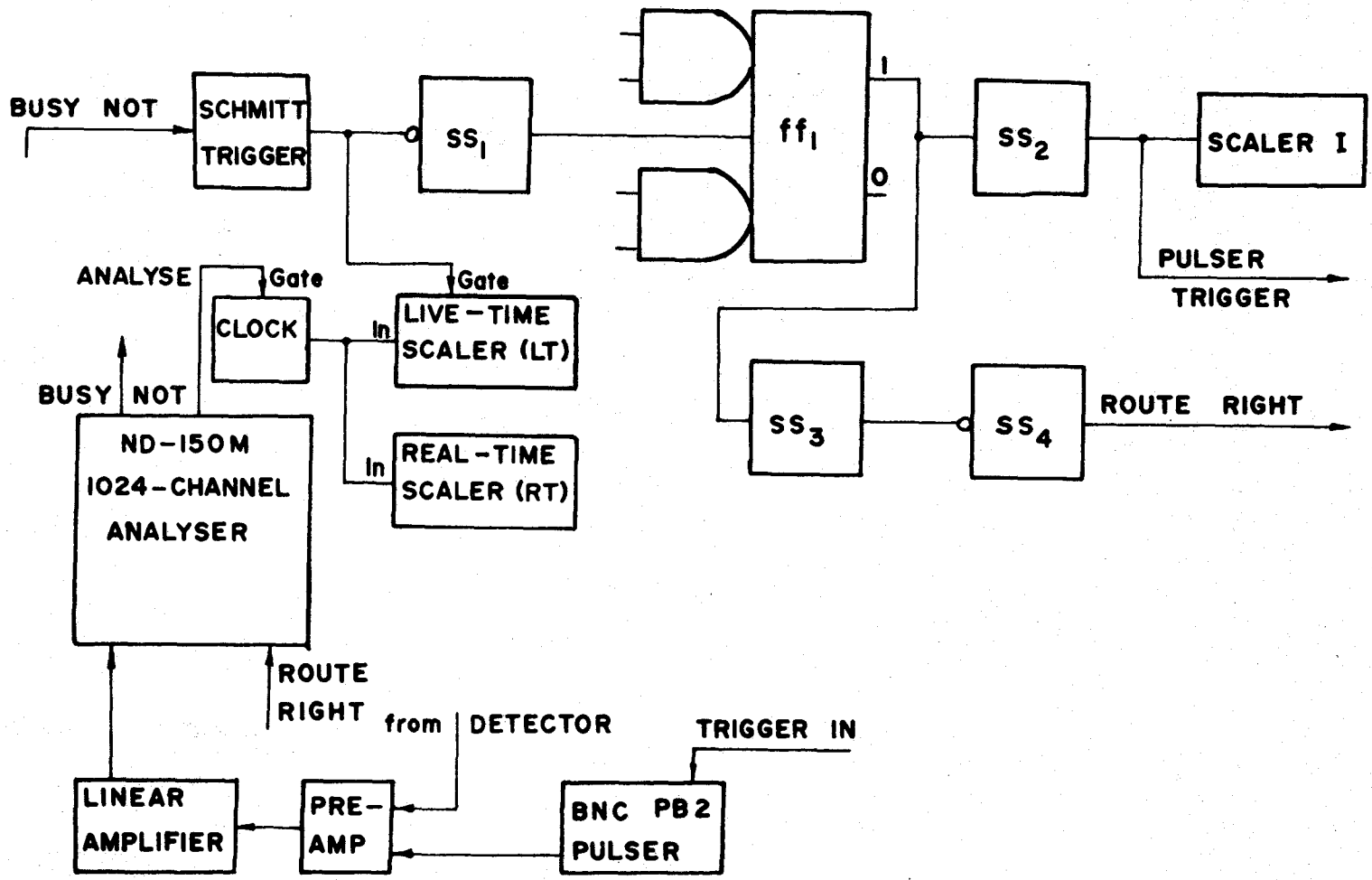

Figure 3-8: Electronic arrangement designed to compensate for random-summing losses. When the Schmitt trigger senses that the PHA has become free, a signal from the single-shot multivibrator SS_1 is used (following appropriate timing) to trigger the pulser and then to direct the analyser to route the generated event into a memory range isolated from that assigned to random events. The flip-flop ff_1 prevents two successive pulser signals, insuring that a generated event will follow a random event only.

timed pulser trigger and data ROUTE signals subsequently generated. The ensuing pulser event is then pulse-height analysed and stored in a second region of the memory. Following this storage cycle, the Schmitt trigger again responds to the change in the state of the BUSY NOT signal, however, this time the bistable multivibrator ff_1 prevents generation of the pulser trigger and ROUTE signals. Only after a random signal arrives for analysis does the sequence repeat itself. The purpose of the alternation between random and pulser events is to insure that the count I recorded by the INTEGRAL scaler represents the integrals of both the random and the pulser spectra. Also, under these conditions, the pulser event will always find the analyser free and, therefore, losses to the recorded pulser peak will in no way be the result of analyser dead times. Corrections for dead-time losses to the source spectra were determined externally by using the Schmitt trigger to inhibit a LIVE-TIME scaler during analyser busy periods. Both the LIVE-TIME (LT) and a REAL-TIME (RT) scalers were fed by a gateable clock which was allowed to operate only when the PHA was in the analyse mode. The resulting dead-time correction, with very little error, is given by $C_{DT} = LT/RT$. Evaluation of live time using an internal PHA facility was purposely avoided to prevent any complications associated with analyser dead times that would be experienced during storage of the live time information.

Having chosen the range of channels over which to integrate in order to determine the area S_o of a peak in the source spectrum, the corresponding pulser area P_o, obtained using identical integration limits, will be related to the random-sum correction term C_{Rs} by $C_{Rs} =$

I/P_o. Since I is the integral of the pulser spectrum, it can be written

$$I = P_o + rP_o + R_{RS}, \qquad 3.3$$

where R_{RS} is the random-sum contribution to the pulser spectrum (beyond the chosen peak integration limits) and r is that fraction of the pulser peak which under conditions of zero random adding falls beyond the chosen peak integration limits. The random-sum correction term may then be written

$$\begin{aligned} C_{RS} &= I/P_o \\ &= (1 + r) + R_{RS}/P_o. \end{aligned} \qquad 3.4$$

The value of r, dependent on the choice of integration limits, is easily determined by recording a pulser spectrum under conditions of zero random summing and then applying equation 3.3 with $R_{RS} = 0$. The corrected signal area S is given by

$$S = C_{DT}\, S_o I/P_o. \qquad 3.5$$

Since P_o is proportional to the total random input rate N_S and since R_{RS} is proportional to the random-sum rate $2\tau N_S^2$ then the term R_{RS}/P_o in C_{RS} can be expected to depend on N_S as well. A measurement of the mass-attenuation coefficient for 279 keV photons (^{203}Hg source) in lead using a narrow beam geometry served as a simple but effective method of determining the validity of this proposed pulser technique.

For any given absorber of thickness x, the observed peak intensity if properly corrected for random-summing and analyser dead-time

losses is given by

$$C_{DT}C_{RS}S_o = \varepsilon N_o e^{-x\mu/\rho} , \qquad 3.6$$

where N_o is the open beam intensity and ε the detector efficiency. For this same target thickness, the ratio R_{RS}/P_o is proportional to N_S which is given by $N_o e^{-x\mu/\rho}$. Consequently, if the correction factor for random-summing effects is adequate then both $C_{DT}C_{RS}S_o$ and R_{RS}/P_o should exhibit identical exponential dependencies on absorber thickness. Semilog plots of the mass-attenuation curve and the R_{RS}/P_o vs target thickness curve are illustrated in figure 3-9. Integration limits of $\pm$ 1.58 σ (where σ is the mean deviation associated with the shape of the peak under zero random-adding conditions) on either side of the mean peak positions were used to establish all points on both curves. Significant input rates reaching as high as 30,000 counts/s for absorber thicknesses of about 2g/cm^2 were experienced in the measurement. The slopes of the mass-attenuation and random-summing curves were found to be 0.442 $\pm$ .004 and 0.443 $\pm$ .002 cm^2/g respectively, their absolute deviation ($\sim$ 1%) being within experimental limits. Grodstein[21] had reported a mass-attenuation coefficient for 279 keV photons in lead of 0.440 cm^2/g. The fact that the corrected mass-attenuation curve continued to show its proper exponential dependence even at rates as high as 30,000 counts/s where random-summing effects were quite severe, clearly established the effectiveness of the pulser technique.

When a series of related intensity measurements are performed under conditions of widely varying signal and background strengths, flexibility in the choice of integration limits is frequently desirable

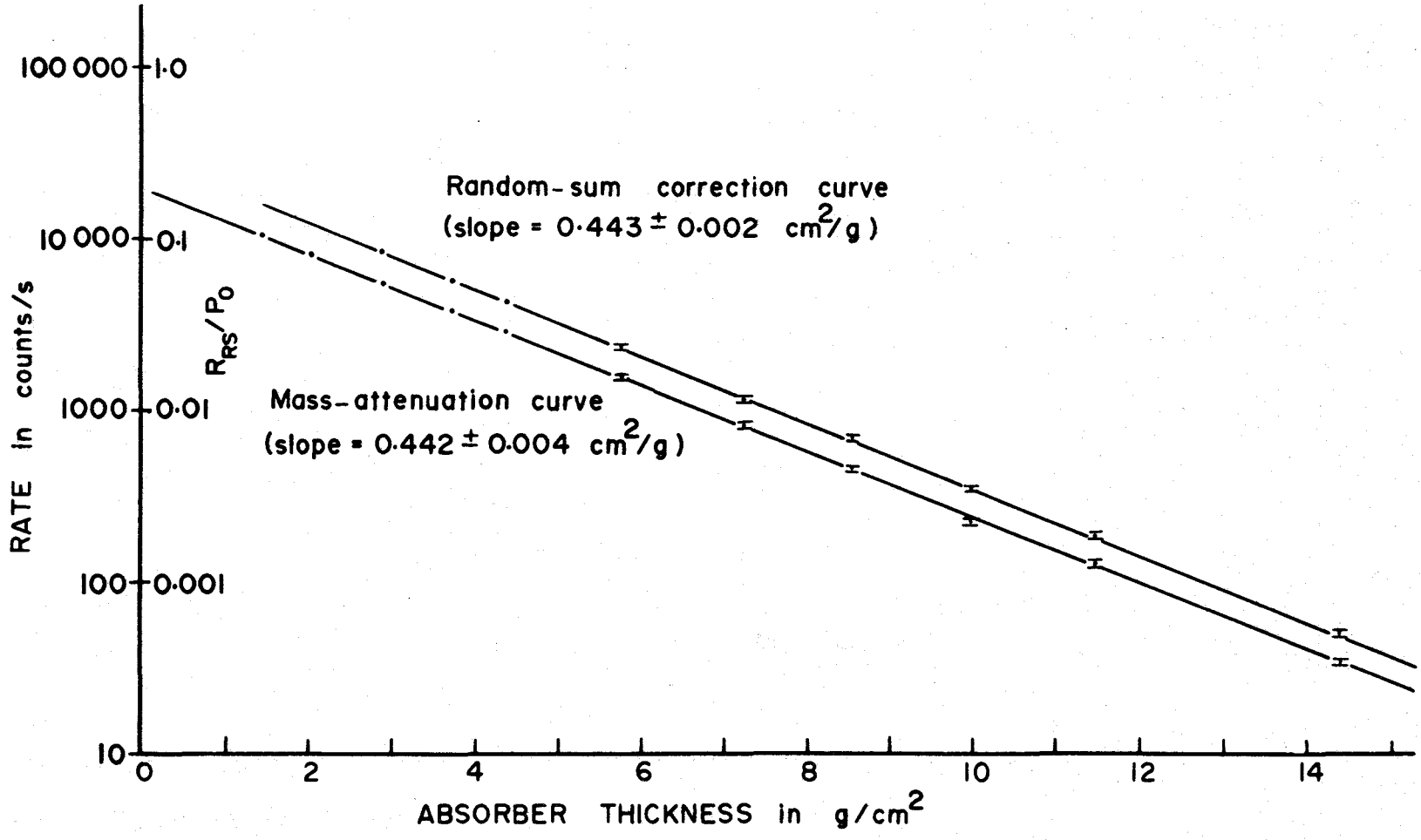

Figure 3-9: Semilog plots of the mass-attenuation and random-summing curves demonstrating the close agreement in their slopes. Analyser dead time for target thicknesses of about 2 g/cm^2 was approximately 80%, corresponding to an input rate of about 30,000 events/s. Random-summing effects are significant in this region and yet the corrected mass-attenuation curve continued to show its proper exponential dependence. Clearly, the pulser technique is effective in accounting for random summing effects.

in order that peak area to background ratios may be maximized for the individual measurements. An examination of the pair spectrum (figure 3-7), typical of spectra expected in the proposed cross section measurement, shows that precisely this situation exists from one peak to another. Since the pulser technique was expected to be used in the cross section measurement, it was decided to do a further evaluation as to the flexibility in choice of integration limits afforded by the technique. The ratio S_o/P_o, proportional to the peak intensity, was evaluated with the upper integration limit varied from zero to 6.38 σ above the respective peak centroids while the lower limit was varied from zero to 1.58 σ below the centroids where it was then held fixed. The S_o/P_o vs integration limits curve shown in figure 3-10 was obtained with an input rate of approximately 30,000 counts/s. It is apparent from the curve that for even the worst case where only a single channel was utilized the ratio S_o/P_o was within 2% of its stable value achieved for integration limits of $\pm\,\sigma$ and beyond. The results of this investigation clearly established that the pulser technique would afford the flexibility in choice of integration limits which would probably be required in the proposed cross section measurement.

Once the effectiveness of the pulser technique had been determined, the problem remained to implement the technique with the proposed cross section measurement. A low-frequency pulser signal would be mixed at the preamplifier input and stored in a corresponding energy region above that of the source spectrum. From equation 3.5 it is seen that the corrected intensity of a particular energy peak would be given by

$$R = (S/T_{LS})(I/T_R)/(P/T_{LP}), \qquad 3.7$$

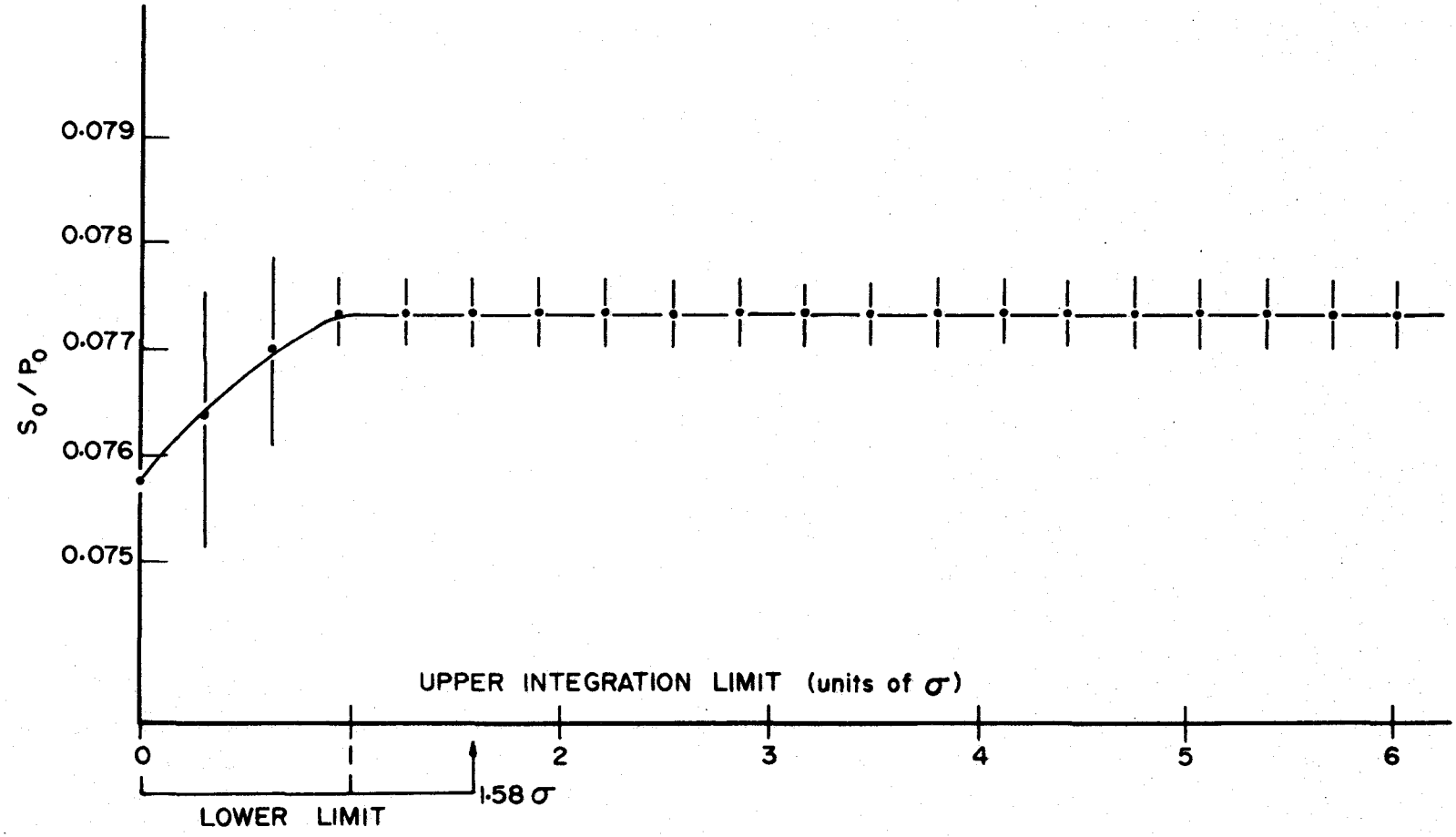

Figure 3-10: S_o/P_o vs integration limits. The excellent stability in the ratio S_o/P_o (which is proportional to the corrected peak intensity) for integration limits of $\pm \sigma$ or greater illustrates the flexibility in choice of integration limits afforded by the pulser method.

where S and P are signal and pulser areas respectively, determined by integrating the two peaks over similar limits. T_{LS} and T_{LP} are the live times experienced by the incoming source and pulser events respectively and I/T_R is the ratio of the number of pulser events to the real time (the pulser frequency). The difference between T_{LS} and T_{LP} lies in the fact that any pulser event arriving at the PHA can find the ADC busy only if a source event is being analysed, whereas, the ADC can be found busy by a random event because another source event or a pulser event is being processed. Since the pulser frequency would be kept low (approximately 8 pulses/s was planned) then $T_{LS} \simeq T_{LP}$ and therefore

$$R \simeq (S/P)I/T_R. \qquad 3.8$$

In this approximation, the dead-time losses relating to the two peaks cancel and the need for any further correction for dead time effects eliminated.

The mass-attenuation coefficient in units of cm^2/g is given by

$$\mu/\rho = \ell n(R_o/R)/x, \qquad 3.9$$

where R and R_o are the corrected intensities given by equation 3.8 for target and no-target measurements respectively and x is the target thickness in g/cm^2. The mass-attenuation coefficient using the pulser technique may then be written

$$\mu/\rho = \ell n[(S_o/P_o)/(S/P)]/x. \qquad 3.10$$

During multi-channel pulse height analysis, the range of the incident spectrum which may be analysed is determined by the ADC zero

level setting and by the electronic gain. The zero level determines the input signal amplitude corresponding to some energy in the spectrum which will be converted to the binary value zero and subsequently stored in the first available memory channel. The electronic gain then determines which energy in the spectrum corresponds to a 10 volt ADC input which is subsequently converted to the full scale binary number and stored in the last available memory channel. During extended periods, electronic gain has a tendency to drift resulting in a variation of the digital value assigned to a particular source energy. This appears in the observed spectrum as a deterioration in energy resolution and can to some degree affect the reliability of measured peak intensities.

In light of the expected pairs rate of approximately 200 counts/s, measurements could be expected to extend into several days thus the requirement for electronic stabilization. The principals involved in electronic stabilization are as follows. Once the zero level and gain have been set, they may be defined by a reference to two prominent source energies (or pulser energies). The stable conversion values (channel numbers) corresponding to these two reference amplitudes are determined and the electronic stabilizers set accordingly. Digital windows are set on either side of the two reference channels and during spectral analysis all counts falling inside the two windows are monitored and centroids continuously established for the two regions. The zero level and gain are continually adjusted by the stabilizers in an effort to keep the centroids positioned on their respective reference channels.

Reference signals would be obtained using the same precision pulser as planned for random summing and dead-time compensation. The

pulser would generate alternately a high and low amplitude signal. The high amplitude pulser signal would be used for gain reference (as well as for random-summing and dead-time compensation) and the low amplitude signal would be used for zero level reference.

(3) Target system:

The target holder and automatically operated pneumatic target-position changer designed for the cross section measurement is shown in figure 3-11. The arrangement required that the targets be solid rods screwed into the aluminium holder. Choice of target material depended primarily on the availability of elements which would provide a reasonable distribution across the atomic number scale. The control unit indicated in the diagram will be discussed in detail later in this chapter. The principal decision required concerning the target system and experimental optimization involved the choice of target thickness and the relative counting times for the target positioned in and out of the beam.

Using the pulser technique to account for random-summing and analyser dead-time losses, the mass-attenuation coefficient for a particular energy and target material was shown to be given by equation 3.10. S and S_o, the measured peak areas, will be obtained from the measured spectra by subtracting off their respective backgrounds B and B_o. Ignoring any error in P, P_o, and x, the statistical variance in the mass attenuation coefficient is given by

$$\sigma^2_{\mu/\rho} = [\partial(\mu/\rho)/\partial S_o]^2\sigma^2_{S_o} + [\partial(\mu/\rho)/\partial S]^2\sigma^2_S$$

$$= [(S_o+2B_o)/S_o^2 + (S+2B)/S^2]/x^2. \qquad 3.11$$

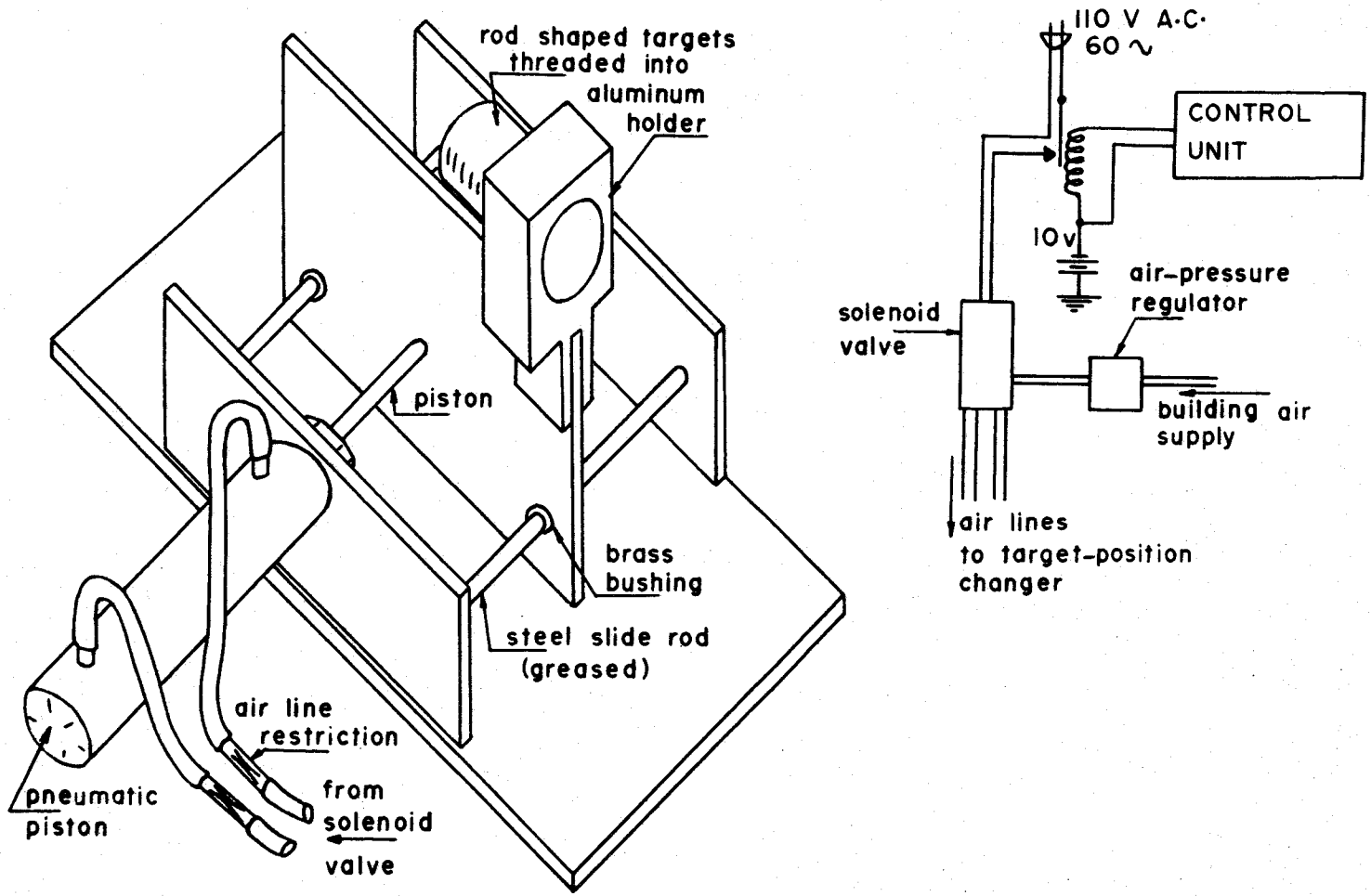

Figure 3-11: Pneumatic target-position changer. Building air supply was reduced to a pressure of approximately 15 psi. With this pressure and the restrictors placed in the lines, a smooth switching motion ($\sim$ 0.5 s) with a minimum shock to the apparatus was achieved.

Using the relationship

$$S = S_o e^{-ut}, \tag{3.12}$$

and the approximation

$$B = B_o e^{-ut}, \tag{3.13}$$

where u is the linear attenuation coefficient for the energy and target material being considered and t is the target thickness in cm, if $(1-\alpha)$ and α represents the fractions of the total counting time spent counting with the target positioned in and out of the beam respectively, then

$$\sigma^2_{\mu/\rho} = \text{CONSTANT} \times [1/\alpha + e^{ut}/(1-\alpha)]/t^2. \tag{3.14}$$

The validity of equation 3.13 relating B and B_o was later established by an examination of the measured backgrounds in target and no target spectra. Minimizing the variance through choice of α using the familiar formula

$$\partial\sigma^2_{\mu/\rho}/\partial\alpha \equiv 0 , \tag{3.15}$$

leads to the result

$$\alpha_o = 1/(1 + e^{ut/2}), \tag{3.16}$$

where α_o is the optimum value for the fraction of the total counting time that should be spent counting the open beam. Minimizing the variance through choice of target thickness t and substitution of α_o for α yields to the results

$$t_o = 2.56/u_o, \tag{3.17}$$

$$\alpha_o = 0.217, \qquad 3.18$$

and

$$(1-\alpha_o) = 0.783, \qquad 3.19$$

and consequently

$$(1-\alpha_o)/\alpha_o = 3.64. \qquad 3.20$$

Since a range of gamma-ray energies were to be studied in one measurement, the optimum target thickness t_o could not be chosen to satisfy all energies simultaneously. Therefore, consideration was given to the distribution and relative intensities of the gamma-ray energies in the spectrum in order to establish an energy region for which an optimum target thickness would prove most beneficial. The conclusion was reached that information on the relatively weak 9.151 MeV gamma ray should be enhanced since it would be particularly significant in bridging the gap between the much stronger 8.3 and 10.8 MeV results.

Equation 3.10, relating the cross section to the measured peak intensities is completely valid only in the limit of vanishingly small beam solid angles. This follows from the fact that equation 3.10 is based on the assumption that each time a photon interacts with and is scattered by a target centre, the secondary or scattered radiation is removed from the beam and cannot possibly be counted as a transmitted event. Since a finite count rate using infinitely small solid angles cannot be obtained in practice, a compromise must be reached whereby some leakage into the detector of scattered radiation is tolerated in order to establish a reasonably high count rate.

In the energy region being considered, two types of scattered events, inelastic (Compton) and elastic (Rayleigh), may reach the counter. Further, they may reach the counter as a result of one (single) scattering interaction or more than one (multiple) scattering interaction. In either case, because of the $\ln(R_o/R)$ dependence, the measured cross section will appear low since the effect of scattered radiation striking the counter is to make R appear too high. In the case of inelastic scattering, the scattered or secondary radiation is decreased in energy from the primary energy E_0 by an amount

$$\Delta E_1 = E_0 \left| 1 - \frac{1}{1 + E_0(1-\cos\theta_1)/mc^2} \right| , \qquad 3.21$$

where θ_1 is the scattering angle and mc^2 is the electron rest mass energy. This secondary radiation with energy $[E_0-\Delta E_1(E_0,\theta_1)]$ may undergo a second inelastic scattering at an angle θ_2 and again experience a degradation in energy given by equation 3.21 with E_0 replaced by the energy of the secondary radiation and θ_1 by θ_2. In general, for multiple scattering ΔE is given by $\Sigma\Delta E_i$. Therefore, if ΔE is of at least the same magnitude as the detector resolution then the scattered event is likely to fall at an energy below the peak integration limits and, therefore, if detected it will probably not be included in the measured peak intensity. An examination of the spectrum in figure 3-7 shows energy resolutions ranging from 6.5 keV at 2.225 MeV to 11 keV at 10.827 MeV. The results of the preliminary study previously discussed showed that a 200 count/s pair rate could be obtained with a 160g melamine + Na source mixture (in the aluminium holder shown in figure 3-3) using beam collimation as illustrated in

figure 3-2. An evaluation of the geometry shown in figure 3-2 revealed that photons scattered by the absorber in a forward direction into a cone of half-angle $\theta_o \lesssim 18$ min of arc may possibly reach the detector. Using equation 3.21, the degradation energies for 2.225 and 10.827 MeV photons single-scattered at an angle of 18 min are approximately 0.1 and 3 keV respectively, indicating that in the proposed cross section measurement collimation rather than energy discrimination would be used predominantly in limiting small angle scattering effects. Use of energy discrimination would be more applicable in the event of multiple scattering where ΔE can be larger for scattered radiation striking the detector; however, as a result of the relatively small probability of multiple-scattered radiation reaching the counter any effects on the measured cross sections would probably be negligible.

A liberal estimate of the effect of small angle scattering into the detector was calculated as follows. In the limit of zero scattering angle the differential incoherent scattering cross section independent of energy is given by

$$d\sigma_{(INCOH)} = Zr_o^2 \, d\Omega, \qquad 3.22$$

and under similar conditions the coherent cross section is given by

$$d\sigma_{(COH)} = Z^2 r_o^2 \, d\Omega, \qquad 3.23$$

where r_o is the classical electron radius (2.818×10^{-13} cm). Therefore, by assuming that these zero-angle values for the differential cross sections prevail over the angle θ_o, a liberal estimation of the

cross sections for Compton and Rayleigh scattering into the cone defined by θ_o may be given by

$$\sigma^{\theta_o}_{(INCOH)} = 2\pi r_o^2 Z \int_o^{\theta_o} \sin\theta \, d\theta = WZ, \qquad 3.24$$

and

$$\sigma^{\theta_o}_{(COH)} = WZ^2 \qquad 3.25$$

The RHS of equation 3.25 must be replaced by the total coherent cross section $\sigma(COH)$, at energies where $\sigma_{(COH)} \leq Z^2W$. This situation will not be experienced for the incoherent cross section at the energies proposed for the study. For $\theta_o \sim 18$ min, $W \sim 5 \times 10^{-6}$ and hence the conclusion that $\sigma^{\theta_o}_{(INCOH)}$ will be negligible for all Z and all energies to be studied. The most significant small-angle coherent scattering effects are indicated for high Z at energies where the total interaction cross section is minimal and where $WZ^2 = \sigma_{(COH)}$; that is, the energy region where the total coherent cross section would still have the significant value of WZ^2 and where it is assumed that its entire effect is contained inside the scattering angle θ_o. An evaluation of this last assumption can be made by considering the equation $\theta_c = \sin^{-1}(0.026\ Z^{1/3}\ mc^2/h\nu)$ where θ_c is the scattering angle inside of which it is expected that approximately 75% of Rayleigh scattering will occur. For Z = 92 and $h\nu$ = 5 MeV ($\sigma_{(COH)} \sim WZ^2 \sim 0.04$ b/atom), the approximation for $\sigma^{\theta_o}_{(COH)}$ would represent only about 0.2% of the total interaction cross section. The actual effect could be expected to be somewhat less since the corresponding value for θ_c is 1.3° whereas it was assumed that the entire coherent scattering effects were confined

to an angle of less than 0.3°.

Since the effects of single and multiple scattering into the detector are a function of target thickness they may be measured, if significant, by studying the effect of target thickness on measured intensities. The semilog, intensity vs target thickness plots for 2.2 and 10.8 MeV photons (figure 3-12) obtained during the previously discussed preliminary investigation show no departure from straight lines as the lead targets were increased in thickness from zero to 52.3 g/cm.

Satisfactory evidence was accumulated to conclude that for all target materials and energies to be studied in the cross section measurement any corrections associated with finite solid angles would be sufficiently insignificant that they could be safely ignored.

(4) Control Unit

Constructed of Digital Equipment Corporation, logic electronic modules, the control unit (figure 3-13) was designed primarily to coordinate the target position with data acceptance and storage and to activate a precision pulser used to establish a compensation factor for random-summing and dead-time losses and to provide electronic stabilization. Operation of the unit would be as follows. The output of the flip-flop ff_2 would serve the dual purpose of determining the target position, either in or out of the beam, and of providing a ROUTE signal during the counting time for one of the target positions. Consequently, the spectra associated with the different target positions would be stored in isolated memory groups. The relay driver fed by ff_2 would make or break a relay switch which in turn would control

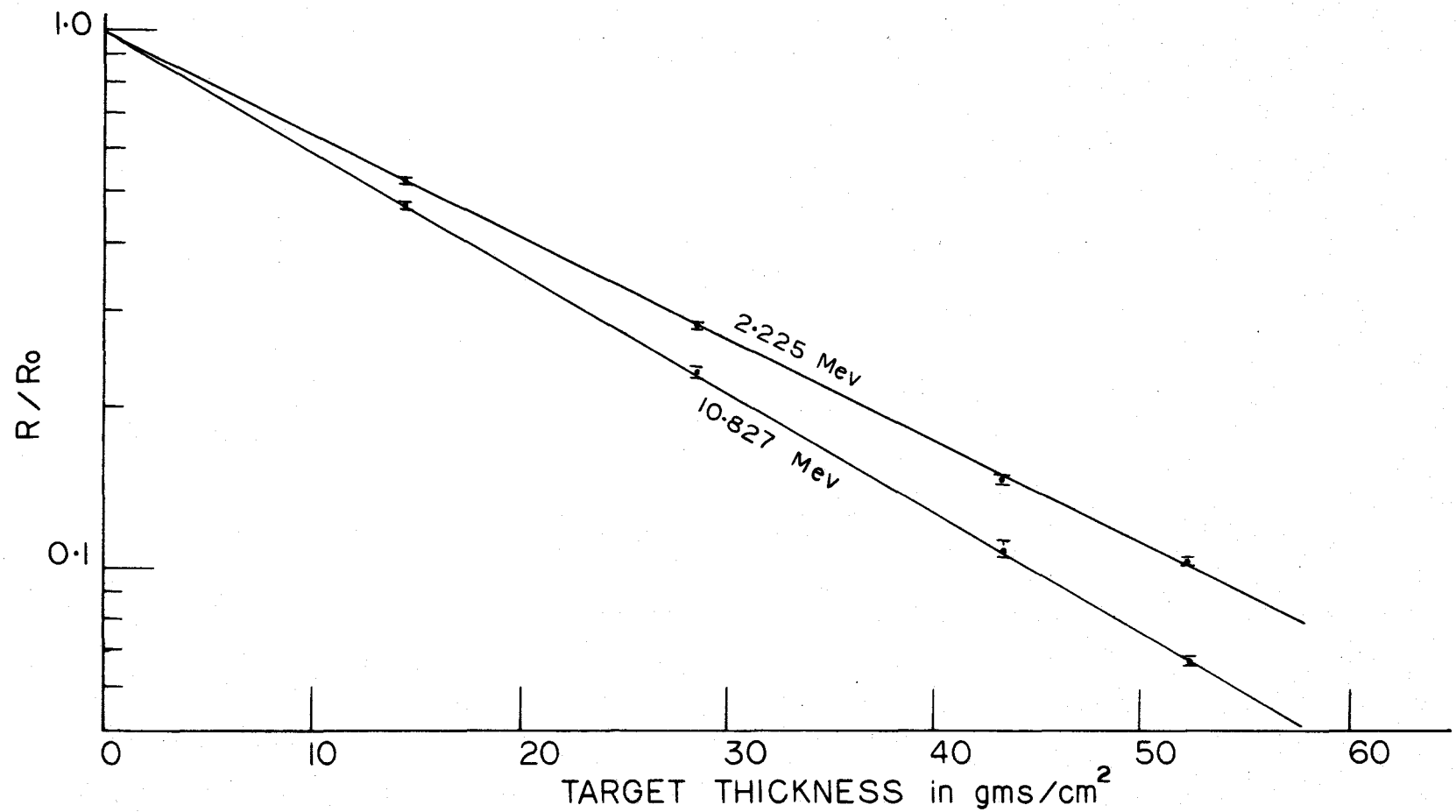

Figure 3-12: Results of a beam intensity vs target thickness study to determine the effect of radiation being scattered into the detector. R and R_0 are the peak intensities at 2.225 and 10.827 MeV measured with a Pb target in and out of the beam respectively. No departure from a straight line (semilog plot) is observed, indicating that the effect of small angle scattering into the detector was not significant.

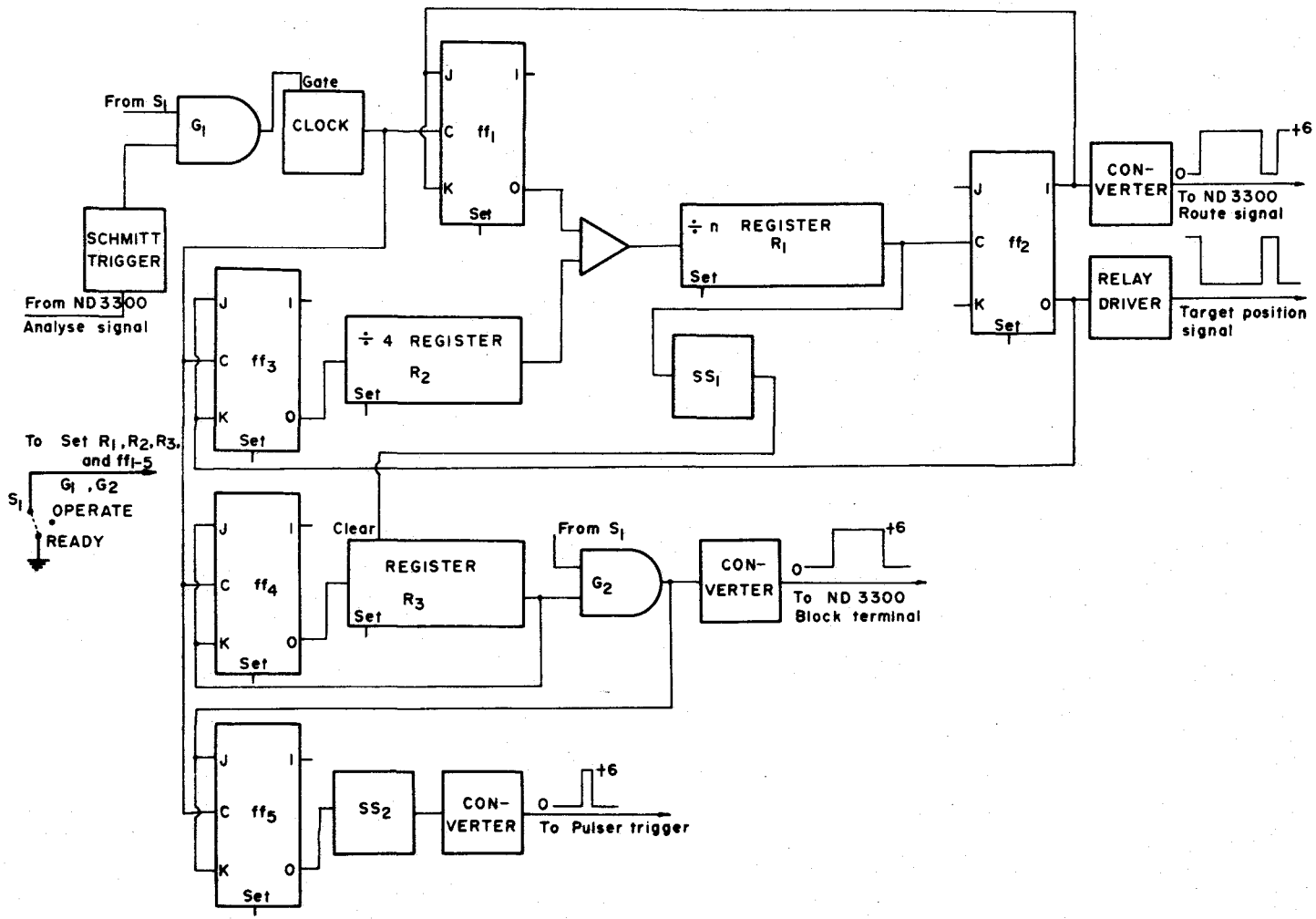

Figure 3-13: Control unit. The control unit functions primarily to determine the target position (in or out of the beam) and to correlate the acceptance and storage of intensity data with the target position. Also, it functions to trigger a precision pulser which is used for electronic stabilization and for determining random-summing and analyser dead-time losses.

the line voltage supply to a solenoid valve (figure 3-11) operating the pneumatic target-positioning piston.

During that part of the cycle when the target is positioned in the beam, the divide-by-four register R_2 will be in the circuit thus extending the counting time by a factor of 4. Proposed in-beam and out of beam counting times, determined by the size of register R_1 and the clock frequency, would be 8 min and 2 min respectively. During a target position change the memory cycle of the PHA would be inhibited by a BLOCK signal determined by the state of the most significant bit of register R_3. The period of this block signal ($\sim$ 2 sec) would be determined by the size of R_3 and the clock frequency.

In the READY position, switch S_1 will set the various registers so that a controlled start would be initiated by the switch to OPERATE. Switching the PHA to READOUT or DISPLAY will stop the clock, suspending all activity in the control unit thus avoiding any interference with the timing and positioning sequence during examination or extraction of stored data.

A final decision was taken to extend the cross section measurement down into the energy region of approximately 100 keV using β-decay gamma-ray sources. After a review of decay schemes, the decision was reached to use a combination ^{152}Eu and ^{64}Cu source which would yield 9 well distributed, relatively intense gamma-ray energies ranging from 121 to 1409 keV (table 3-2). The energies and intensities for ^{152}Eu were given by Dzhelepov[22]. During this measurement the through tube would be removed and the β-decay source inserted to a distance of approximately 6 feet into the external collimator as indicated in figure 3-2. Effects of any solid angle differences associated with

Table 3-2: Energies and relative intensities for gamma rays, suitable for the total cross section measurement, obtained following β-decay by the indicated isotopes.

Energy in keV (E_γ)	Relative Intensities (I_γ) per 100 decays		
	^{152}Eu	^{64}Cu	^{24}Na
121	60		
245	11		
344	29		
511		38	
779	12		
965	13		
1087	10		
1113	12		
1369			100
1409	20		
2754			100

the β-decay and (n,γ) source positions would be relatively insignificant since the through tube system was so tightly collimated to begin with. Reactor background would be reduced by placing a 12" bismuth block on the forward through tube support thus shielding the external collimator from the pool.

Besides the target thicknesses to be used for the high energy measurement, two additional thicknesses would be required to cover the energy region from 121 to 1409 keV, one for the 121-779 keV range and the other for the 344-1409 keV range. Overlap in these two sets of measurements would be useful in estimating the precision obtained in determining target thicknesses. In order to establish an overlap in results between the (n,γ) and β-decay source measurements, a reactor power shut down was planned following the high energy measurement so that the 1369 and 2754 keV gamma rays from the sodium component of the internal source could be studied using the medium thickness (344-1409 keV range) targets. The 2754 keV results, common to both the thick (high energy) and medium thick targets would be useful in further establishing the degree of precision obtained in determining target thicknesses. The 1369 keV ^{24}Na results could then be compared to the 1409 keV ^{152}Eu results in order to test for any apparent effects related to the different solid angles associated with the two source positions.

3.3 Measurement of the Total Cross Section

The general experimental arrangement illustrated in figure 3-2 was used in the measurement of the total gamma-ray cross section. The experimental geometry defined in figure 3-2, was such that any photon

scattered by the target in a direction of more than 18 min off the forward axial direction would be unlikely to strike the detector. Nine target elements, namely C, Al, Ti, Cu, Mo, Cd, W, Pb, and U were used in the study and in most cases, three different target thicknesses were required to cover the full 121 keV to 10.8 MeV energy region. Target thicknesses and the energy regions for which they were used are given in table 3-3. All measurements utilized the pulser technique of compensation for random-summing and analyser dead-time losses as well as electronic stabilization. For these purposes, use was made of the dual-amplitude precision pulser[23] discussed previously. The high amplitude pulser events used to establish P and P_o for random-summing and analyser dead-time compensation were recorded in the same 4096 channel memory group as their respective source spectra but in the upper channels region well above those assigned to the 10.8 MeV source gamma ray.

The automatic, pneumatic target-position changer shown in figure 3-11 used the building air supply reduced to about 15 psi. Air-line flow restrictors were used to insure a smooth position change, the resulting switching time obtained being approximately 0.5 sec. A 10 minute counting cycle was used, the target-in and target-out of the beam counting times being 8 minutes and 2 minutes respectively. During target position changes, data storage was inhibited by applying a BLOCK signal (of approximately 2 sec duration) at the PHA.

In order to effectively study the entire energy region from 121 keV to 10.8 MeV, four measurements were required on each of the nine target elements. Two types of photon sources, (n,γ) and β-decay,

Table 3-3

Target Thicknesses

Target thicknesses shown in column 1 were used in the high energy Na-Melamine study. Those in columns 2 and 3 were used in the lower energy ^{152}Eu and ^{64}Cu measurements. Column 2 targets were also used in the 1369 and 2754 keV measurement. An overlap in results obtained with the different target thicknesses and energy sources provided an evaluation of the precision in determining target thicknesses. Errors in target thicknesses are estimated to be approximately 0.5%.

Target Material	Target Thickness in g/cm^2		
Carbon	77.4	15.1	15.1
Aluminium	101.	38.4	15.5
Titanium	88.4	35.8	9.82
Copper	81.8	39.5	9.28
Molybdenum	80.5	36.4	3.18
Cadmium	69.4	37.5	2.05
Tungsten	55.8	28.8	1.08
Lead	52.3	23.0	.838
Uranium	49.7	23.5	.783

involving two different source positions were required to span the entire energy region. Further, three target thicknesses were required in order to facilitate efficient data accumulation. Considerable effort was taken in establishing an overlap of results obtained with the two source positions and three target thicknesses. Overlapping results would be used to obtain some estimate of the precision attained in measuring target thicknesses and to determine if the effects of the change in solid angles associated with the two source positions were significant. Three specific energy regions studied were the 121-779 keV, the 344-1409 keV, and the 1.779-10.8 MeV ranges using, respectively, the thin, medium, and thick targets listed in columns 3, 2, and 1 of table 3-3. The fourth measurement, taken on 1369 and 2754 keV gamma rays involved the medium target thicknesses. Experimental procedures and conditions for each of the 9 target elements studied in any one of the specific energy regions were essentially the same as a result of the similar influences on count rates held by any one column (table 3-3) of target thicknesses.

Details of specific procedures used in each of the four measurements follow:

(1) Photons with energies distributed from 1.779-10.8 MeV were generated by the ^{1}H, ^{12}C, ^{14}N, ^{23}Na, ^{27}Al (n,γ) reactions using the internal irradiation facility. Column 1, table 3-3 (thick) target thicknesses were studied.

160g of an NaF-melamine mixture (10g of NaF) contained in an aluminium holder as illustrated in figure 3-3 was positioned adjacent to the reactor core in a thermal neutron flux of approximately 5×10^{12} neutrons/

cm^2/sec. The triple coincidence, pair spectrometer illustrated in figure 3-5 was used to record the spectra associated with the two absorber positions. Energy resolutions obtained using the 25 cc, Ge(Li) solid-state detector ranged from approximately 6 keV at 1.779 MeV to 11 keV at 10.827 MeV. An open-beam, pair count rate of approximately 250 counts/sec was obtained. Spectroscopic counting time for each target element was approximately 100 hours. Approximately every 12 hours, accumulated data was transferred from the PHA memory onto magnetic tape. Reactor power charts were carefully monitored throughout each 12 hour counting period and recorded data discarded if any severe power fluctuations had been encountered.

(2) 1369 and 2754 keV gamma rays were obtained following β-activity from the sodium component of the internal source. Column 2, table 3-3 (medium) target thicknesses were studied.

Following completion of the high energy (1.779-10.8 MeV) measurement, advantage was taken of a 4-day reactor power shut down to study the 1369 and 2754 keV 15-hour activity following the β-decay of ^{24}Na. Single parameter sampling was used for data accumulation. Counting periods for the different target materials, initially about 5 hours, were gradually increased at a rate which would compensate for the decreased source activity (15-hour half life). Respective energy resolutions of approximately 6 and 6.5 keV were observed for the 1369 and 2754 keV gamma-ray energies.

(3) 344-1409 keV photons were studied following the β-decay of ^{152}Eu and ^{64}Cu sources positioned in the external collimator. Column 2, table 3-3 (medium) target thicknesses were used.

The through tube was removed and 30 mCi, ^{152}Eu and ^{64}Cu sources inserted into the external collimator to a distance of 6 feet as illustrated in figure 3-2. A 12" long x 6" diameter bismuth block was positioned on the forward through tube support in order to shield the detector from any reactor pool activity. Single parameter sampling was used and the counting time for each target was approximately 36 hours. The 12-hour ^{64}Cu activity was renewed at approximately 10-hour intervals. Observed energy resolutions ranged from approximately 4.5-5.0 keV.

(4) The 121-779 keV gamma rays from ^{152}Eu and ^{64}Cu were studied using column 3, table 3-3 (thin) target thicknesses.

Counting time for each of the target elements was approximately 30 hours, and energy resolutions ranged from 3.5-4.5 keV. Identical procedures to those used in measurement (3) were followed in this measurement.

3.4 Results on the Total Cross Section

The mass-attenuation coefficient [cm^2/g] for a particular photon energy and target material of thickness x [g/cm^2] was shown to be given by

$$\mu/\rho = \ln [(S_o/P_o)/(S/P)]/x \ . \qquad 3.26$$

In this form, compensation has been made for both dead-time and random-summing effects. It is of interest at this time to establish some estimate of the degree of influence these effects (particularly random-summing) would have had on the final result had they been ignored. As discussed earlier, equation 3.26 is an approximation taken from

$$\mu/\rho = \ell n\ [R_o/R]/x\ , \qquad 3.27$$

where R and R_o are the target and no-target peak intensities respectively. These intensities (consider R as example) were shown to be given by

$$R = (S/T_{LS})(I/T_R)/(P/T_{LP}), \qquad 3.28$$

where I/T_R is the pulser frequency and where the live times T_{LS} and T_{LP} are given by

$$T_{LS} = \text{Real time} - (T_{DS} + T_{DP}) \qquad 3.29$$

and

$$T_{LP} = \text{Real time} - T_{DS}. \qquad 3.30$$

T_{DS} and T_{DP} are the analyser dead times resulting from analysis of source events and pulser events respectively. Equations 3.29 and 3.30 state that a source event can find the analyser dead because another source event or a pulser event is being processed; however, the low frequency pulser events can only find the analyser dead when a source event is being analysed. Equation 3.26 follows from equations 3.27 and 3.28 with the assumption that $T_{LS} = T_{LP}$.

Consider the following experimentally observed conditions;

(i) $I/T_R \underset{\sim}{\sim} 8$ pulses/sec,

(ii) No-target (open-beam) pair rate $\underset{\sim}{\sim} 250$ counts/sec,

(iii) Target (closed-beam) pair rate $\underset{\sim}{\sim} 20$ counts/sec,

and consider the following details concerning the discharge-type ADC (Wilkinson[24]) used in the measurement;

(a) 10 Volts input corresponds to full scale conversion,

(b) Full scale conversion used = 4096 channels,

(c) Conversion clock frequency = 20 Mc,

(d) Set-up and storage time $\sim$ 10 μs and, therefore,

(e) Analysis time for an input pulse of amplitude V (volts) where $0 < V \leq 10$ volts is given by

$$T_{PHA}(V) \sim (V/10)(4096/20) + 10\ \mu s. \qquad 3.31$$

Using these facts, an estimate can be made of analyser dead times by assuming an average signal (random and pulser) amplitude of 5 Volts which corresponds to an event analysis time of approximately 110 μs. This would result in an open-beam ($\sim$ 260 counts/sec) dead time of approximately 3% as compared to a closed-beam ($\sim$ 30 events/sec) dead time of about 1/3%. Clearly, if dead time effects had been ignored, an error of approximately 3% would have resulted. Since the greatest dead-time losses in measured intensities would have occured with the open-beam condition, the resulting cross section would have appeared low.

The assumption $T_{LS} = T_{LP}$ can be evaluated by considering the maximum effects that would occur if the extreme values for analysis time were required. Suppose the maximum analysis time ($\sim$ 210 μs) is required for each pulser event while the analysis time T_{PHA} required for random events is $10 \leq T_{PHA} \leq 210$ μs. Using these extreme values for T_{PHA} in equations 3.29 and 3.30 it is seen that for both the open and closed-beam states $T_{LS}/T_{LP} \sim 1.002$. Therefore, for any peak intensity calculation the assumption that $T_{LS} = T_{LP}$ introduces an approximate error of only 0.2%. However, since the mass-attenuation

coefficient is obtained from the ratios of open and closed-beam intensities the error tends to cancel.

The random-summing effects experienced in a measurement can be approximated by considering the ratio

$$C_o/C = (I_o/1.03P_o)/(4I_o/P), \qquad 3.32$$

where C and C_o are the random-sum correction terms associated with the spectra obtained during the target and no-target states respectively and I_o is the number of pulser events (actually a measure of the real time) generated during the no-target beam analysis. The factors 4 and 1.03 in equation 3.32 account for the different counting times used and dead times experienced with the target in its two positions. Figure 3-14 displays the pulser spectra used to obtain P and P_o for the Pb-target study with the important difference that the no-target pulser spectrum has been normalized to its corresponding target spectrum using the factor 4 x 1.03 as discussed above. The random-sum contribution, resulting in a tail on the high energy side of the peak obtained with the higher open-beam rate is clearly evident from a comparison of the two spectra. Integration limits of $\pm$ 10 channels either side of the peak positions were used to determine P and P_o and substitution of these pulser areas into equation 3.32 showed the ratio C_o/C to be approximately 1.1 indicating that if random summing had been ignored, an error of approximately 10% would have resulted.

Statistical standard deviations in the measured mass-attenuation coefficients, given by

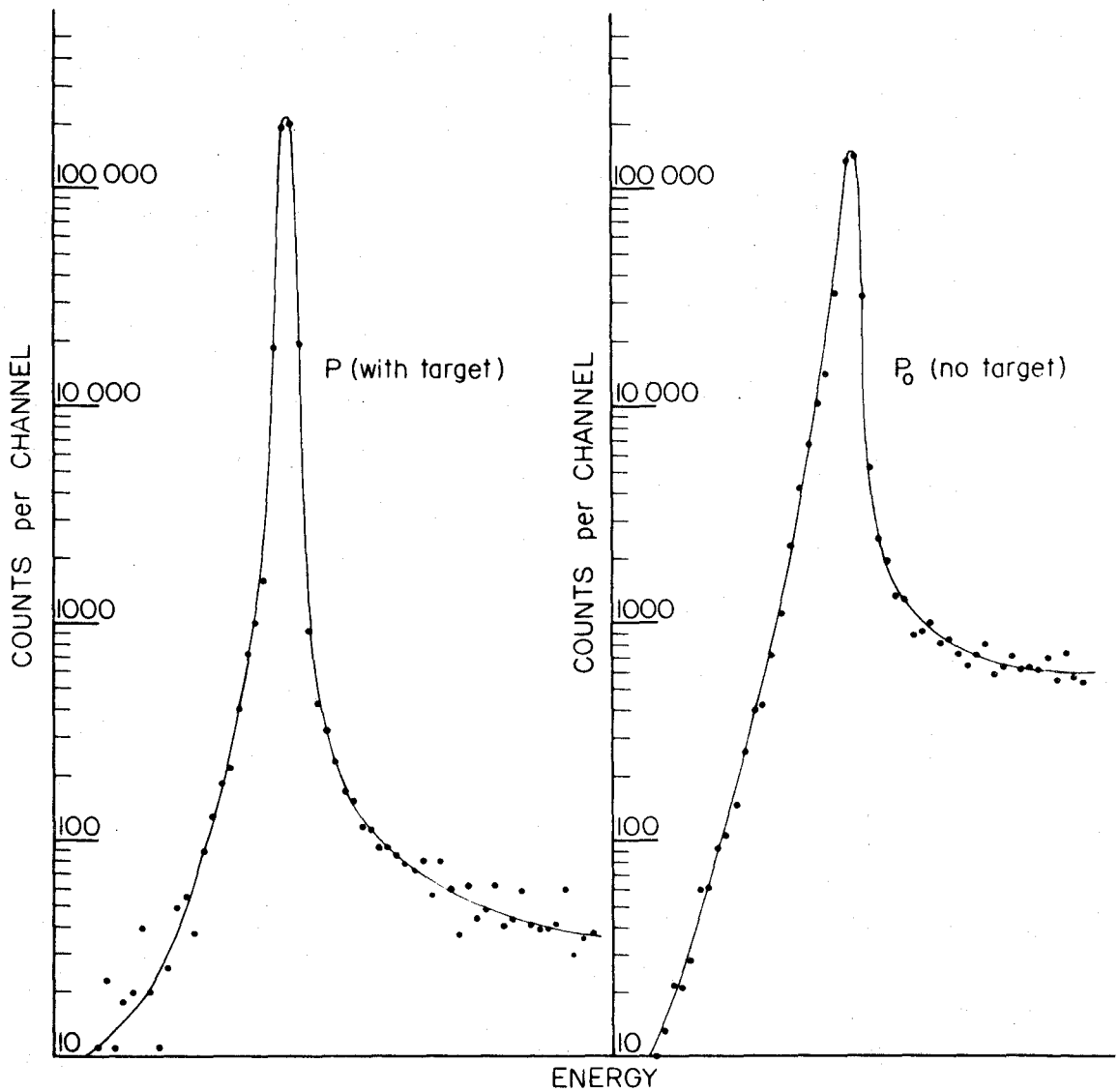

Figure 3-14: Pulser spectra observed with and without the Pb target positioned in the beam. The RHS pulser spectrum, obtained with the beam open, has been normalized to the closed-beam spectrum using the factor 4 x 1.03.

$$\sigma_{\mu/\rho} = [(S_o + 2B_o)/S_o^2 + (S + 2B)/S^2]^{1/2}/x, \qquad 3.33$$

were found in all cases to be less than 0.5% with an average deviation being approximately 0.1 - 0.2%. Error associated with the evaluation of target thicknesses x was estimated to be 0.5%. Consequently, considering these two sources of error, it was concluded that an error of 1% assigned to all measured coefficients would be reasonable and, if anything, would allow for a small margin of safety in most cases. Before reaching this conclusion, overlapping results obtained using the different target thicknesses and source positions were carefully examined. The purpose of this examination was to establish if, in fact, the solid-angle effects relating to the change in source position were insignificant and if the expected precision in target thickness evaluations had been realized.

Percent deviations in results obtained on the 2754 keV gamma ray for the thick and medium sized targets (table 3-3, columns 1 and 2 respectively) using the same source geometries (measurements (1) and (2), section 3.3) are shown in table 3-4. Since the expected statistical error, obtained from equation 3.33, for the 2754 keV results was approximately 0.2%, an examination of the observed deviations shown in table 3-4 indicates that the estimate of 0.5% error in the involved target thicknesses is at least reasonable, if not slightly high. Further, it is seen from the observed deviations (table 3-5) in the overlapping results obtained using the medium and thick target sizes (measurements (3) and (4)) that again the expected precision in target thickness evaluations has probably been achieved.

The cross section results obtained from measurement (3) using

Table 3-4: Percent deviations observed in cross section results obtained for 2754 keV photons (measurements (1) and (2)) using the thick and medium target sizes (table 3-3, columns 1 and 2 respectively).

Δ = 100 x [(1) - (2)]/(Average of (1) and (2)) percent

Target Element	Δ (percent)
Carbon	+1.1
Aluminium	+0.1
Titanium	+1.1
Copper	+0.6
Molybdenum	-0.3
Cadmium	+0.3
Tungsten	-0.1
Lead	+0.1
Uranium	-0.1

Table 3-5: Percent deviations observed in cross section results obtained from measurements (3) and (4) using medium and thin target sizes (table 3-3, columns 2 and 3 respectively). Note that only one carbon thickness was used for both measurements and that either the 344 keV or the 779 keV results were used for comparison depending on which offered the better statistics.

Δ = 100 x [(3) - (4)]/(Average of (3) and (4)) percent

	(Percent)	
Target Element	344 keV	779 keV
Carbon	---	---
Aluminium	-0.2	---
Titanium	0.0	---
Copper	+0.6	---
Molybdenum	-1.5	+0.7
Cadmium	+1.3	+1.0
Tungsten	---	-1.2
Lead	---	+1.0
Uranium	---	-0.8

the ^{152}Eu source and medium target thicknesses were used to obtain interpolated values for the 1369 keV cross sections. These interpolated values were then compared with the 1369 keV results obtained from measurement (2) using the ^{24}Na through tube source but the same medium target thicknesses. The resulting deviations, shown in table 3-6, clearly indicate that the change in solid angles associated with the two source positions had no significant effect on the measured cross sections.

Total cross sections for 29 well distributed energies from 121 keV to 10.8 MeV in 9 target materials ranging from carbon to uranium have been realized and in each case the experimental error has been assessed to be 1% or less. Measured results on the total cross section are shown in table 3-7.

Table 3-6: Percent deviations in interpolated 1369 keV cross section results obtained from measurement (3) using the ^{152}Eu source and those obtained from measurement (2) using the ^{24}Na through tube source. Both sets of results were taken using the medium thick targets (table 3-3, column 2).

Δ = 100 x [(2) - (3)]/(Average of (2) and (3)) percent

Target Element	Δ (Percent)
Carbon	-1.0
Aluminium	-0.8
Titanium	+1.0
Copper	-0.8
Molybdenum	0.0
Cadmium	+0.3
Tungsten	+1.0
Lead	-0.8
Uranium	+0.2

Table 3-7: Experimental Results for total photon cross sections in barns/atom. Estimated errors are less than 1%.

Energy (MeV)	Carbon	Aluminium	Titanium	Copper	Molybdenum	Cadmium	Tungsten	Lead	Uranium
.121	2.85	6.89	16.3	31.6	109.	169.	781.	1160.	1660.
.245	2.28	5.13	9.20	13.5	28.8	38.6	143.	211.	308.
.344	2.02	4.45	7.78	10.7	18.9	24.5	74.5	103.	146.
.511	1.72	3.75	6.43	8.70	13.7	16.8	40.5	53.5	74.0
.779	1.42	3.14	5.34	7.01	10.6	12.6	25.4	31.0	42.1
.965	1.30	2.83	4.81	6.33	9.44	11.2	20.6	25.0	32.8
1.087	1.20	2.65	4.53	5.95	8.93	10.5	18.8	22.7	29.2
1.113	1.20	2.59	4.49	5.88	8.82	10.3	18.1	22.0	27.9
1.369	1.06	2.34	4.07	5.29	8.00	9.15	16.1	18.5	23.5
1.409	1.07	2.33	3.97	5.23	7.96	9.00	15.4	18.4	23.0
1.779	.941	2.04	3.44	4.63	6.88	8.14	14.0	16.2	20.2
1.889	.930	1.99	3.35	4.52	6.68	7.71	13.7	16.1	19.6
2.225	.844	1.85	3.14	4.26	6.27	7.42	12.9	15.2	18.3
2.519	.781	1.75	2.96	4.05	6.02	7.03	12.6	14.5	17.8
2.754	.750	1.66	2.85	3.92	5.88	6.97	12.3	14.3	17.5
3.098	.695	1.57	2.70	3.76	5.72	6.94	12.2	14.3	17.4
3.530	.653	1.47	2.62	3.67	5.63	6.65	12.1	14.1	17.2
3.675	.639	1.44	2.61	3.59	5.57	6.59	12.2	14.2	17.2
3.982	.605	1.40	2.52	3.55	5.52	6.56	12.2	14.1	17.4
4.508	.572	1.33	2.45	3.43	5.50	6.62	12.2	14.3	17.3
4.945	.545	1.28	2.38	3.37	5.49	6.52	12.5	14.3	17.4
5.278	.530	1.26	2.35	3.34	5.49	6.60	12.4	14.6	17.7
5.542	.518	1.23	2.33	3.32	5.51	6.64	12.5	14.8	17.9

Table 3-7 (Continued)

Energy (MeV)	Carbon	Aluminium	Titanium	Copper	Molybdenum	Cadmium	Tungsten	Lead	Uranium
6.321	.483	1.17	2.29	3.27	5.52	6.71	12.8	15.1	18.3
7.299	.450	1.12	2.25	3.25	5.62	6.87	13.4	15.6	18.9
7.724	.442	1.11	2.25	3.27	5.62	6.81	13.5	15.9	19.2
8.308	.422	1.09	2.23	3.25	5.72	7.03	13.8	16.1	19.6
9.151	.402	1.07	2.21	3.28	5.85	7.25	14.3	16.7	20.2
10.827	.379	1.03	2.23	3.33	6.06	7.44	15.1	17.7	21.6

CHAPTER IV

A RELATIVE MEASUREMENT OF THE PAIR PRODUCTION CROSS SECTION

4.1 Introduction

Pair cross sections may be obtained indirectly from the total cross sections by subtracting the predicted values for all other effects contributing to the total. This technique, however, is limited to photon energies well above the pair production threshold where the pair cross section is at least competitive with the other contributing cross sections. In order to obtain significant results on the pair cross section in the energy region near threshold, direct measurement of the partial cross section is required.

The most familiar technique used in measuring partial pair cross sections is to observe the energy distributions of the created positron-electron pair. The pair cross section may then be obtained by integration over these energy distributions. Usually a thin target or radiator material is bombarded by photons with energies above the pair threshold and the resulting positron-electron pair, produced with forward momenta, are then subjected to a homogeneous magnetic field. The kinetic energies with which they were produced are then related to their radii of curvature in the magnetic field.

A second technique, and the one proposed for this present study, involves an intensity analysis of the radiation spectra following the annihilation of positrons created in the pair process. This method

will frequently be referred to as a direct measurement of the pair cross section (in contrast to using the total cross section to deduce the pair contribution) but clearly, the term direct is not completely correct since it is the annihilation rather than the creation process that is being observed. During the discussion of experimental planning and design, considerable effort will be given to resolving any differences in the results that would be obtained by studying these two different processes.

4.2 Experimental Planning and Design

The general experimental arrangement proposed for the relative pair cross section measurement is illustrated in figure 4-1. A collimated beam of photons with energies above the pair threshold is incident on a target positioned midway between two detectors. Following pair creation by a photon in the target and the subsequent annihilation of the created positron, the resulting pair of 511 keV quanta, each propagating in opposite directions, may strike, interact with, and deposit their respective energies in the two detectors. Thus, the simultaneous detection of 511 keV radiation in each of the two opposite detectors is interpreted as the occurence of a pair production interaction. A one to one correspondence between a pair event and a radiation pattern consisting of two oppositely directed 511 keV photons would be ideal; however, in reality every pair event does not lead to such a particular radiation pattern.

In almost all cases following pair production, the created positron is slowed to a near rest state prior to its annihilation with a free electron. The principles of energy and momentum conservation then

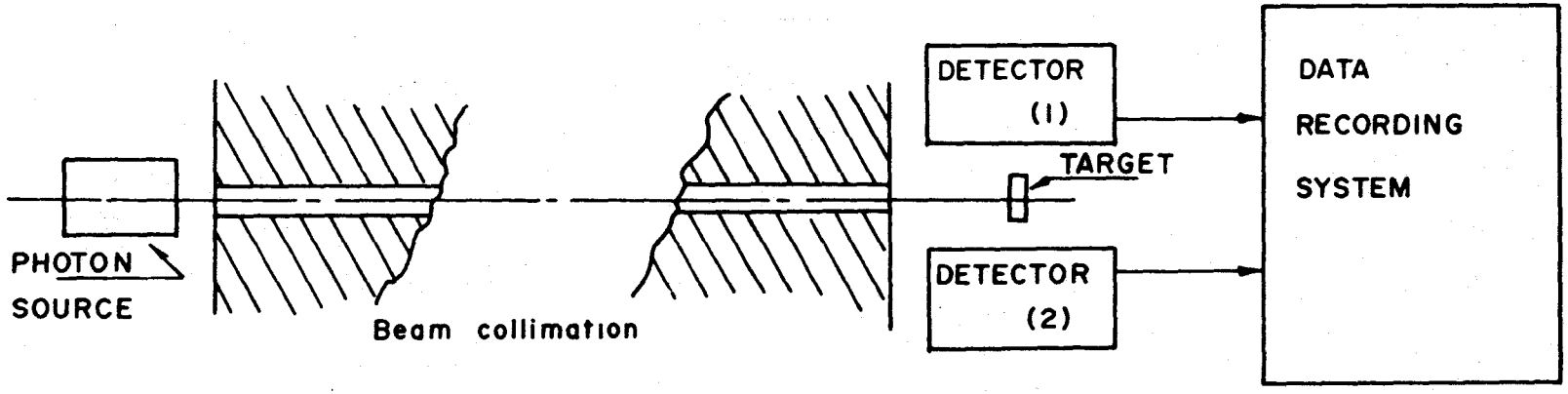

Figure 4-1: Basic experimental system suitable for a relative measurement of the partial pair cross section.

require that the annihilation radiation consist of two 511 keV photons propagated in opposite directions. Other possibilities for annihilation, however small, do exist and they relate primarily to the positron momentum at annihilation or to the actual degree of freedom experienced by the electron involved in the annihilation process. In the event of in-flight positron annihilation, the resulting radiation pattern must conserve the kinetic energy and momentum of the positron as well as the usual two units of electronic rest-mass energy. Consequently, the resulting pair of quanta may be expected to differ somewhat in energy from 511 keV. Further, they may be expected to propagate in somewhat different than opposite directions in order to conserve the positron's momentum. The probability of inflight annihilation, however, decreases rapidly with positron velocity[25] and the effect will not be a contributing factor considering typical detector resolutions and experimental solid angles. Single-quantum annihilation[26], although considerably less probable than the two-quanta type, may occur when the electron is bound to its atom since the atom can then take up the necessary momentum required for conservation purposes. This effect, although very small, increases with atomic number.

These effects, along with others concerning positron annihilation in the target will be further dealt with later in the discussion. As was the case for the total cross section measurement, details concerning planning of the partial pair cross section are best delt with by considering specific areas. From figure 4-1 it is seen that the general problem of experimental design can be divided into the areas concerning (1) the detector system and related electronics, (2) the target system, and (3) the photon source.

(1) Detector System and Related Electronics

The detector system chosen for the study was, in principle, similar to that used in the total cross section measurement. The NaI(Tℓ) annulus would again be used; however, the central solid-state detector would be replaced by the particular target material to be studied. In recollection, during the total cross section measurement an event was recorded when an incident photon with energy E_γ underwent a pair production interaction in the Ge(Li) counter providing that both 511 keV quanta following annihilation of the created positron managed to escape the detector and deposit their respective energies in each of two opposite NaI quadrants. When such a condition was met, a coincidence logic signal was generated and subsequently used to enable an ADC input gate permitting pulse height analysis of the $E_\gamma - 2mc^2$ main channel radiation. In the proposed partial pair cross section measurement, replacing the central detector with the target material eliminates any opportunity to observe the $E_\gamma - 2\ mc^2$ distribution. Instead, the monoenergetic annihilation spectra observed simultaneously in opposite NaI quadrants will be of central interest. In fact, all that is essentially required from the detector system is a measure of the rate of simultaneous detection of opposite quadrant 511 keV radiation relating to the pair production process. This suggests two possible methods of data accumulation using the NaI-annulus detector system. The first method would be to simply scale the coincidence logic signal generated when the proper conditions have been met. The second method would use the coincidence signals to gate a pair of ADC inputs permitting two-parameter pulse height analysis of the annihilation spectra associated with

opposite NaI channels. The coincidence rate for detection of the annihilation radiation would then be obtained through an intensity analysis of the recorded 511 keV peak.

The scaler technique, the simpler of the two possible methods proposed for data accumulation, would function as follows. Following linear amplification, the signals from two opposite NaI quadrants would be fed into separate single-channel pulse height analysers with energy-selection windows set to accept only those pulses corresponding to 511 keV annihilation radiation. The outputs of these two single-channel analysers would then be ANDed and the resulting coincidence logic signals, corresponding to the occurance of pair events in the target, scaled. Although simple in principle, this method does have some serious drawbacks which lead to uncertainties in the measured results. Variations in recorded rates caused by electronic gain shifts in the amplifier stages or by shifts in the width and (or) position of the single-channel analyser energy-selection windows cannot be measured simultaneously with the accumulation of data on the cross section. Although the cross section measurement can be frequently interrupted in order to test the selection window settings, some uncertainty will still remain as to the actual state of the system during the period in which the pair data was recorded. A similar problem involving the differentiation of recorded true and chance events arises using the scaler technique. In a later discussion, it will be seen that the chance or background contributions to the energy regions defined by the energy-selection windows are actually dependent on the energy distribution of the photon source as well as on the atomic number of the target being studied. Because of the complexity of the chance distribution,

different for each source and target combination to be studied, it would be of definite advantage to record the annihilation coincidence spectra so that a more positive approach to background evaluation could be taken. As a result of the uncertainties relating to selection windows and chance distributions, use of the scaler technique was abandoned in favour of the more sophisticated two-parameter spectral analysis method.

The two parameter, coincidence spectrometer proposed for the partial pair production cross section measurement is illustrated in figure 4-2. When the conditions, corresponding to a pair event in the target, are satisfied, the amplified X and Y-channel signals will be accepted at separate ADC inputs, pulse height analysed, and subsequently assigned the digital values E_i and E_j (i, j = 1, 2, 3, ---, 128) respectively, corresponding to the energies deposited in the detectors. The digital record held in memory location M_{ij} will then be incremented by 1. The spectrum, accumulated over some period of time, will define a two-dimensional 128 x 128 channel surface given by $M(E_i, E_j)dE_i dE_j$. The energy peak associated with the annihilation radiation will approximate a two-dimensional Gaussian characterized by its standard deviations σ_i and σ_j and its centroid $M(i_o, j_o)$.

(2) Target System

In reaching a final decision concerning size, shape, and composition of the targets, it was necessary to first examine the general experimental problem, the relationship between the pair cross section σ_{PAIR} and the experimentally observable 511 keV peak intensity R_p. Consider a collimated beam of I monoenergetic ($E_\gamma > 2\ mc^2$) photons

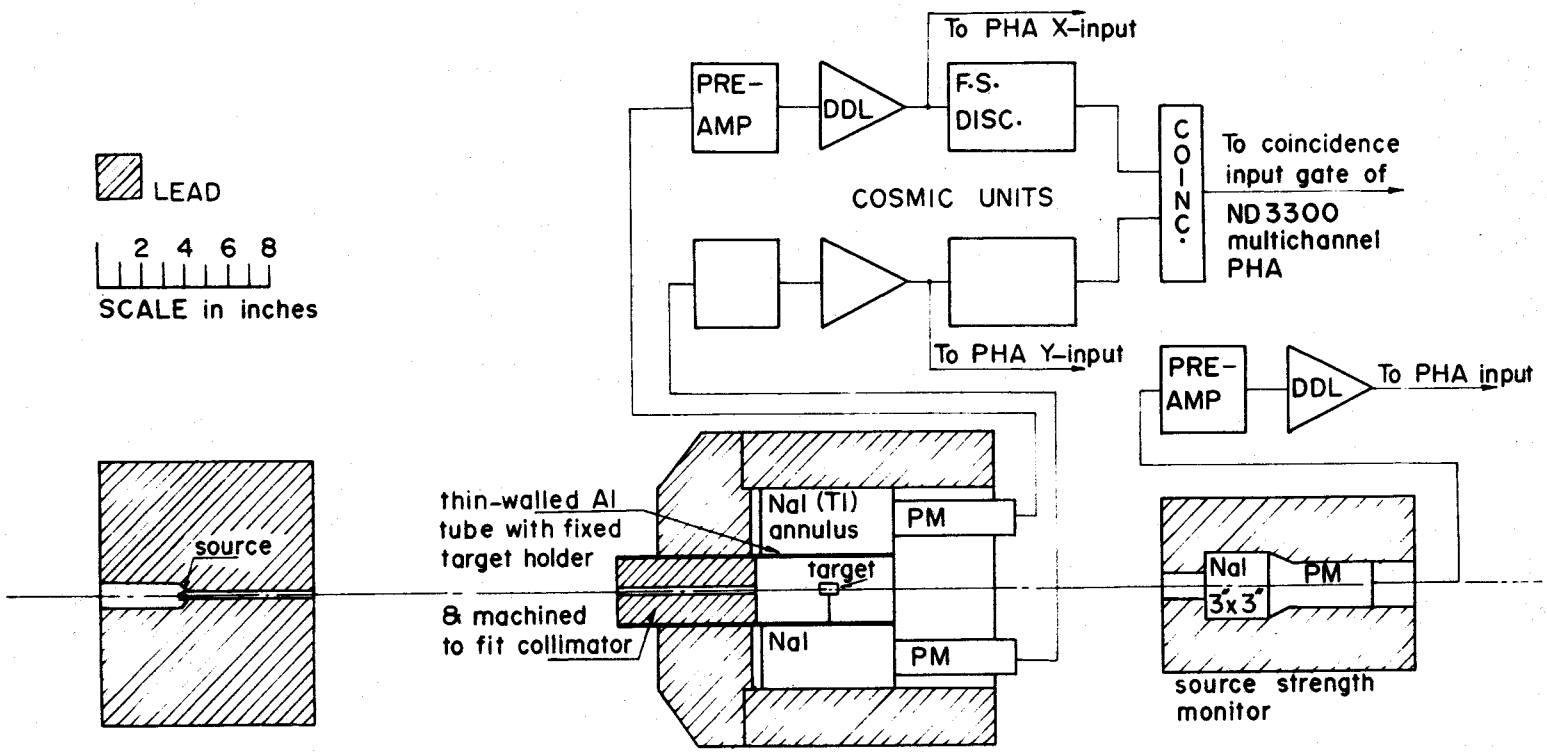

Figure 4-2: Experimental arrangement for the relative measurement of the pair production cross section. The annihilation radiation following pair production by source gamma rays in the target is observed using the two-parameter, coincidence spectrometer shown. Source and target collimation are sufficient to define a beam 1.2 cm in diameter. The beam was carefully centred on the 1.3 cm diameter target. The system, aligned on the axis defined by the reactor internal irradiation facility (Fig. 3-2), was shielded from any pool activity by a 12" shield position between the source holder (above) and the external, through tube collimator. The Pb was removed only for the 2.225 MeV gamma-ray study where the $^{1}H(n,\gamma)^{2}H$ reaction was used.

incident per second on a disc shaped target radially and longitudinally centred in the annulus and having a thickness X and a diameter just sufficiently large to fully intercept the beam. The general equation relating the 511 keV coincidence rate R_P to the pair cross section σ_{PAIR} will then be given by

$$R_P = I(1-e^{-\sigma_T X}) \frac{\sigma_{PAIR}}{\sigma_T} F \omega_1 \varepsilon_1 \omega_2 \varepsilon_2, \qquad 4.1$$

where σ_T is the total gamma-ray cross section for the particular energy and target material being considered. $(1-e^{-\sigma_T X})\ \sigma_{PAIR}/\sigma_T$ represents the fractional probability that a photon arriving at the target will undergo pair production in the target. ω_k and ε_k are respectively, the solid angles associated with the target and NaI detectors and the NaI efficiencies for 511 keV radiation emanating from the target. F represents the probability that a positron created in the pair process will annihilate in the target and the resulting radiation, consisting of a pair of 511 keV quanta, will subsequently escape the target. In general, the product $F\omega_1\varepsilon_1\omega_2\varepsilon_2$ represents the probability that the occurance of a pair production event will result in a recorded event contributing to the 511 keV coincidence peak. Clearly, this product has a strong and complicated dependence on the target material, the target size and density and on the overall geometry of the target-detector system. F must also account for the possibility that the pair production process will be followed by a type of positron annihilation other than that which results in a pair of oppositely directed 511 keV quanta. This introduces into the product weak depencences on the incident gamma-ray energy and on the atomic number of the target as expected from the earlier discussion of the annihilation processes. In

view of the presence of the (E_γ, Z) dependence in the product $F\omega_1\varepsilon_1\omega_2\varepsilon_2$ (equation 4.1), if relative pair cross sections were to be realized, the ultimate choice of target system would necessarily provide a means of determining or at least accounting for this product.

A familiar technique, used particularly in gamma-ray elastic scattering cross section measurements[27] involves a second measurement, in a sense simulating the first, in order to eliminate the effects of target-detector solid angles and detector efficiencies. In the actual measurement involving the pair production model, the two-parameter 511 keV peak intensity R_p is given by equation 4-1. Now suppose that the gamma-ray beam is shut off but that the target contains a small quantity of a uniformly distributed β^+ emitter. This will be frequently referred to as the β^+ model. Spectroscopic intensity analysis of the two-parameter annihilation radiation would then yield

$$R_{\beta^+} = AF'\omega_1'\varepsilon_1'\omega_2'\varepsilon_2' \ , \qquad 4.2$$

where A is the β^+-decay activity.

Using the assumption

$$F\omega_1\varepsilon_1\omega_2\varepsilon_2 = F'\omega_1'\varepsilon_1'\omega_2'\varepsilon_2' \ , \qquad 4.3$$

the ratio R_p/R_{β^+} is given by

$$R_p/R_{\beta^+} = (I/A)(1-e^{-\sigma_T X})\frac{\sigma_{PAIR}}{\sigma_T} \ . \qquad 4.4$$

Since the object of the measurement is the realization of relative pair cross sections $\sigma_{PAIR}(E_\gamma,Z)$ then clearly, relative values for I/A must be obtained. Values for the total photon cross section σ_T

required in equation 4-4 would be taken from the measured results on the total cross section given in Chapter III.

The validity of the assumption given by equation 4-3 was necessarily examined in detail in order that a degree of significance could be assigned with some certainty, to the results on the pair cross section obtained through application of equation 4-4. Consider first the pair production model mathematically described by equation 4-1. Monoenergetic source gamma rays with energy $E_\gamma > 2\ mc^2$ are incident at a rate of I photons/sec on a powder target with atomic number Z, right-circular cylindrically shaped and with a diameter Δd larger than that defined by the photon beam. At any point t along the axis of the target (relative to the source end of the target) the beam strength is given by Ie^{Ut} where $U(E_\gamma,Z)$ is the linear attenuation coefficient. Pair activity involving primary source gamma rays will, therefore, be exponentially biased toward the source end of the target and will be excluded from the target skin of thickness $\Delta d/2$ which extends in the radial direction beyond the beam dimensions. Following pair production, the positron created with an energy of approximately $(E_\gamma - 2\ mc^2)/2$ will probably be slowed to a rest or very near rest state prior to annihilation with an electron. According to theory[28], in-flight annihilation is limited to about a 2% effect and even then, it could be expected that part of this smaller effect would occur with sufficiently low positron energies that it would not be spectroscopically distinguishable from the far more pronounced 98% effect. Since the gamma energies proposed for the measurement are to extend from near threshold to the 2754 keV ^{24}Na energy one would expect the average initial positron energies to range from approximately zero to 900 keV. Following anni-

hilation, both 511 keV quanta must escape the target and simultaneously deposit their energies in opposite quadrant NaI detectors. Otherwise, no event will be recorded inside the energy dimensions of the recorded annihilation peak.

Now consider the β^+ model mathematically described by equation 4-2. A small quantity (say 1% by weight) of a β^+-emitter is unformly mixed with the same target powder as described in the pair model. The target is similarly positioned in the annulus but no external photon source is present. In this case, positrons are created uniformly throughout the target with a typical β^+-decay distribution of energies extending from zero to the end point energy E_o. Since the decision was made to use 12 hour ^{64}Cu as the β^+ emitter E_o is given by 660 keV. Again, in approximately 98% of the cases the positron would be slowed to rest prior to annihilation and the resulting gamma radiation subjected to nearly similar attenuation in the target as was experienced in the pair production model. The probability of in-flight annihilation, small in any event, would be similar with both models as would be the probability of the positron escaping the target prior to annihilation. Further, the probability of single-quantum annihilation with a bound electron would be similar with both models. Thus, with the application of equation 4-4 these effects, expected to be small, would further cancel.

Two rather significant differences do exist however. With the β^+ model, the annihilation centres would be uniformly distributed over the entire target volumes whereas, the pair model would feature the exponential distribution of centres as well as the skin effect as discussed earlier. Consequently, the 511 keV radiation associated with

the two models could experience somewhat different attenuation effects in the target as well as slightly different solid angle and NaI detector efficiency effects. In a following discussion, it will be shown using numerical integration techniques that for the proposed range of target materials and gamma-ray energies the use of the assumption given by equation 4-3 would lead to no more than a 1 1/2% effect in the measured results on the relative pair cross section.

At this stage, experimental planning and design of the relative pair measurement had developed as follows. Right-circular, cylindrically shaped targets with diameters approximately 1 mm larger than the beam dimension would be constructed from powders and would include a small quantity ($\sim$ 1% by weight) of uniformly distributed active copper additive. Caution would necessarily be taken to insure that all copper additives used with the different targets would be uniformly activated so that the 511 keV gamma ray activity given by A in equation 4.2 would be directly proportional to the weights of copper additives. Target materials would be best contained in thin walled capsules constructed of low Z material so that gamma ray interactions with the walls of these capsules would contribute as little as possible to the total effect. Thick side walls would have the tendency to attenuate the annihilation radiation (in both the pair and β^+ models) while the end walls, visible to the beam, would contribute to the pair production activity as well. The decision was reached to use lucite (primarily a hydrogen-carbon compound) capsules with 1 mm side and end walls which would be precision machined from available rod material. A 1.2 cm diameter photon beam would be carefully centred on 1.3 cm diameter targets as illustrated in figure 4-2. The encapsulated targets would be

held snugly in a second thin-walled lucite tube rigidly centred in a very thin-walled ($\sim$ 0.012") aluminium tube machined to fit the annulus. A lead collimator (figure 4-2) would be carefully machined to fit the aluminium tube so that the photon beam could be near perfectly aligned with the target. Since only a 0.5 mm margin of overlap between target and beam was planned considerable caution would be required.

In reaching some conclusions concerning choice of target thicknesses, the following conditions, apparent from equations 4-1 and the discussions concerning the pair production and β^+ models, were considered:

(i) the rate of pair activity in the target increases with target thickness,

(ii) the relative loss in rate resulting from created positrons escaping the target before annihilation decreases with target thickness,

(iii) the relative contribution to the measured pair rate resulting from interactions with the lucite end walls and the air column visible to the beam decreases with target thickness,

(iv) the probability of 511 keV annihilation quanta escaping the target decreases with target thickness,

(v) the beam intensity decreases exponentially with target thickness, consequently, the distribution of positron annihilation centres (511 keV radiation) is exponentially biased towards the source end of the target.

Any effects relating to conditions (ii) and (iv), however significant, tend to cancel when the ratio $R_p/R_{\beta+}$ is used to determine the cross section. Although the approximate effects of condition (iii) may be

calculated, the best approach would be to reduce them to a limit of insignificance. The most important conditions to be contended with are (i) and (v). Clearly, a substantial count rate is desirable; however, the targets must not be so thick that the asymmetries associated with the exponential distribution of 511 keV pair centres would produce severe effects. Excessively thick targets would result in the annulus detector system seeing significantly different 511 keV source distributions for different atomic number targets and different source energies. Further, and most important, the distribution seen in the case of the pair model would differ in varying degrees from that of the β^+ model thus tending to invalidate the assumption given by equation 4.3. The decision was taken to make all targets the same physical size and shape. Although the number of pairs created in the targets would decrease with decreasing atomic number, the losses due to attenuation of the annihilation radiation would also decrease, tending somewhat to maintain a reasonably constant count rate across the proposed atomic number range. The compromise reached on target size was that all targets would be approximately 2 cm in length and have a diameter of 1.3 cm. With this information, the validity of the assumption relating the two models may now be evaluated.

A mathematical evaluation of the effects relating to dissimilarities in the pair production and β^+ models was considered using numerical integration techniques which would be suitable for computer solution. The effects of model dissimilarities, associated with the distributions of annihilation centres, are most pronounced in the situation where low energy ($E_\gamma \gtrsim 2\ mc^2$) source gamma rays and high Z

target materials are being studied. Under these conditions, the exponential fall off of annihilation activity with target depth (pair model) is most severe. Further, the outer skin of the target (Δr = 0.5 mm), void of annihilation centres (pair model), offers most resistance to the escape of annihilation radiation when the target consists of high Z material. The numerical analysis was, therefore, directed at the situation where E_γ = 1120 keV (^{46}Sc source) and Z = 82 (Pb target) since this particular combination, proposed for the pair cross section measurement, would suffer the most significant effects associated with the model dissimilarities.

The numerical evaluation of the effects of model dissimilarities proceded as follows. The distributions of annihilation centres associated with the two models were first divided into discs of equal activity. Since the centres are uniformly distributed in the β^+ model, equal disc thicknesses $(\Delta z)_i$ are given simply by

$$(\Delta z)_i = 2\ell/M, \qquad 4.5$$

where 2ℓ (= 2 cm) is the target length and M is the number of discs or divisions. The decision was made to use M = 40; consequently, for the β^+ model the disc thicknesses were approximately 0.5 mm. In the pair production case, attenuation of the photon beam in the target required that the discs be chosen progressively thicker with beam penetration. The criterion for disc thickness is given by

$$e^{-\sigma_T \rho z_{i-1}}(1-e^{-\sigma_T (\Delta z)_i \rho})\frac{\sigma_{PAIR}}{\sigma_T} = \frac{1}{M}(1-e^{-2\ell\sigma_T\rho})\frac{\sigma_{PAIR}}{\sigma_T}, \qquad 4.6$$

and therefore

$$(\Delta z)_i = \ell n \left| \frac{Me^{-\sigma_T \rho z_{i-1}}}{Me^{-\sigma_T \rho z_{i-1}} - 1 + e^{-2\sigma_T \ell \rho}} \right| \Big/ \rho\sigma_T \,, \qquad 4.7$$

where z_{i-1} is the target thickness the beam must penetrate before encountering the i^{th} target disc, ρ is the target density in g/cm^2, and σ_T the mass-attenuation coefficient in cm^2/g. In both cases, the mean disc position $\overline{z_i}$ was determined using

$$\overline{z_i} = z_{i-1} + (\Delta z)_i/2. \qquad 4.8$$

Each disc was further divided into rings of equal activity, this being accomplished simply by choosing equal volume elements. Therefore, the outer radius of the j^{th} ring is given by

$$r_j^2 = jR^2/N, \qquad 4.9$$

where N (=12) is the number of rings chosen, R (=0.65 cm) is the target radius, and j = 1, 2, 3, ---, N_k (k = 1, 2 relates to the β^+ and pair models respectively) where N_1 and N_2 are the number of these rings, for the β^+ and pair models respectively, over which integration is to be carried out. Clearly then, for the β^+ model $N_1 = N = 12$. In order to account for the absence of annihilation activity in the outer region of the target not seen by the photon beam (pair model) a value of $N_2 = 10$ was chosen. Since this assumes that the activity in the pair model situation is contained in the first 10 rings while that of the β^+ model is distributed over all 12 rings, a normalization factor

$(0.65^2/0.60^2)$ must be applied to the calculated pair model results. If the effective volumes associated with the two models are to contain the same amount of activity then clearly, the pair model with its reduced (0.60 cm) effective radius must have a greater average density of annihilation centres. Thus, the above normalization factor. Mean radii $\overline{r_j}$ of the ring elements were chosen using

$$\overline{r_j}^2 = \frac{R^2}{N}\left(\frac{2j-1}{2}\right). \qquad 4.10$$

A target of length 2ℓ (=2 cm) and radius R (=0.65 cm) is centred inside of the annulus of length 2D (=15.2 cm) and inner radius A (=3.8 cm). The target is visualized as being divided into M (=40) discs of equal activity with mean positions L_i (measured from the source end of the target) limited to $0 < L_i < 2\ell$. Each disc is further divided into N (=12 for the β^+ model and 10 for the pair model) rings, again with equal activity, with mean radii a_j where $0 < a_j < R$ for the β^+ model and $0 < a_j < R - 0.5$ mm for the pair production model.

A coordinate system is then chosen so that the particular disc under consideration, with mean position L relative to the source end of the target, is centred as illustrated in figure 4-3 at the origin. Then, any point on the surface of the target is given by (R,z) when

$$-(\ell+L) < z < (\ell-L)\ , \qquad 4.11$$

and is given by (r, z_o) when

$$z_o = -(\ell+L) \qquad 4.12$$

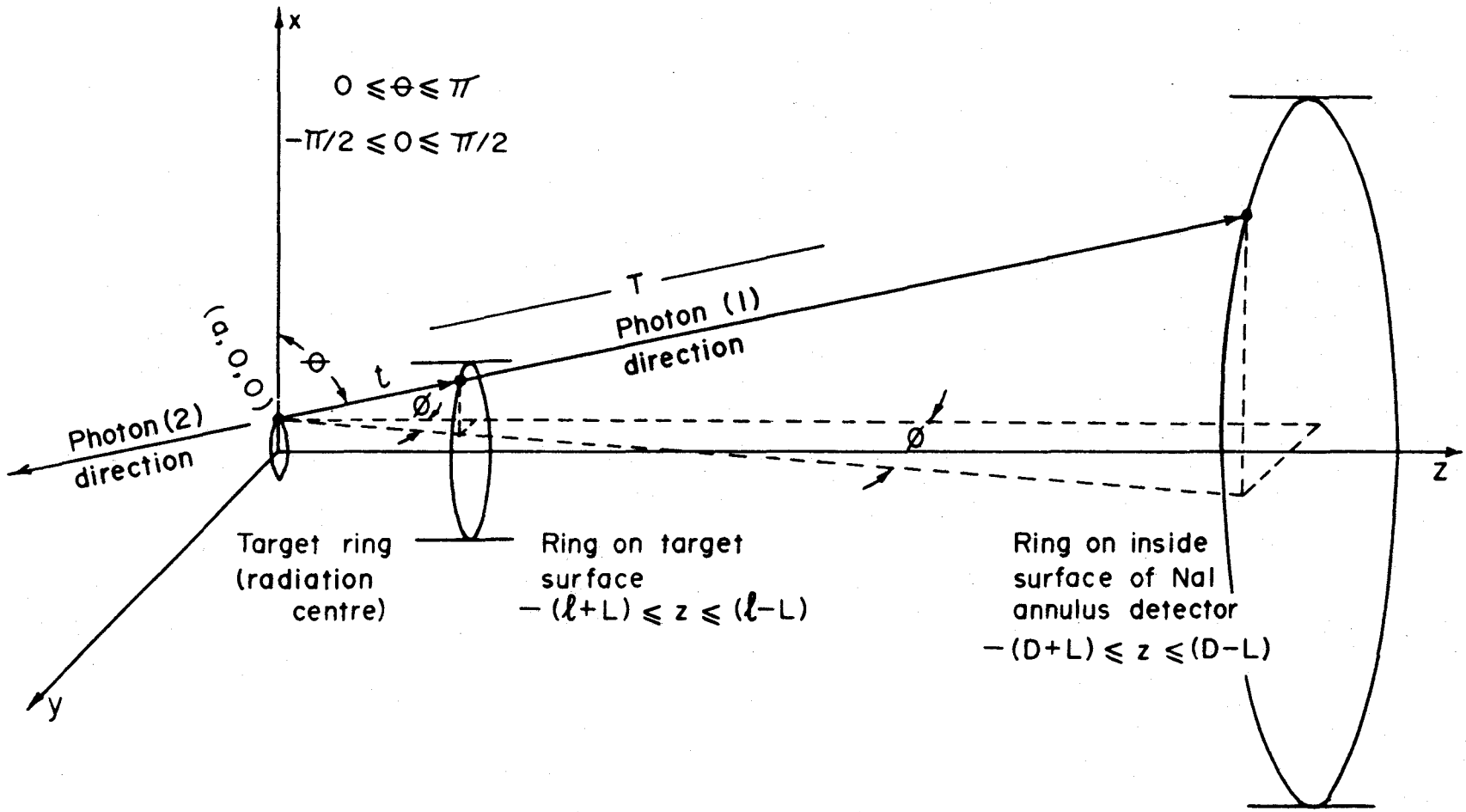

Figure 4-3: Geometrical problem associated with the numerical integration technique used to evaluate the similarities in the pair production and β^+ models.

or

$$z_o = (\ell - L) \ , \qquad 4.13$$

and where

$$r^2 = x^2 + y^2. \qquad 4.14$$

Similarly, any point on the inside surface of the annulus is given by (A,z) where

$$-(D+L) \leq z \leq (D-L) \qquad 4.15$$

Now consider one of the 511 keV annihilation quanta emanating from a point on one of the rings, with mean radius a, and belonging to the disc located at the origin. For convenience this point is chosen as (x = a, y = 0, z = 0). This photon (it will be referred to as the first of the pair) has a uniform probability of being propagated in all directions. Once its direction is established, however, the direction of the second photon is determined since it must propagate in the opposite direction. Since the two photons are indistinguishable, it is sufficient to limit the direction of the first photon to include only one-half of all space. The second photon will, accordingly, occupy the other hemisphere. Allowing the first photon to occupy all space would simply introduce a factor of 2 into the previous result.

Suppose the first photon is restricted to the directions (θ,ϕ) where

$$0 \leq \theta \leq \pi \ , \qquad 4.16$$

and

$$-\pi/2 \leq \phi \leq \pi/2, \qquad 4.17$$

where θ and ϕ are defined as illustrated in figure 4-3. With respect to figure 4-3, the first photon is able to occupy the hemisphere corresponding to positive z directions. Any point $P_1(x,y,z)$ in the path of this first photon with directions (θ,ϕ) is given by

$$x = z + t \cos \theta \ , \tag{4.18}$$

$$y = t \sin \theta \sin \phi, \tag{4.19}$$

and

$$z = t \sin \theta \cos \phi, \tag{4.20}$$

where t is the distance travelled by the photon from its formation at $(a,0,0)$ to the point $P_1(x,y,z)$. Consequently, the distance the first photon must travel (subject to 4.16 and 4.17) in order to escape the target is given by t_1 in the equation

$$R^2 = a^2 + t_1^2 (\cos^2\theta_1 + \sin^2\theta_1 \sin^2\phi_1) + 2at_1 \cos \theta_1, \tag{4.21}$$

where $z < (\ell-L)$. Otherwise, t_1 is determined from

$$z_1 = t_1 \sin \theta_1 \cos \phi_1, \tag{4.22}$$

with $z_1 = (\ell-L)$.

The distance travelled by the second photon is obtained using equation 4.21, when $-(\ell+L)<z_2$, replacing t_1, θ_1 and ϕ_1 with t_2, $\theta_2 = \theta_1 + \pi$ and $\phi_2 = \phi_1 + \pi$. When $z_2 = -(\ell+L)$, equation 4.22 is used with the appropriate substitutions to obtain t_2.

The integration procedures are carried out as follows. The disc is chosen, subject to the conditions of either equations 4.5 or 4.6,

and the z-axis transformed so that the disc is centred at the origin. A particular ring with mean radius a is then chosen and the annihilation radiation assumed to emanate from one point (a,0,0) on this ring. As a result of symmetry, integration around the ring would merely introduce a factor of 2π and could therefore be ignored. Once the origin of the annihilation quanta has been established, their directions given by (θ_1, ϕ_1) and $(\theta_2 = \theta_1+\pi, \phi_2 = \phi_1+\pi)$ are chosen with θ_1 and ϕ_1 being subject to the conditions given by equations 4.16 and 4.17. The equation

$$A^2 = a^2 + T_k^2 (\cos^2\theta_k + \sin^2\theta_k \sin^2\phi_k) + 2aT_k \cos\theta_k , \qquad 4.23$$

(where k = 1, 2 refers to the first and second annihilation quanta) is then used to solve for T_1, and T_2, the distances travelled by the two photons in striking the annulus with inside radius A but assumed to be infinite in length. T_1 and T_2 are then substituted into equation 4.22 using the appropriate angles in order to obtain z_1 and z_2 at the points of interception with the infinitely long annulus. If $z_1 \leq (\ell-L)$ and if $-(\ell+L) \leq z_2$, then both photons are directed so as to strike the finite, 15.2 cm annulus and a calculation of the probability of both photons escaping the target may then procede. Otherwise, either one or both of the photons would miss the detectors and a zero probability would result. Having established that θ_1, ϕ_1 and θ_2, ϕ_2 are such that both photons are directed toward the annulus, equation 4.21 is applied in order to establish t_1, and t_2, the distances that the two photons must travel in order to escape a target of radius R but assumed to be infinitely long. Again, substituting t_1, and t_2 in equation 4.22 yields

the values for z_1 and z_2 at the points of emergence from the infinitely long target. If $z_1 > (\ell-L)$, then the first photon emerges from the end face of the finite, 2 cm target and therefore equation 4.22 with $z_1 = (\ell-L)$ is used to obtain the correct value for t_1. If $z_1 < (\ell-L)$ then the value for t_1, already obtained from equation 4.21 is correct. A similar procedure is carried out for the second photon to determine whether equation 4.21 or 4.22 should be applied in obtaining a value for t_2. Once t_1 and t_2 have been correctly established, the probability of the pair of properly directed annihilation quanta escaping the target is given by

$$dP = e^{-\sigma_T \rho t_1} \, e^{-\sigma_T \rho t_2} \, d(\text{disc}) \, d(\text{ring}) \, d\theta \, d\phi. \qquad 4.24$$

The total probability, approximately proportional to $F\omega_1\omega_2\varepsilon_1\varepsilon_2$ or $F'\omega_1'\omega_2'\varepsilon_1'\varepsilon_2'$ depending on the model, is then obtained by integrating over all possible photon directions and target dimensions. The total probabilities for the two models are then used to determine the divergence of the ratio $F\omega_1\omega_2\varepsilon_1\varepsilon_2/F'\omega_1'\omega_2'\varepsilon_1'\varepsilon_2'$ from unity.

The results of the numerical investigation into the effects relating to the dissimilarities in the pair production and β^+ models involving 1120 keV gamma rays and a Pb target were as follows:

(i) The effects relating to the exponential distribution of annihilation centres in the pair model (as opposed to the uniform distribution in the β^+ model) were very small. This conclusion was reached by integrating both distributions over the entire target volume, thus ignoring any effects relating to the absence of annihilation centres in the outer region of the target (pair model).

(ii) When both effects were considered, the ratio was found to differ by 1 1/2% from unity, the pair result being lower, as expected, because of the absence of annihilation centres at the target surface.

Calculated results of the probabilities associated with each of the target discs are shown in figure 4-4. As expected, the results obtained using the uniform (β^+ model) distribution of target centres is symmetric about the target centre. The curve pertaining to the exponential distribution only (pair model, (i) above) is seen to differ only very slightly from that of the β^+ model. $F_1\omega_1\omega_2\varepsilon_1\varepsilon_2/F'_1\omega'_1\omega'_2\varepsilon'_1\varepsilon'_2$ was found, by integrating over all target discs, to be $38.6/38.8 \tilde{=} 0.995$ thus differing from unity by only 0.5%. The third curve obtained by considering both the exponential distribution and the "skin" effects ((ii) above) is seen to be consistently lower than that of the β^+ model with the integrated value for $F\omega_1\omega_2\varepsilon_1\varepsilon_2/F'\omega'_1\omega'_2\varepsilon'_1\varepsilon'_2$ being $38.2/38.8 \tilde{=} 0.985$. Since the effects of model dissimilarities for E_γ = 1120 keV and Z = 82 would be the most severe experienced in the cross section measurement, the conclusion was reached that using the assumption (equation 4.3) leading to equation 4.4 would introduce a maximum of 1 1/2% error in the measured cross sections. This error, relatively independent of the incident photon energy would, however, decrease rather rapidly with a decrease in target atomic number.

A final consideration concerning the target system involved the actual preparation of the powdered targets. The quantity of activated copper powder, not more than 1% (by weight) of the target material must

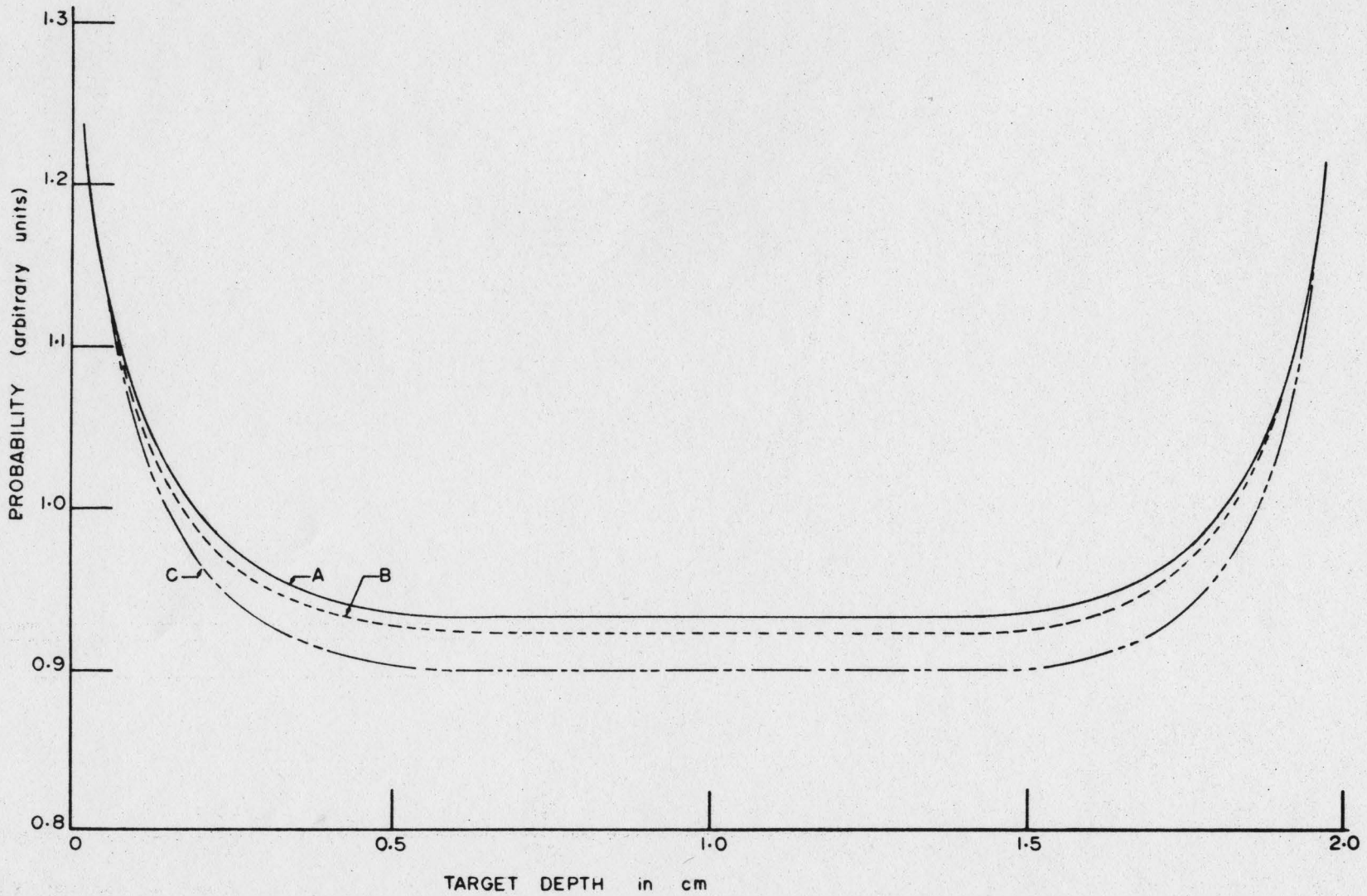

Figure 4-4: Results of the study into the similarities of the pair production and β^+ models for 1120 keV photons in a Pb target. $F_{\omega_1 \omega_2 \varepsilon_1 \varepsilon_2}$ for the particular model is proportional to the integral of its appropriate curve.
(A) β^+ model
(B) Pair production model considering only the exponential distribution source centres.
(C) Pair production model including the "skin effect" as well as (B).

be uniformly mixed with the target material. A step by step procedure proposed for target encapsulation is outlined in figure 4-5. Precaution would be necessarily taken to prevent any loss of target material or copper additive during encapsulation and to insure that a reasonably uniform distribution of copper additive would be realized. Further precaution would be taken to insure that the powders would be sufficiently packed since any shifting of material during the pair measurement would have the effect of changing the target density and, consequently, the effective target thickness.

Following encapsulation, the β^+ activity would be counted in the annulus, in the proposed experimental geometry, with the target capsule sitting at various degrees of rotation in its holder. These measurements would then be repeated with the target direction reversed. The results of such measurements would be used to estimate the degree of uniformity accomplished in distributing the copper additive throughout the target material.

(3) Photon Source

Alignment of the experimental system, illustrated in figure 4-2, on the axis defined by the reactor internal irradiation facility (Chapter III) would allow for a choice in methods of generating the photon beam. Gamma rays following β-decay of radioactive isotopes positioned as indicated in figure 4-2 or gamma rays generated in the $X(n,\gamma)Y$ reaction using the internal irradiation facility could be used in the pair cross section study. Sources proposed for the measurement are given in table 4-1 along with information concerning gamma-ray energies, relative intensities, and source half lives.

Table 4-1: Gamma-ray sources proposed for the relative pair cross section measurement. Table includes information concerning gamma ray energies, relative intensities, and source half lives.

Energy in MeV (E_γ)	Source	Half Life ($T_{1/2}$)	No. gamma rays/ Interaction (I_γ)
1.120	^{46}Sc	84 days	100
1.172	^{60}Co	5.3 years	100
1.333			100
1.369	^{24}Na	15 hours	100
2.754			100
1.560	^{142}Pr	19 hours	
2.225	$^{1}H(n,\gamma)^{2}H$	---	100

Since the reactor produced β-decay sources were to have substantial activities ($\sim$ 20-30 mCi), the decision was taken to leave the sources in their aluminium irradiation cans in order to minimize handling requirements. A thin-walled quartz holder in which the source materials would be sealed, was designed to insure that the sources would remain well centred in their irradiation cans. The irradiation can would then fit snugly into the lead collimator and source holder illustrated in figure 4-2. During the measurement, the source, once positioned, would not be touched until all target materials had been studied.

From experience, it was known that a small amount of 15 hour ^{24}Na contamination from the irradiation can could be expected as well as the 2.6 hour ^{31}Si activity from the quartz holder. An examination of the half lives provided in table 4-1 indicates that in each case a sufficient waiting period could be taken following irradiation in order to eliminate the silicon component. However, in the case of the 19 hour ^{142}Pr, correction for the ^{24}Na contamination would be necessary.

Since the proposed measurement was to yield relative cross sections, then according to equation 4.4 it would be necessary to determine the relative strengths of the proposed gamma-ray sources. For this purpose, a 3" x 3" NaI detector would be positioned on the beam axis as indicated in figure 4-2. An evaluation of the photo-efficiencies offered by this detector to the proposed gamma-ray energies ($1120 \leq E_\gamma \leq 2754$ keV) was, therefore, required. An examination of the literature (for instance reference 29) concerning scintillation detector efficiencies in the energy region from 1100-2754 keV led to the conclusion that

$$\log \varepsilon = \log(\text{Constant}) + n \log E \qquad 4.24$$

was an appropriate expression for the efficiency ε as a function of photon energy. The contribution to the full energy peak as a result of pair production in the counter (followed by the capture of both annihilation quanta) which results in an upward curvature of the efficiency function would not be sufficiently large, even at an energy as high as 2754 keV, to significantly affect the validity of equation 4.24.

Using the model $\varepsilon = kE^n$, n was readily obtained by measuring the counter response to the equally intense 1369 and 2754 keV gamma rays from a ^{24}Na source positioned at the source location indicated in figure 4-2. Relative intensities for the remaining energies to be included in the pair measurement were then taken from the straight line log ε vs log E curve connecting the two ^{24}Na points. As an added check, the relative counter responses to the equally intense 889 and 1120 keV radiation from a ^{46}Sc source and the near equally intense 1172 and 1333 keV radiation from a ^{60}Co source were examined and found to agree well with the values predicted by the simple efficiency model chosen. Detector efficiencies for the photon energies indicated in table 4-1 are given in table 4-2 where the 1369 keV result has been normalized to unity.

The experimental arrangement illustrated in figure 4-2 is such that the NaI monitor would intercept the entire photon beam as would the target when in position. Consequently, the rate at which gamma rays of energy E_γ would strike the target would be identical to the rate at which they would strike the NaI detector in the absence of a target. This rate is given by

Table 4-2: Relative efficiencies for the 3" x 3" NaI detector (figure 4-2) used for source strength evaluation. Errors are expected to be better than 1 1/2%.

Energy in MeV) (E_γ)	Relative Efficiency
1.120	1.17
1.173	1.12
1.333	1.02
1.369	1.00*
1.560	.890
2.223	.670
2.754	.561

* 1.369 MeV result normalized to unity

$$\frac{I_0(E_\gamma)\omega}{4\pi} = S(E_\gamma)/\varepsilon(E_\gamma)t, \qquad 4.25$$

where S is the peak area accumulated in counting time t, I_0 is the source activity, and ω the solid angle subtended at the NaI detector (and at the target when positioned) by the source.

Since some of the sources proposed for the study would have sufficiently short half lives, it would be necessary to define an initial time $t_0 = 0$, at which time $(I_0\omega)_{t_0}$ would be measured. In each case, as a consequence of the substantial source strengths proposed, the counting time that would be required in obtaining $(I_0\omega)_{t_0}$ would be much shorter than the life time of the source and, therefore, the source activity would be essentially constant over this period of measurement. During the actual pair cross section measurement, $(I_0\omega)_{t_0}$ would be corrected using the appropriate exponential decay constant.

As indicated in table 4-1, a cross section measurement was planned using the internal irradiation facility and the $^1H(n,\gamma)^2H$ reaction, the proposed through-tube source being about 10 g of water. The same collimation as indicated in figure 4-2 would be used in this study except in this situation the beam passing through the source collimator indicated in the diagram will have been already transmitted through the external through-tube collimator (figure 3-2). Equations 4.24 and 4.25 would remain applicable with this geometry and the 3" x 3" NaI detector would have the added purpose of monitoring the 2.225 MeV capture gamma-ray intensity which would fluctuate with reactor power levels.

Analysis of data taken on the pair cross section will involve

the evaluation of the two-parameter 511 keV peak volumes associated with positron annihilation following pair production in the target by source gamma rays and following positron emission by the ^{64}Cu additive. The appropriate form of equation 4.4 must then be applied in order to relate the pair cross section σ_{PAIR} to the experimentally observed peak volumes S_P and $S_{\beta+}$. Equation 4.4 may be written in the form

$$S_P/S_{\beta+} = \text{constant} \times (I_0\omega)_{t_0}\, T(1-e^{-\sigma_T X})\, \frac{\sigma_{PAIR}}{\sigma_T} \,/\, \Lambda_0\tau\,, \qquad 4.26$$

where in this case, T and τ are the experimental counting times (real) used in accumulating S_P and $S_{\beta+}$ and Λ_0 is simply the weight of copper additive used. Values for $\sigma_T(E_\gamma,Z)$, the total photon cross section, applicable to the proposed study are shown in table 4-3. These values for σ_T were taken from smoothed curves drawn through the data obtained earlier in the total cross section measurement.

In order to compensate for finite half lives of the sources proposed for the study, the numerator of equation 4.26 would necessarily be modified to the form

$$S_P = \text{constant} \times (I_0\omega)_{t_0} \int_{T_1}^{T_2} e^{-t\ell n2/T_{1/2}}dt \cdot \frac{T_{LIVE}}{\Delta T}\,(1-e^{-\sigma_T X})\,\frac{\sigma_{PAIR}}{\sigma_T}, \qquad 4.27$$

where T_1 and T_2 are respectively the start and stop counting times defined with respect to the initial time $t_0 = 0$ at which $(I_0\omega)_{t_0}$ had been measured. ΔT is a given by T_2-T_1, $T_{1/2}$ is the half life of the particular source being considered, and T_{LIVE} the total live time used in the measurement of S_P. $T_{LIVE}/\Delta T$ is, therefore, a correction factor

Table 4-3: Total cross sections σ_T used in determining the pair cross section. Values for σ_T were taken from the results on the total cross section measurement (Chapter III), using interpolation procedures when required. 1% errors were assigned to all values.

Energy in MeV (E_γ)	σ_T in barns/atom					
	Titanium	Copper	Molybdenum	Cadmium	Tungsten	Lead
1.120	4.48	5.87	8.80	10.3	18.1	22.0
1.172	4.38	5.73	8.62	10.0	17.6	21.1
1.333	4.11	5.37	8.10	9.29	16.1	19.1
1.369	4.05	5.29	8.00	9.15	15.9	18.6
1.560	3.76	4.96	7.45	8.54	14.8	17.2
2.225	3.14	4.26	6.27	7.38	12.9	15.2
2.754	2.85	3.92	5.88	6.97	12.3	14.5

for analyser dead time. The terms $(I_0\omega)_{t_0} \int e^{-t\ell n2/T_{1/2}}\, dt$ in equation 4.27 represent the total number of gamma rays striking the target during the period ΔT. In the limit that $T_{1/2} >> \Delta T$, then the integral in equation 4.27 reduces to ΔT and, consequently

$$S_P = \text{constant} \times (I_0\omega)_{t_0}\, T_{LIVE}\, (1-e^{-\sigma_T X})\, \sigma_{PAIR}/\sigma_T \,. \qquad 4.28$$

Otherwise, integration in equation 4.27 leads to the result

$$S_P = \text{constant} \times (I_0\omega)_{t_0}\, \frac{T_{1/2}T_{LIVE}}{\Delta T\ \ell n2}\, (e^{-T_1\ell n2/T_{1/2}} - e^{-T_2\ell n2/T_{1/2}}) \times$$

$$(1-e^{-\sigma_T X})\, \sigma_{PAIR}/\sigma_T \,. \qquad 4.29$$

Identical reasoning concerning the $S_{\beta+}$ term (the denominator of equation 4.26) leads to the result

$$S_{\beta+} = \text{constant} \times W_{Cu}\, \frac{\tau_{1/2}\tau_{LIVE}}{\Delta\tau\ \ell n2} \times$$

$$\left(e^{-\tau_1\ell n2/\tau_{1/2}} - e^{-\tau_2\ell n2/\tau_{1/2}}\right), \qquad 4.30$$

where W_{cu} and $\tau_{1/2}$ refer to the weight and half life of the copper additive. The start and stop counting times τ_1 and τ_2 are defined with respect to some initial time common to all the $S_{\beta+}$ measurements.

If the photon source is monoenergetic at energies above pair threshold, the general equation relating the measured parameters (the 511 keV peak volumes) to the relative pair cross section is given by $S_p/S_{\beta+}$ using equation 4.30 and either 4.28 or 4.29 depending on source

life times. Variations are then required for cases involving two or more gamma energies above threshold energy. These variations will be discussed later in the chapter when dealing with the analysis of measured data obtained using the individual sources.

4.3 Measurement of the Partial Pair Cross Section

Powdered Ti, Cu, Mo, Cd, W, and Pb targets were prepared using the procedures outlined in figure 4-5. In each case, the amount of material required in forming a well-packed 2 cm long target was first obtained in a preliminary procedure. The resulting target thicknesses in g/cm^2, given by X = target weight/target cross sectional area, are shown in table 4-4 as are the amounts of copper additives used in each target. The entire quantity of copper additive required for all targets was irradiated as a single unit in the reactor core, then well mixed before being divided into the individual target portions. This insured that the β^+-decay activity mixed with each target would simply be proportional to the weight of copper additive.

Immediately following encapsulation and prior to the two-parameter measurement of S_{β^+}, a set of measurements was taken in order to obtain an estimate of the degree of success achieved in uniformly distributing the active copper throughout the target. The targets, each in turn, were positioned in the annulus (minus the external source) as indicated in figure 4-2 and their 511 keV annihilation activities counted using one of the NaI quadrant detectors and scaling the logic output of a single channel PHA having a window set to accomodate approximately 90% of the annihilation peak. Each target was counted in three positions

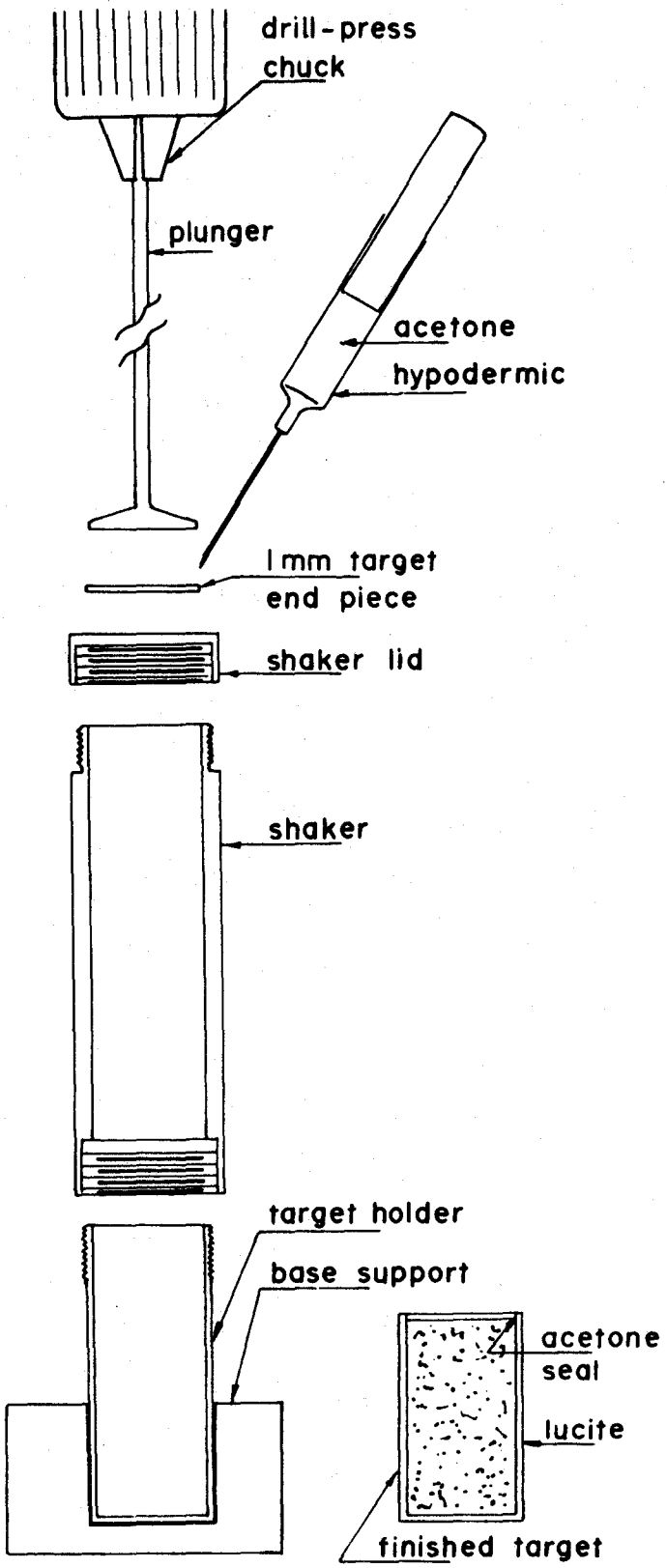

Figure 4-5: Target Preparation.
(1) The target holder plus shaker were first weighed, then a quantity of target material (determined in a preliminary check) added and the combination reweighed.
(2) A known quantity of uniformly activated copper powder was added and the shaker lid screwed on tightly. Care was taken to insure a uniform mixture of the compound.
(3) The system was jarred slightly, allowing the mixture to settle as far down as possible into the target holder.
(4) The apparatus was positioned in the base support on a drill-press platform and the shaker lid removed. A 1 mm lucite end piece was lightly stuck to the plunger base using a dab of grease, then inserted into the shaker and target holder.
(5) With the end piece positioned under pressure, the shaker was unscrewed and slid up the plunger free of the target holder. The end piece was then fused to the target holder using acetone released from the hypodermic.
(6) The unused part of the target holder was carefully trimmed away and the top surface smoothed.

Table 4-4: Target thicknesses and weights of copper additives. Errors in thicknesses are estimated at 1/2%. Errors in weights of Cu additives are negligible.

Atomic Number	Target Thickness (g/cm^2)	Weight of Cu Additive (g)
22	4.50	.0732
29	4.94	.0981
42	7.40	.1141
48	9.78	.0862
74	12.0	.0868
82	16.5	.1611

of rotation in the capsule holder. Agreement in observed intensities for any one target was sufficiently close in each case to draw the conclusion that a reasonably uniform copper mixture had, in fact, been realized.

The 128 x 128 channel coincidence spectra, associated with the β^+-decay of the ^{64}Cu additives, were recorded for each of the 6 targets using the apparatus and spectrometer illustrated in figure 4-2. Counting times of approximately 5 hours were required for each of the targets in order to reduce the statistical error in the two-parameter peak intensity to approximately 0.5%. Room background was first measured and found to be negligible. Following each target measurement, the recorded spectrum, requiring all 16K of memory, was transferred to magnetic tape. The targets were then allowed to sit for approximately 5 days, allowing the 12-hour ^{64}Cu activity to decay away, before proceding with the measurement of R_p.

Following insertion of each of the photon sources into the source holder and collimator (or through tube facility in the case of the $^1H(n,\gamma)^2H$ study), values for $(I_0\omega)_{t_0=0}$ were obtained using the geometry as illustrated in figure 4-2 with no target in the holder. Counting times of approximately 5 minutes were required in each case to determine $(I_0\omega)_{t_0}$ with a statistical error of 0.5% or better. Once a source was positioned and $(I_0\omega)_{t_0}$ measured, the source was not moved until all the target measurements had been completed. Live times used in determining $(I_0\omega)_{t_0}$ and R_p (as well as R_{β^+}) were obtained using the ND-3300 PHA internal live time recording facility. A discussion of particular techniques involved in the measurements of $(I_0\omega)_{t_0}$ and R_p follows, with each photon source study being considered individually.

(1) 1120 keV, ^{46}Sc Gamma Rays

The relatively long-lived ^{46}Sc source (84 days as compared to 15 hour ^{24}Na) was allowed to decay for 10 days following irradiation in order to eliminate the ^{24}Na contamination present from the irradiation can. Consequently, the singles spectrum recorded in the $(I_0\omega)_{t_0}$ measurement, using the 3" x 3" NaI monitor detector, displayed no gamma ray peaks, other than that at 1120 keV, at energies above the pair production threshold.

The rather low pair cross section for 1120 keV gamma rays limited the measurement of R_p to the higher atomic number, Mo, Cd, W, and Pb targets. Counting time used for each of the 4 targets studied was approximately 20 hours.

(2) 1369 and 2754 keV, ^{24}Na Gamma Rays

Since both photons (1369 and 2754 keV) following β^+-decay in ^{24}Na have equal intensities, it is expected that $(I_0\omega)_{t_0}^{1369} = (I_0\omega)_{t_0}^{2754}$. Using the relative detector efficiencies established earlier and given in table 4-2 the two values obtained for $(I_0\omega)_{t_0}$ showed a deviation of only 0.2%. The ^{24}Na source was allowed to stand for approximately 15 hours following irradiation in order to eliminate any contribution to the source spectrum from the 2.6 hour ^{31}Si activity from the quartz source holder. For obvious reasons, the ^{24}Na contamination from the irradiation can was of no consequence to the measurement.

All 6 target elements were studied and counting times ranged from 10 min for the Pb target to 1 1/2 hours for the Ti target.

(3) 1560 keV, ^{142}Pr Gamma Rays

Because of the comparable half lives of the ^{142}Pr (19 hours) source and the ^{24}Na contamination, it was impossible to wait for the latter to decay away. Consequently, it was necessary to obtain values for the $(I_0\omega)^{1369}_{t_0}$ and $(I_0\omega)^{2754}_{t_0}$ contamination components as well as a value for $(I_0\omega)^{1560}_{t_0}$. A correction could then be made to the measured R_p result. A wait of approximately 20 hours following irradiation was taken, however, in order to eliminate the ^{31}Si component.

All 6 target elements were studied and counting times ranged from 1 hour for the Pb target to 5 hours for the Ti target.

(4) 1172 and 1333 keV, ^{60}Co Gamma Rays

The 5.3 year ^{60}Co source was allowed to stand for approximately one week following irradiation, thus eliminating any contamination effects. $(I_0\omega)^{1172}_{t_0}$ and $(I_0\omega)^{1333}_{t_0}$ were measured and found to be within 1%.

All 6 target elements were studied and counting times ranged from 1 hour for the Pb target to 6 hours for the Ti target.

(5) 2.225 keV, ^{1}H(n,γ)^{2}H Gamma Rays

The 12" Pb shielding protecting the apparatus of figure 4-2 from any reactor pool activity was removed and a 10 g water sample, sealed in a thin quartz holder and secured in the through tube, was positioned in a thermal neutron flux of approximately 5 x 10^{12} neutrons/cm^2/sec. A value for $(I_0\omega)_{t_0}$ was obtained in the same manner as used for the β-decay sources, a 5 min counting time being used. Beam strength checks were then made approximately every 40 minutes, between target measurements, in order to obtain correction factors for $(I_0\omega)_{t_0}$. Reactor power charts were closely monitored to insure a reasonably steady

beam strength had been maintained throughout a target measurement.

All 6 target elements were studied and counting times ranged from 20 minutes for the Pb target to 70 minutes for the Ti target.

4.4 Results on the Partial Pair Cross Section

The 511 keV peak volumes (total number of counts) S_p and $S_{\beta+}$ relating to pair production and ^{64}Cu β-decay respectively were obtained from the recorded two-parameter spectra M_{ij} (where i, j = 1, 2, 3, ---, 128) through an intermediate, iterative process. The centroid (i_0, j_0) and standard deviations σ_i, σ_j associated with the X and Y dimensions of a particular 511 keV peak were estimated to the nearest channel, primarily by visual inspection, using the familiar relationship FWHM = 2.35 σ. The two-parameter spectrum was then transformed into a pair of single-parameter spectra associated with the X and Y planes using

$$A_i = \sum_j M_{ij} \ , \qquad 4.31$$

where $(i = 1, 2, 3, ---, 128)$ and $(j_0 - 2.0\,\sigma_j \leq j \leq j_0 + 2.0\,\sigma_j)$ and

$$A_j = \sum_i M_{ij} \ , \qquad 4.32$$

where $(j = 1, 2, 3, ---, 128)$ and $(i_0 - 2.0\,\sigma_i \leq i \leq i_0 + 2.0\,\sigma_i)$. Backgrounds were then subtracted from the single-parameter spectra A_i and A_j and standard deviations and peak centroids established, this time to a tenth of a channel. A final value for the peak volume S was then determined using the latest values for the peak centroids and standard deviations in the summation

$$S = \sum_{i} (A_i - B_i) \qquad 4.33$$

where $(i_0 - 2.0\sigma_i \leq i \leq i_0 + 2.0\ \sigma_i)$ and where A_i was determined using equation 4.31 again with the improved centroid and standard deviation values.

Examples of the single-parameter spectra A_i, obtained by compressing the appropriate range of X-planes (determined by j_0 and σ_j) into a single plane as discussed above are shown in figure 4-6. Examination of the spectral shapes (as a function of E_γ and Z) associated with the pair production model clearly shows that the chance or background component B_i (i = 1, 2, 3, ---, 128) depends primarily on the degree, and energy distribution, of Compton scattered radiation by the target into the detectors. Because of this complication relating to background evaluation, it was decided that the best possible technique in evaluating the chance contribution to the recorded peaks would simply involve fitting a curve smoothly to the backgrounds on either side of the peak. Except for the E_γ = 1120 keV measurements, the true/chance ratio was sufficiently high that the evaluation of background was not critical.

In estimating experimental error in the measured cross sections, the following considerations were given. Error in target thickness was estimated to be 0.5% while the error in the quantity of copper additive was considered negligible. Possible error in the measurement of $(I_0\omega)_{t_0}$ was estimated as 1 1/2%. Lifetimes involved in making necessary corrections for the natural decay of source activity (as well as the ^{64}Cu activity in the β^+ model) were assumed to be good to

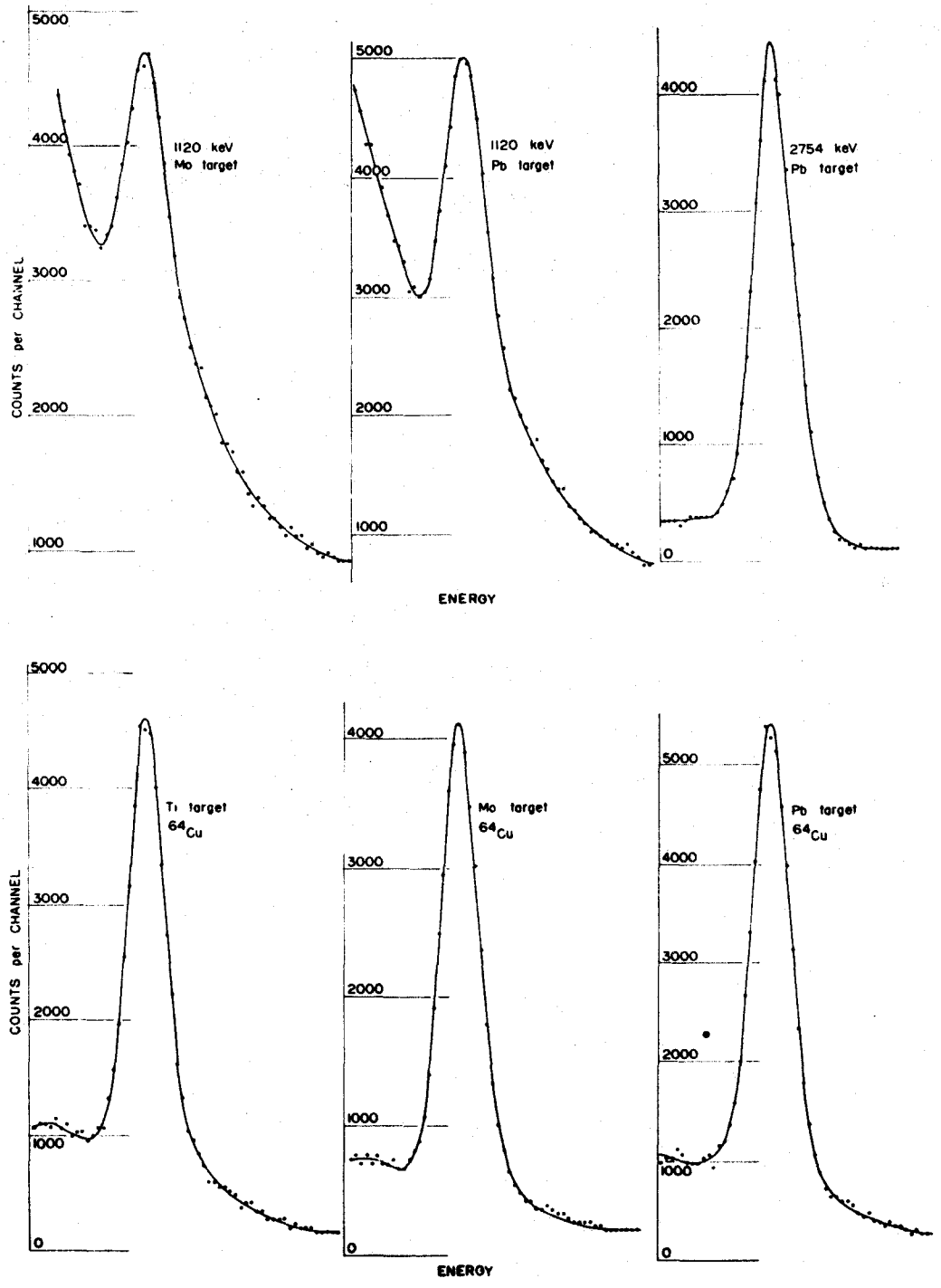

Figure 4-6: Examples of single parameter spectra obtained by compressing the two-parameter observed spectra into a single plane. The top three illustrations indicate the strong dependence of the background on E_γ and Z.

1%. Sufficient statistics were accumulated in each case that values for $S_{\beta+}$ could be quoted with 0.5% or better error while the estimated error in S_P was set at 1% except for the ^{46}Sc (E_γ = 1120 keV) results. Because of the uncertainties relating to background contributions to the 1120 keV results, an additional 5% was included in the error assigned to S_P.

Using the familiar formula for determining the variance

$$\sigma_{mf}^2 = \left(\frac{\delta f}{\delta x}\right)^2 \sigma_{mx}^2 + \left(\frac{\delta f}{\delta y}\right)^2 \sigma_{my}^2 + - - -, \qquad 4.34$$

where $f = f(x, y ---)$, an error in σ_{PAIR} of approximately 3% ($\lesssim$ 8% for E_γ = 1120 keV) was established. Because of a number of small uncertainties not considered in the application of equation 4.34, relating to the assumption given by equation 4.3, an additional 2% was added to each of the error estimates.

The general equation relating the relative pair cross section to the measured parameters for a monoenergetic (above pair threshold) source was given earlier as $S_P/S_{\beta+}$ where

$$S_P = \text{constant} \times (I_0\omega)_{t_0} \, T_{LIVE} \, (1-e^{-\sigma_T x}) \, \sigma_{PAIR}/\sigma_T \, , \qquad 4.35$$

if T_1, $T_2 \ll T_{1/2}$, otherwise

$$S_P = \text{constant} \times (I_0\omega)_{t_0} \, \frac{T_{1/2} T_{LIVE}}{\Delta T \, \ell n 2} \times \left(e^{-T_1 \ell n 2/T_{1/2}} - e^{-T_2 \ell n 2/T_{1/2}}\right)\left(1-e^{-\sigma_T x}\right) \frac{\sigma_{PAIR}}{\sigma_T}, \qquad 4.36$$

and where

$$S_{\beta+} = \text{constant} \times W_{Cu} \frac{\tau_{1/2}\tau_{LIVE}}{\Delta\tau\ \ell n2} \left(e^{-\tau_1 \ell n2/\tau_{1/2}} - e^{-\tau_2 \ell n2/\tau_{1/2}}\right). \quad 4.37$$

Since variations of the equations for S_p are required in order to account for more complicated spectra, the experimental results will be considered by dealing with one source study at a time. For any one source, a maximum of two gamma-ray energies above threshold were observed, the origin of these energies being due either to the actual source spectrum or to the ^{24}Na contamination from the irradiation can. Results on the relative pair cross sections are given in table 4-5 where it is seen that the value obtained for $\sigma_{PAIR}(E_\gamma = 2754$ keV, $Z = 82)$ has been normalized to 3.3 barns/atom. It will be seen later in this study that this value of 3.3 barns/atom coincides with the result obtained indirectly from the total cross section data (Chapter III). Further, it will be seen that this value agrees well with the theoretical cross section[21,30].

(1) 1120 keV, ^{46}Sc Results

Since ^{46}Sc has only one gamma-ray energy above pair threshold and since any ^{31}Si and ^{24}Na contamination was allowed to dissipate prior to the measurement, the general equation $S_p/S_{\beta+}$ using equations 4.36 and 4.37 was applicable in obtaining σ_{PAIR} (1120, Z). Pair cross sections were obtained for Z = 42, 48, 74, and 82 and an error of 10% assigned to all results.

(2) 2754 keV, ^{24}Na Results

^{31}Si contamination was allowed to dissipate prior to use of the

Table 4-5: Measured pair cross sections in units of barns/atom. $\sigma_{PAIR}(E_\gamma = 2754, Z = 82)$ has been normalized to a value of 3.30 barns/atom.

Energy in MeV (E_γ)	σ_{PAIR} in barns/atom					
	Titanium	Copper	Molybdenum	Cadmium	Tungsten	Lead
1.120	---	---	.0026 ± .0003	.0030 ± .0003	.0071±.0007	.0089±.0009
1.172	.0013 ± .0001	.0028 ± .0003	.0075 ± .0007	.010 ± .001	.029 ± .003	.039 ± .004
1.333	.00770 ± .00039	.0158 ± .0008	.0421 ± .0021	.0574 ± .0029	.175 ± .009	.248 ± .012
1.560	.0304 ± .0015	.0559 ± .0028	.133 ± .007	.182 ± .009	.509 ± .025	.703 ± .035
2.225	.108 ± .005	.205 ± .010	.481 ± .024	.633 ± .032	1.63 ± .08	2.20 ± .11
2.754	.189 ± .009	.371 ± .018	.771 ± .038	1.03 ± .05	2.59 ± .13	3.30 ± .16

^{24}Na source. Since two energies (1369 and 2754 keV) contribute to the measured quantity S_p, then S_p is given by $S_p(1369) + S_p(2754)$. Therefore, since both energy photons have equal intensities

$$S_p = \text{constant } (I_0\omega)_{t_0} \left| (1-e^{-\sigma_T(1369)X}) \frac{\sigma_{PAIR}^{(1369)}}{\sigma_T(1369)} + (1-e^{-\sigma_T(2754)X}) \frac{\sigma_{PAIR}(2754)}{\sigma_T(2754)} \right| \times \frac{T_{1/2}T_{LIVE}}{\Delta T \ \ell n2} \left(e^{-T_1 \ell n2/T_{1/2}} - e^{-T_2 \ell n2/T_{1/2}} \right). \quad 4.38$$

The pair cross sections for 2754 keV gamma rays were then determined using the general form S_p/S_β with equation 4.37 and equation 4.38 using the appropriate form of the substitution

$$\kappa = \sigma_{PAIR}(1369)/\sigma_{PAIR}(2754) \ . \quad 4.39$$

The values for κ were obtained from theory, using the Bethe-Heitler pair cross sections and the ratios $\sigma_{PAIR}/\sigma_{(B-H)_{PAIR}}$ obtained from the illustrated results of Øverbø et al[31] using interpolation procedures when required. Although compensation for the 1369 keV contribution to S_p was made, an evaluation of $\sigma_{PAIR}(1369)$ was not attempted because of its relatively small contribution ($\sigma_{PAIR}(1369)/\sigma_{PAIR}(2754) \simeq 0.04$) to the total effect. An error of 5% was assigned to the pair cross section results obtained on all 6 target elements studied.

(3) 1560 keV, ^{142}Pr Results

Although ^{142}Pr has only a single energy, a correction for the

^{24}Na contamination from the irradiation can was necessary. This created little difficulty, however, since the contamination intensity $(I_0\omega)^{C}_{t_0}$ was measured at the same time as $(I_0\omega)^{Pr}_{t_0}$ and the already established $\sigma_{PAIR}(2754)$ results could be used in the correction. The quantity S_p which includes $S_p(1560) + S_p(1369) + S_p(2754)$ is then written

$$S_p = \text{constant} \times (I_0\omega)^{Pr}_{t_0} \frac{T_{1/2}T_{LIVE}}{\Delta T\ \ell n2} \left(e^{-T_1 \ell n2/T_{1/2}} - e^{-T_2 \ell n2/T_{1/2}} \right) \times$$

$$\left(1-e^{-\sigma_T(1560)X}\right) \frac{\sigma_{PAIR}(1560)}{\sigma_T(1560)} \qquad 4.40$$

$$+ (I_0\omega)^{C}_{t_0} \frac{T_{1/2}T_{LIVE}}{\Delta T\ \ell n2} \left(e^{-T_1 \ell n2/T_{1/2}} - e^{-T_2 \ell n2/T_{1/2}} \right)$$

$$\times \left| (1-e^{-\sigma_T(1369)X}) \frac{\kappa\sigma_{PAIR}(2754)}{\sigma_T(1369)} + (1-e^{-\sigma_T(2754)X}) \frac{\sigma_{PAIR}(2754)}{\sigma_T(2754)} \right|,$$

where κ was discussed earlier in considering the 2754 keV results and where $T_{1/2}$ in the first and second terms refer to the half lives of ^{142}Pr and ^{24}Na respectively. Equations 4.40 and 4.37 were then used in applying the general equation $S_p/S_{\beta+}$. An error of 5% was assigned to the pair cross section results obtained for all 6 targets studied.

(4) 1172 and 1333 keV, ^{60}Co results

As a result of the substantial, 5.3-year lifetime of ^{60}Co, the simplified expression for S_p, given by equation 4.28, was applicable for each of the two gamma-ray energies involved. Further, contamination was allowed to dissipate before the measurements of S_p were taken. The two energies involved were assumed to have the same intensities

and, consequently, S_p, which includes $S_p(1172) + S_p(1333)$ becomes

$$S_p = (I_0\omega)_{t_0} \left| (1-e^{-\sigma_T(1172)X}) \frac{\sigma_{PAIR}(1172)}{\sigma_T(1172)} + (1-e^{-\sigma_T(1333)X}) \frac{\sigma_{PAIR}(1333)}{\sigma_T(1333)} \right| . \qquad 4.41$$

The pair cross sections for both energies were then obtained by making the appropriate substitutions

$$\kappa = \sigma_{PAIR}(1172)/\sigma_{PAIR}(1333) , \qquad 4.42$$

where κ was obtained in a similar manner as discussed for the case involving the ^{24}Na source.

(5) 2.225 keV, $^1H(n,\gamma)^2H$ Results

The general equation applicable to this measurement is similar to the one that would be used for a very long lived, monoenergetic source. However, since the deuteron intensity was subject to reactor power fluctuations, regular beam strength checks were required and a correction factor for $(I_0\omega)_{t_0}$ established. Beam strength checks were carried out every 40 min and the reactor power charts closely monitored. Since individual runs were necessarily less than 40 min in duration, more than one run was required for the lower-Z targets in order to obtain sufficient statistics. The sum of the peak volumes over the required number of runs is given by $S_p = \sum_i S_p^i$ and, therefore, can be related to the pair cross section by

$$S_P = \text{constant} \times (I_0\omega)_{t_0} (1-e^{-\sigma_T X}) \frac{\sigma_{PAIR}}{\sigma_T} \sum_i f_i T^i_{LIVE} , \qquad 4.43$$

where f_i are the source strength correction factors for each run, taken from a smooth curve drawn through the results of the 40 min interval checks, and T^i_{LIVE} are the live times for the individual runs. Equation 4.43 was then used with equation 4.37 to form the general equation $S_P/S_{\beta+}$ and an estimated error of 5% was assigned to the results obtained for all targets studied.

CHAPTER V

DISCUSSION OF RESULTS

5.1 The Total Cross Section

Total cross sections σ_T for 29 well distributed energies from 121 keV to 10.8 MeV in 9 target elements ranging from carbon to uranium have been realized and an accuracy of approximately 1% achieved. The results are shown in table 3-7.

In the energy region below 6 MeV, experimental results on the total cross section were in excellent agreement with the theoretical values compiled by Storm and Israel[30] and by Grodstein[21]. Grodstein indicates slightly lower values for the photoelectric contribution to the total cross section than reported by Storm and Israel; however, no significant differences in the two reports are apparent. The excellent agreement between measured and theoretical cross sections for 121 keV to 6 MeV photons is clearly illustrated in figure 5-1. The theoretical cross sections used for comparison are those proposed by Storm and Israel.

Values for the inelastic (Compton) scattering cross section $\sigma_{(INCOH)}$ in the energy region from 1-3 MeV were deduced from the measured total cross sections σ_T using

$$\sigma_{(INCOH)} = \sigma_T - \left|\sigma_{PHOTO} + \sigma_{(COH)} + \sigma_{(PAIR)}\right|_{theory}. \qquad 5.1$$

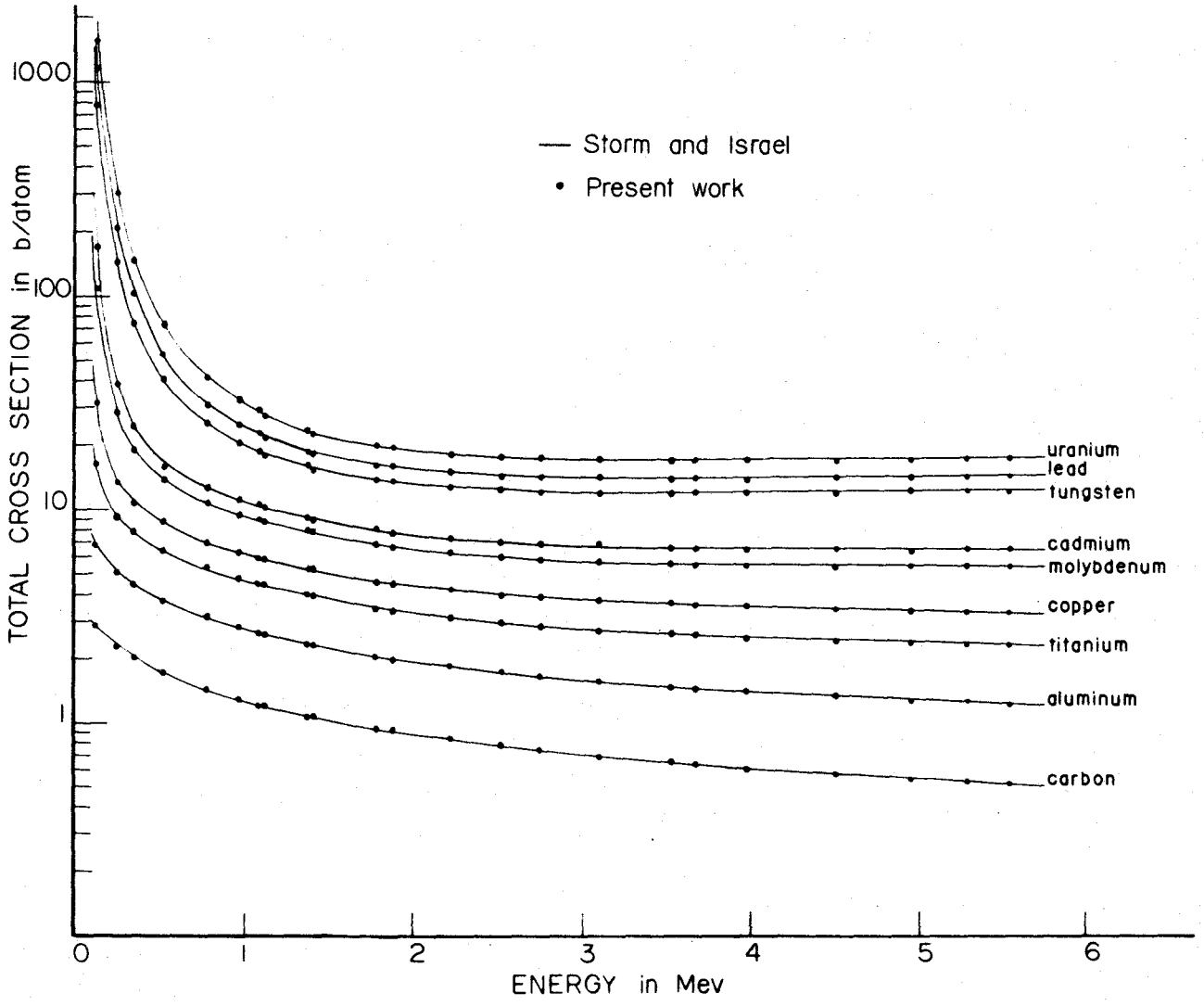

Figure 5-1: Total cross section results for 121 keV to 6 MeV gamma rays. Experimental error is reflected in the size of the data points.

Theoretical values for photoelectric absorption σ_{PHOTO}, coherent (Rayleigh) scattering $\sigma_{(COH)}$, and pair production σ_{PAIR} were taken from smooth curves drawn through the values provided by Storm and Israel. The coherent scattering cross sections were reported to have been calculated from the equation

$$d\sigma_{(COH)} = r_o^2/2\ (1 + \cos^2\theta)\ [F(q,Z)]^2 d\Omega \qquad 5.2$$

by numerical integration over angle. The form factors F(q,Z) were reported to be those of Cromer[32] and Hanson[33]. The photoelectric cross sections in the region of 1-3 MeV were credited to Rakavy and Ron[34] and to Schmickley and Pratt[35]. In a further effort to verify the photoeffect, K edge τ_a/τ_k ratios measured by Kirchner[36] were used to extend Pratt's[37] cross sections to include the outer electronic shells. The two sets of values showed good agreement. The reported pair production cross sections had been obtained by interpolation of the data compiled by Hubbell and Berger[38] for some 11 elements over a range of 1.5-100 MeV. These values had been calculated using the Born approximation with the Bethe-Heitler high energy approximation. They include radiative and screening corrections. These results were found to agree with those calculated from Maximum's simplified expression of the Racah formula as reported by Motz[9].

Results obtained on the incoherent cross section $\sigma_{(INCOH)}$ (using equation 5-1) are compared in table 5-1 to the cross sections calculated using the Klein-Nishina formula, the percent deviations being shown in each case. An examination of these deviations and the total

Table 5-1: Percent deviations between inelastic scattering cross sections deduced from the total cross section measurement and those calculated from the Klein-Nishina formula.

$\Delta = [\sigma_{(INCOH)} / \sigma_{K-N}] \times 100\%$

Energy (MeV)	Carbon	Aluminium	Titanium	Copper	Molybdenum	Cadmium	Tungsten	Lead	Uranium	Average Δ
.965	+0.9	+0.9	+0.9	0.0	-0.5	+0.9	0.0	-1.4	+2.8	+0.5
1.087	-1.5	0.0	+0.5	-0.5	+0.5	+0.5	-0.5	-1.0	+4.5	+0.5
1.113	0.0	-1.0	+1.0	0.0	+0.5	+1.0	-2.5	0.0	+0.5	-0.1
1.369	-1.7	-0.6	+2.2	0.0	+2.2	0.0	+1.7	-2.2	+1.7	+0.4
1.409	+0.6	0.0	+0.6	0.0	+2.8	-0.6	-2.8	-1.1	+0.6	0.0
1.779	+0.6	-0.6	-2.6	-0.6	-1.3	+1.3	+0.6	0.0	+2.6	0.0
1.889	+2.6	0.0	-2.6	-0.7	-1.3	-2.0	+1.3	+2.6	+2.0	+0.2
2.225	+1.4	+0.7	-2.2	0.0	-1.4	-0.7	0.0	0.0	+0.7	-0.2
2.519	+1.6	+1.6	-2.3	0.0	-1.6	-2.3	0.0	-2.3	+0.8	-0.5
2.754	+2.5	+0.8	-1.6	+0.8	-0.8	0.0	-0.8	-2.5	+1.6	0.0
3.098	+1.8	+0.9	-1.8	0.0	-1.8	+1.8	-1.8	-0.9	+0.9	-0.1
Average Δ	+0.8	+0.2	-0.7	-0.1	-0.2	0.0	-0.4	-0.6	+1.7	

cross section results shown in figure 5-1 leads to the following conclusions:

(i) below 6 MeV, and particularly in the 1-3 MeV region, the experimental and theoretical total cross sections are in excellent agreement and,

(ii) the values for the inelastic scattering cross section obtained using the Klein-Nishina formula agree well with the measured values in the low atomic number region where Compton scattering is the only significant interaction and agreement appears to be nearly as good at higher Z values where the results obtained for $\sigma_{(INCOH)}$ using equation 5.1 are less reliable due to the uncertainties in the theoretical values used for σ_{PHOTO}, $\sigma_{(COH)}$, and σ_{PAIR}.

Measurement of the total interaction cross section in the energy region covered by long-lived beta-decay sources has an extensive history. Consequently, the reliability of the theoretical cross section σ_T, has been well established in the energy region from 1-3 MeV. The Compton scattering cross section has also been examined in detail and the reliability of the Klein-Nishina formula well established in this energy region. Therefore, the conclusion that the present experiment is relatively free from significant systematic errors can be reached with reasonable certainty. Further, the error of 1% (primarily statistical in origin) assigned to the measured total cross sections appears to be reasonable.

In the energy region from 1-3 MeV where the cross section is

well understood, measured results show excellent agreement (certainly within the 1% assigned error) with theoretically predicted values. Consequently, the measured results in the region from 3-11 MeV, obtained in the same measurement as the lower energy cross sections, should be equally reliable.

At photon energies above 6 MeV, particularly in high Z target materials, the measured total cross section showed a definite trend towards values higher than those quoted by Storm and Israel. Log-log plots of the observed deviation in the measured and quoted total cross sections for the higher energy and atomic numbers studied are shown in figure 5-2 (a)-(e). The deviation plotted against energy in figure 5-2 (f) for Z = 92 reveals an exponential dependence on energy. The departure of the measured total cross section from the theoretical values can be safely related to the pair production cross section by a simple argument of the magnitude of the deviation and the observed dependence on energy and atomic number. Consider $\Delta\sigma_T$ (E = 10 MeV, Z = 92) $\underset{\sim}{\sim}$ 0.9 barns (figure 5-2 (f)). Storm and Israel quote the values σ_{PHOTO}(10 MeV, 92) = 0.295 barns and $\sigma_{(INCOH)}$(10 MeV, 92) = 4.7 barns. Therefore, $\Delta\sigma_T$ (10 MeV, 92) would represent a 300% effect in the quoted photoelectric absorption cross section and a 20% effect in the Klein-Nishina cross section. Such relative effects, which would further increase with energy, are already too large to be credible. On the other hand, $\Delta\sigma_T$ would represent a reasonable 6% effect in the quoted pair production cross section.

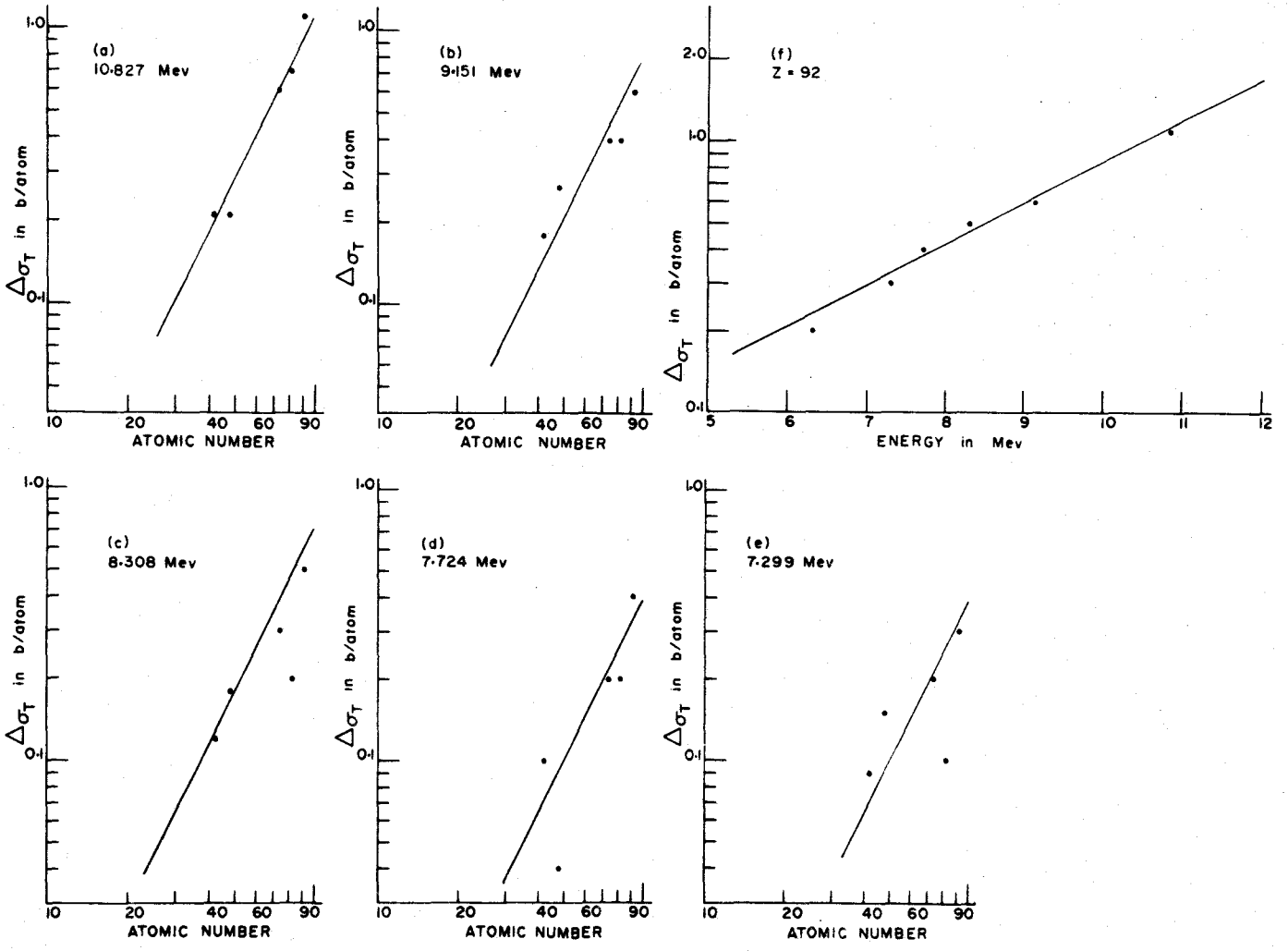

Figure 5-2: Deviation of measured total cross sections from those proposed by Storm and Israel[30]. Solid lines in figures (a) to (e) are not intended to represent the best fit but rather to indicate the slope corresponding to a Z^2 dependence.

5.2 Deduction of the Pair Production Cross Section From the Measured Total Cross Section

When a positron and an electron are created through the absorption of a sufficiently energetic photon, momentum must necessarily be transferred to a third particle, which may be either a nucleus or an electron, in order that the conservation laws be satisfied. Since all three particles, the created pair and the third body, are charged, the momentum transfer to the nucleus (or electron) is brought about through the Coulomb interaction between the nucleus and the created pair. In the case of pair production in the field of a nucleus, the nucleus, being much heavier than either the positron or electron, will carry away only a negligible amount of recoil energy and, consequently

$$E_+ + E_- \simeq E_\gamma - 2\,mc^2 , \qquad 5.3$$

where E_+ and E_- are the energies imparted to the positron and electron at their creation. Thus, nuclear pair production is frequently referred to as elastic pair production. In the case of pair production in the field of an electron, the recoiling electron may carry away considerable energy and, consequently

$$E_+ + E_- = E_\gamma - (2\,mc^2 + E_{RECOIL}). \qquad 5.4$$

Thus pair production in the field of an electron is frequently referred to as inelastic pair production or, more frequently, triplet production,

relating to the created pair plus the third, recoiling electron. While the photon threshold energy for elastic pair production is 2 mc^2, conservation of energy and momentum requires that the triplet production threshold be 4 mc^2.

The ratio of the triplet cross section for all Z atomic electrons to the nuclear pair production cross section (assuming both interactions are energetically possible) can be written[39]

$$\sigma_{TRIPLET}/\sigma_{PAIR} = 1/kZ, \qquad 5.5$$

where k has an energy dependence (k is expected to be about 2-3 at 6.5 MeV, about 1.2 at 100 MeV, and to approach unity as E approaches ∞) but is independent of Z. The total pair cross section $\sigma_{PAIR+TRIPLET)}$ may then be written

$$\sigma_{(PAIR+TRIPLET)} = \sigma_{PAIR}[1 + 1/kZ]. \qquad 5.6$$

For a particular photon energy,

$$\sigma_{(PAIR+TRIPLET)} = a^2Z + b^2Z^2, \qquad 5.7$$

where

$$\sigma_{PAIR} = b^2Z^2 \text{ and } \sigma_{TRIPLET} = a^2Z.$$

Values for the total pair cross section $\sigma_{(PAIR+TRIPLET)}$ were deduced from the measured total cross section σ_T (table 3-7) using

$$\sigma_{(PAIR+TRIPLET)} = \sigma_T - \left| \sigma_{(COH)} + \sigma_{(INCOH)} + \sigma_{(PHOTO)} + \sigma_{NUCL} \right| , \qquad 5.8$$

where again, the theoretical values used for $\sigma_{(COH)}$, $\sigma_{(INCOH)}$, and σ_{PHOTO} were those provided by Storm and Israel. The contribution of photo nuclear effects σ_{NUCL} to the total cross section was expected to be quite small for even the highest photon energies studied and the necessity for considering the effects just marginal. Consequently, using the discussion of Rosenblum, Shrader and Warner[40] concerning these effects, a very rough estimate was made for 10.8 MeV photons (0.3, 0.2, and 0.1 barns/atom for U, Pb, and W respectively). σ_{NUCL} was then assumed to fall off very rapidly with energy.

In the energy region from 2-11 MeV, for the low Z carbon and aluminium targets, $\sigma_{(PAIR+TRIPLET)}$ was determined using the simpler expression

$$\sigma_{(PAIR+TRIPLET)} = \sigma_T - \sigma_{KLEIN-NISHINA}, \qquad 5.9$$

since the other interactions are not competitive in this region of energy and atomic number. The results obtained for $\sigma_{(PAIR+TRIPLET)}$ for carbon and aluminium are shown in figure 5-3. These results were smoothed (as indicated by the solid lines in figure 5-3), then used in equation 5.7 to determine the inelastic component $\sigma_{TRIPLET}$ of the pair production process.

The results obtained on the triplet cross section $\sigma_{TRIPLET}/Z$ are shown in figure 5-4 along with the recently calculated values (solid line) of Mork[41]. Results on the triplet cross section were

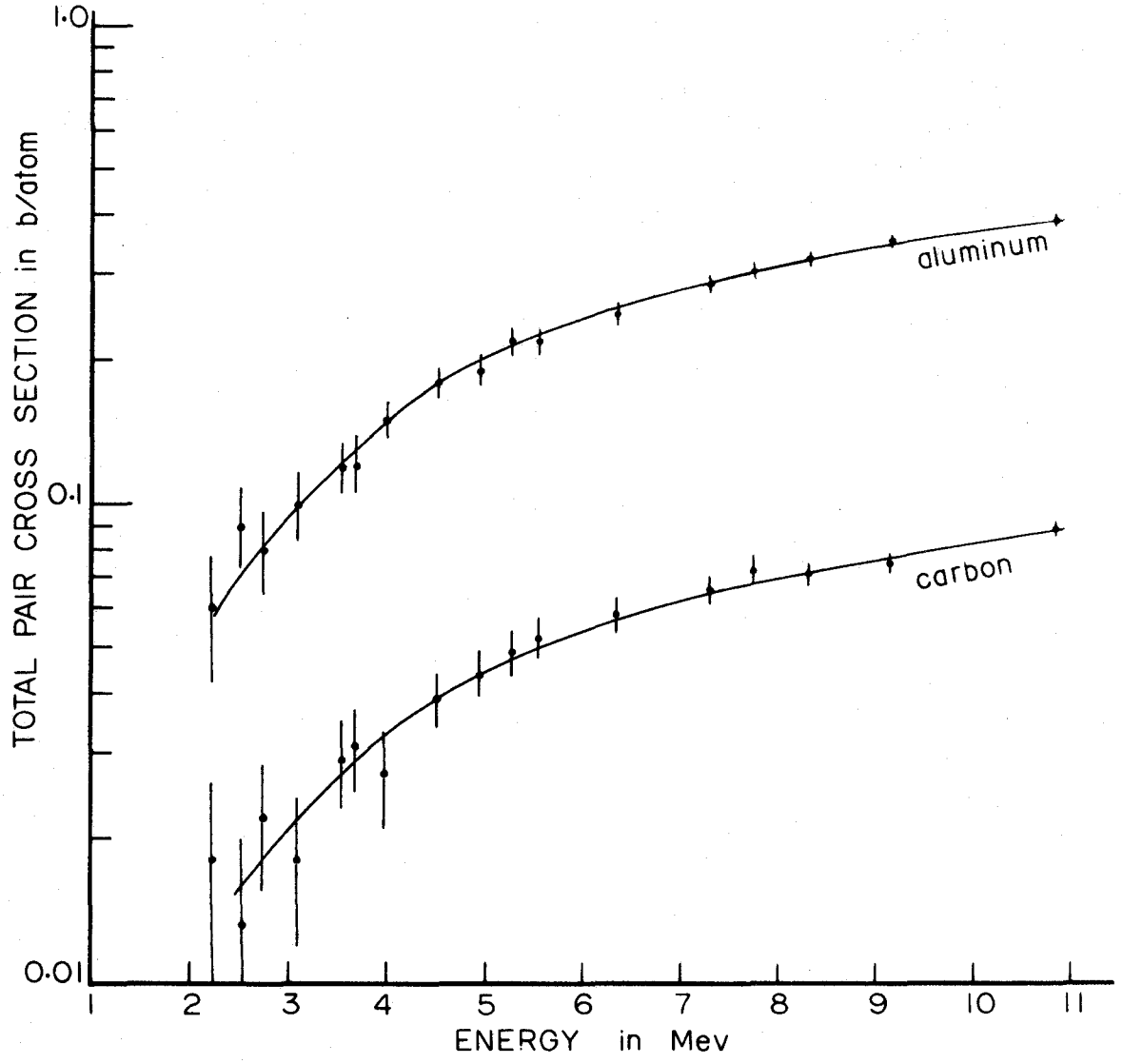

Figure 5-3: Total pair cross sections $\sigma_{(PAIR+TRIPLET)}$ for carbon and aluminium targets. Smoothed values (solid lines) were used to evaluate the contribution due to pair production in the field of an electron.

limited to carbon and aluminium materials since, according to equation 5.5, the triplet process represents a significant contribution to the total effect only for low Z materials. At Z = 6 and E_γ = 10 MeV, $\sigma_{TRIPLET}/\sigma_{(PAIR+TRIPLET)}$ is expected to be about 0.09 while for Z = 92 and E_γ = 10 MeV the ratio is expected to be only about 0.007. Similarly, the study was limited to energies above 4.5 MeV.

As indicated in figure 5-4, the present results on the triplet cross section are in good agreement with the calculated values of Mork and, therefore, Mork's values were used to obtain the elastic pair production cross sections σ_{PAIR} from the total pair cross sections $\sigma_{(PAIR+TRIPLET)}$ obtained in the manner described by equation 5.8. The resulting values for the nuclear pair cross section are shown in table 5-2.

Grodstein[21] suggests the following semi-empirical equation for σ_{PAIR} for $h\nu > 5$ MeV.

$$\sigma_{PAIR} = \sigma_{BH(SCREENED)} - \Delta_{KC} + b^2(\ell n\alpha)/\alpha \ , \qquad 5.10$$

where

$$\Delta_{KC} = (28/9)Z^2r_o^2/137\left\{a^2[(1+a^2)^{-1} + 0.20206 - 0.0369\ a^2 + 0.0083\ a^4 - 0.002\ a^6]\right\} \ , \qquad 5.11$$

where $a^2 = (Z/137)^2$ and where α is the photon energy in mc^2 units, $\sigma_{BH(SCREENED)}$ is the Bethe-Heitler cross section for a screened nucleus, Δ_{KC} is a Coulomb correction term calculated at very high energies accounting for the fact that the negatron and positron undergo attraction and repulsion, respectively, by the Coulomb force, and b^2 is an

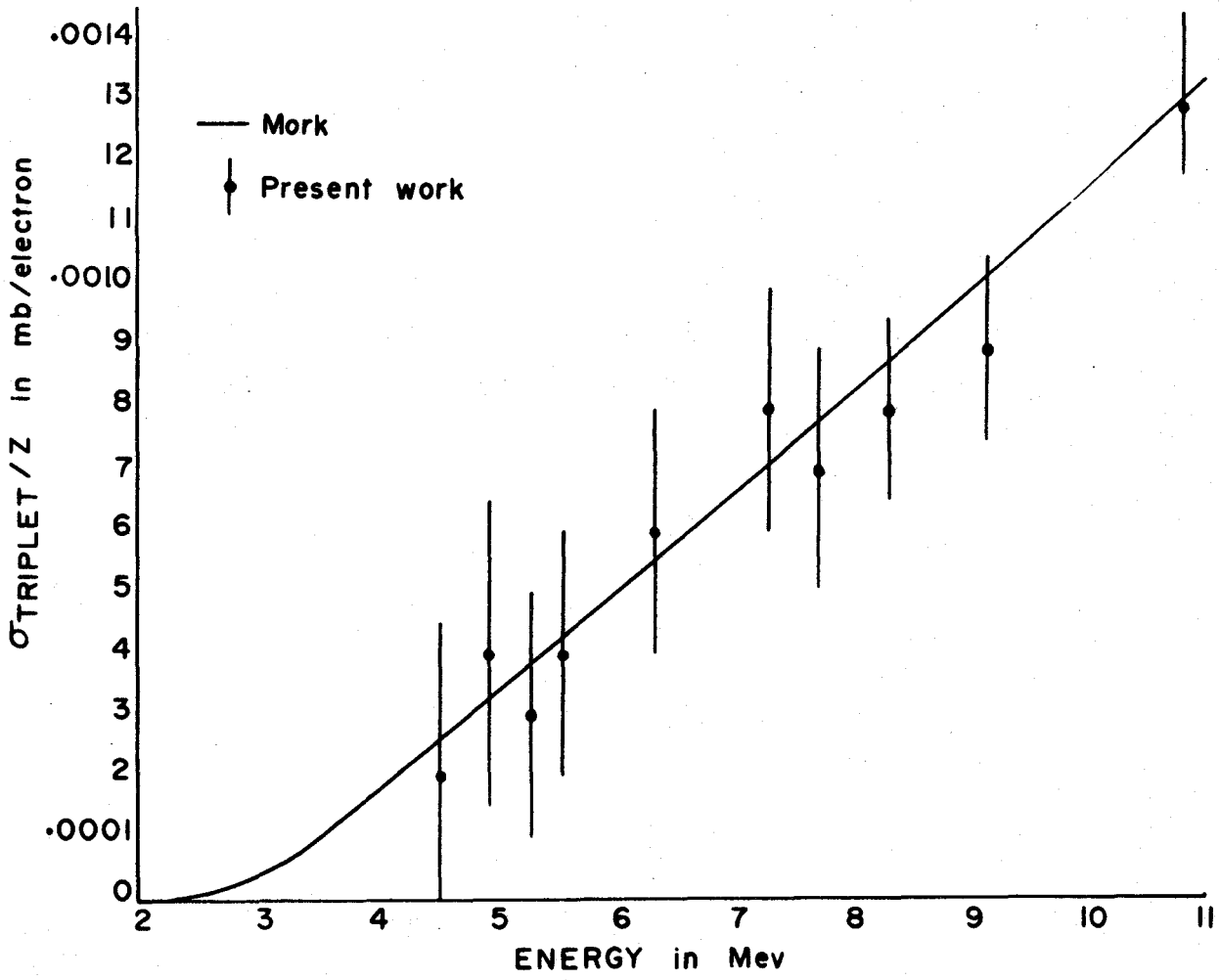

Figure 5-4: Results on the triplet production cross section.

Table 5-2: Pair production cross sections obtained indirectly from the total cross section data using $\sigma_{PAIR} = \sigma_{PAIR+TRIPLET} - \sigma_{TRIPLET}$.
(Equation 5.8) (MORK)

Energy in MeV (E_γ)	C	Al	Ti	Cu	Mo	Cd	W	Pb	U
2.225	.018 ± .008	.06 ± .02	.10 ± .03	.24 ± .04	.45 ± .12	.64 ± .14	1.6 ± 0.2	2.2 ± 0.3	2.7 ± 0.3
2.519	.013 ± .008	.09 ± .02	.14 ± .03	.32 ± .04	.57 ± .10	.74 ± .13	2.2 ± 0.2	2.6 ± 0.3	3.6 ± 0.3
2.754	.022 ± .008	.08 ± .02	.18 ± .03	.39 ± .04	.73 ± .10	1.02 ± .13	2.5 ± 0.2	3.1 ± 0.3	4.2 ± 0.3
3.098	.017 ± .007	.10 ± .02	.21 ± .03	.48 ± .04	.92 ± .10	1.42 ± .12	3.2 ± 0.2	4.0 ± 0.2	5.3 ± 0.3
3.530	.029 ± .007	.12 ± .01	.33 ± .03	.64 ± .04	1.21 ± .10	1.57 ± .12	3.9 ± 0.2	4.7 ± 0.2	6.2 ± 0.3
3.675	.031 ± .006	.12 ± .01	.38 ± .03	.64 ± .04	1.27 ± .10	1.64 ± .12	4.2 ± 0.2	5.1 ± 0.2	6.5 ± 0.3
3.982	.027 ± .006	.15 ± .01	.40 ± .03	.75 ± .04	1.43 ± .10	1.86 ± .11	4.6 ± 0.2	5.5 ± 0.2	7.3 ± 0.3
4.508	.038 ± .006	.17 ± 0.1	.49 ± .02	.84 ± .03	1.73 ± .09	2.29 ± .11	5.2 ± 0.2	6.4 ± 0.2	8.1 ± 0.3
4.945	.043 ± .005	.19 ± .01	.54 ± .02	.94 ± .03	1.94 ± .09	2.45 ± .11	6.0 ± 0.2	6.9 ± 0.2	8.8 ± 0.3
5.278	.049 ± .005	.22 ± .01	.58 ± .02	1.01 ± .03	2.10 ± 0.9	2.70 ± .11	6.2 ± 0.2	7.5 ± 0.2	9.5 ± 0.3
5.542	.052 ± .005	.22 ± .01	.62 ± .02	1.06 ± .03	2.26 ± .09	2.80 ± .10	6.5 ± 0.2	8.0 ± 0.2	10.0 ± 0.3
6.321	.057 ± .005	.25 ± .01	.73 ± .02	1.21 ± .03	2.51 ± .09	3.26 ± .10	7.3 ± 0.2	8.9 ± 0.2	11.1 ± 0.2
7.299	.063 ± .005	.28 ± .01	.83 ± .02	1.38 ± .03	2.90 ± .08	3.75 ± .10	8.4 ± 0.2	10.0 ± 0.2	12.4 ± 0.2
7.724	.070 ± .004	.30 ± .01	.89 ± .02	1.47 ± .03	3.00 ± .08	3.81 ± .10	8.7 ± 0.2	10.5 ± 0.2	13.0 ± 0.2

Table 5-2 (Continued)

Energy in MeV (E_γ)	C	Al	Ti	Cu	Mo	Cd	W	Pb	U
8.308	.068 ± .004	.32 ± .01	.93 ± .02	1.54 ± .03	3.23 ± .08	4.17 ± .10	9.3 ± 0.2	11.0 ± 0.2	13.7 ± 0.3
9.151	.071 ± .004	.35 ± .01	1.00 ± .02	1.68 ± .03	3.53 ± 0.8	4.58 ± .10	10.1 ± 0.2	11.9 ± 0.2	15.1 ± 0.3
10.827	.084 ± .004	.39 ± .01	1.15 ± .02	1.90 ± .03	3.98 ± .08	5.06 ± .10	11.3 ± 0.2	13.5 ± 0.2	16.8 ± 0.3

experimentally determined parameter. The cross sections obtained with this equation in the energy region of 10 MeV using the b^2 values proposed by Grodstein fall several percent below the results of this present study. Øverbø, Mork, and Olsen[42] apparently transfer the screening effects from the theoretical Bethe-Heitler term to the experimental term by suggesting the following modification to Grodstein's equation:

$$\sigma_{PAIR} = \sigma_{BH(UNSCREENED)} - \Delta_{KC} + b^2 \ell n(\alpha-0.75)/\alpha \ , \qquad 5.12$$

where $\sigma_{BH(UNSCREENED)}$ is the Bethe-Heitler cross section for an unscreened nucleus. For Z = 82, Øverbø gives $b^2 = 16.8$ as does Grodstein. This value was also established in this present study using Øverbø's version of the equation. Agreement with Øverbø's results extended across the entire target materials studied and in each case the value determined for b^2 agreed well with Grodstein's value. In Table 5-3, values for σ_{PAIR} determined from equation 5.12 are compared with the results of Øverbø's formula for W, Pb and U using b^2 values determined in the present study. Excellent agreement is observed.

Results obtained on the elastic pair production cross section are compared in Figures 5.5 and 5.6 to the values proposed by Storm and Israel[30] which, as previously mentioned, agree well with the values proposed by Grodstein[21]. Also, in figure 5-6, cross sections calculated from Øverbø's modified form of the Grodstein semi-empirical formula are included (dashed lines) and their agreement with the results of this present study (Z = 42, 48, 74, 82, 92) is shown to be well

Table 5-3: Experimental results for elastic pair production cross sections compared to values calculated from ∅verb∅'s[42] semi-empirical formula. Cross sections are in units of barns/atom and b^2 values used in ∅verb∅'s formula were measured in this present work.

Energy in MeV (E_γ)	Tungsten		Lead		Uranium	
	Present Work	∅verb∅ (Semi-empirical) $b^2 = 11.8$	Present Work	∅verb∅ (Semi-empirical) $b^2 = 16.7$	Present Work	∅verb∅ (Semi-empirical) $b^2 = 24.9$
1.778	0.9 ± .3		0.9 ± .3		1.6 ± .4	
1.888	1.1 ± .3		1.4 ± .3		1.9 ± .4	
2.225	1.6 ± .2		2.2 ± .3		2.7 ± .3	
2.519	2.2 ± .2		2.6 ± .3		3.6 ± .3	
2.754	2.5 ± .2		3.1 ± .3		4.2 ± .3	
3.098	3.2 ± .2		4.0 ± .2		5.3 ± .3	
3.530	3.9 ± .2	4.03	4.7 ± .2	4.92	6.2 ± .3	6.25
3.675	4.2 ± .2	4.23	5.1 ± .2	5.15	6.5 ± .3	6.53
3.982	4.6 ± .2	4.64	5.5 ± .2	5.64	7.3 ± .3	7.11
4.508	5.2 ± .2	5.31	6.4 ± .2	6.44	8.1 ± .3	8.05
4.945	6.0 ± .2	5.84	6.9 ± .2	7.06	8.8 ± .3	8.80
5.278	6.2 ± .2	6.22	7.5 ± .2	7.52	9.5 ± .3	9.35
5.542	6.5 ± .2	6.52	8.0 ± .2	7.87	10.0 ± .3	9.80
6.321	7.3 ± .2	7.35	8.9 ± .2	8.86	11.1 ± .2	11.0
7.299	8.4 ± .2	8.31	10.0 ± .2	10.0	12.4 ± .2	12.3
7.724	8.7 ± .2	8.70	10.5 ± .2	10.4	13.0 ± .2	12.9

Table 5-3 (Continued)

Energy in MeV (E_γ)	Tungsten		Lead		Uranium	
	Present Work	∅verb∅ (Semi-empirical) $b^2 = 11.8$	Present Work	∅verb∅ (Semi-empirical) $b^2 = 16.7$	Present Work	∅verb∅ (Semi-empirical) $b^2 = 24.9$
8.308	9.3 ± .2	9.21	11.0 ± .2	11.1	13.7 ± .3	13.7
9.151	10.1 ± .2	10.0	11.9 ± .2	12.0	15.1 ± .3	14.8
10.827	11.3 ± .2	11.4	13.5 ± .2	13.6	16.8 ± .3	16.8

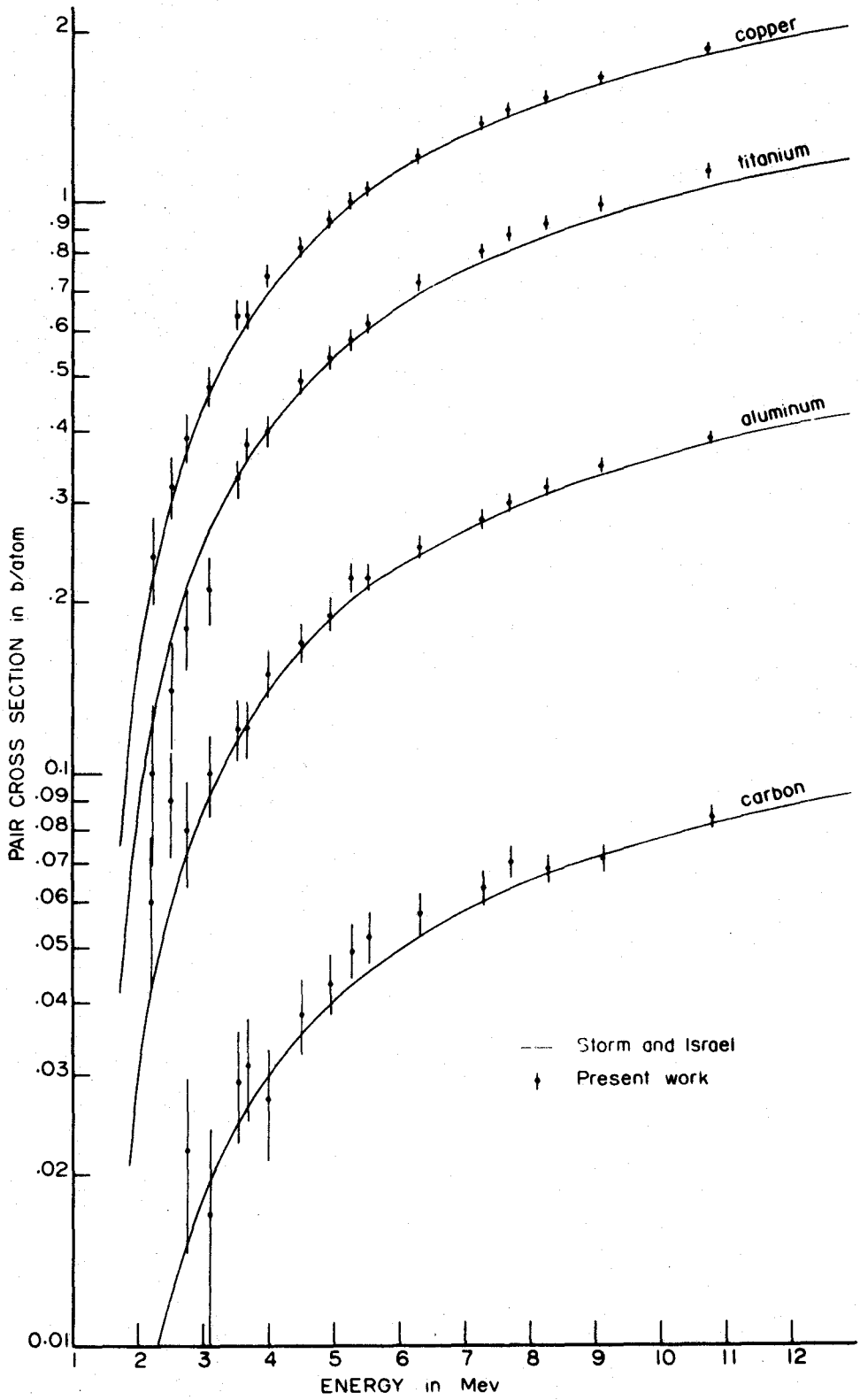

Figure 5-5: Elastic pair production cross sections deduced from the total photon cross section data.

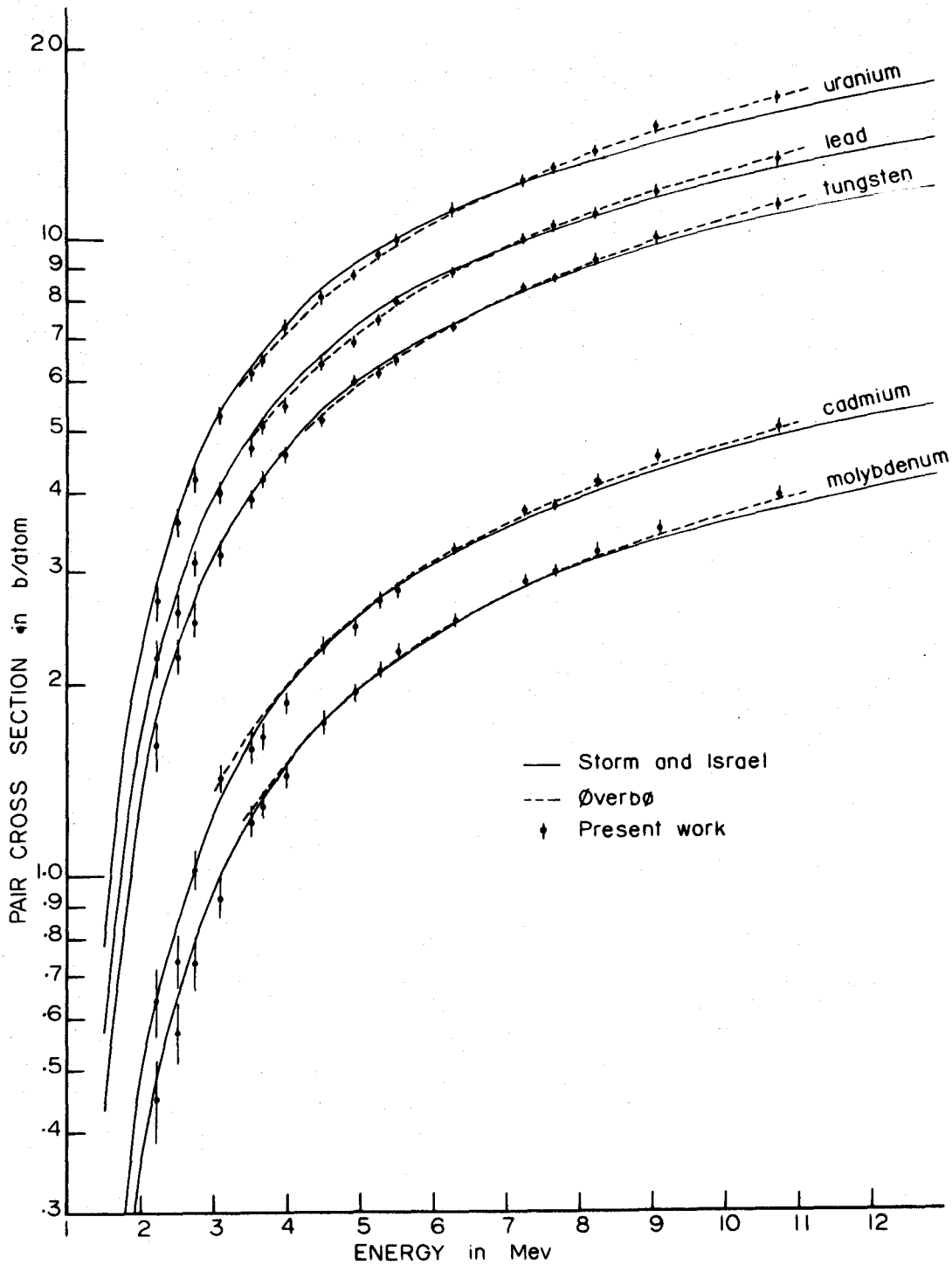

Figure 5-6: Elastic pair production cross sections deduced from the total photon cross section data.

within experimental error.

5.3 Pair Production Cross Sections Obtained by Direct Measurement

Through an intensity analysis of the positron annihilation radiation following pair production, relative information was obtained on the partial cross section for pair production by photons ranging in energy from 1120 to 2754 keV in some 6 target elements ranging from titanium to lead. Relative values for the pair cross sections were realized for E_γ = 1120 keV in Mo, Cd, W, and Pb target elements and for E_γ = 1172, 1333, 1560, 2225, and 2754 keV in Ti, Cu, Mo, Cd, W, and Pb target materials. Error in the results obtained from the 1120 and 1172 keV measurements was estimated to be 10% while the higher energy results were assigned an error of 5%. Absolute values for the cross section (table 4-5) were obtained by normalizing the $\sigma_{PAIR}(E = 2754 \text{ keV}, Z = 82)$ result to 3.30 barns/atom, a value obtained for the pair cross section earlier from the total cross section data. This value of 3.30 barns/atom is in agreement with the value proposed by Storm and Israel[30] and by Grodstein[21].

Exact calculations for pair production in a variety of elements by photons with energies below about 2.5 MeV have recently been made by Øverbø, Mork, and Olsen[42]. They have presented their results by comparison with the Bethe-Heitler cross section, plotting $\sigma_{\text{ØVERBØ}}/\sigma_{BH}$ as a function of energy for some 7 target elements ranging from argon to uranium. Figure 5.7 represents a reproduction of this set of curves (Figure 3, ref. 42, excluding the uranium data) with the inclusion of the experimental data points $\sigma_{EXPT}/\sigma_{BH}$ obtained in this present study. The values for σ_{EXPT} used in determining the ratios are those given in table 4-5. Agreement with the results presented by Øverbø is seen to be quite good, particularly below E_γ = 2.0 MeV, where the presently established ratio are within 10% in almost all cases. In comparing the results of their calculation

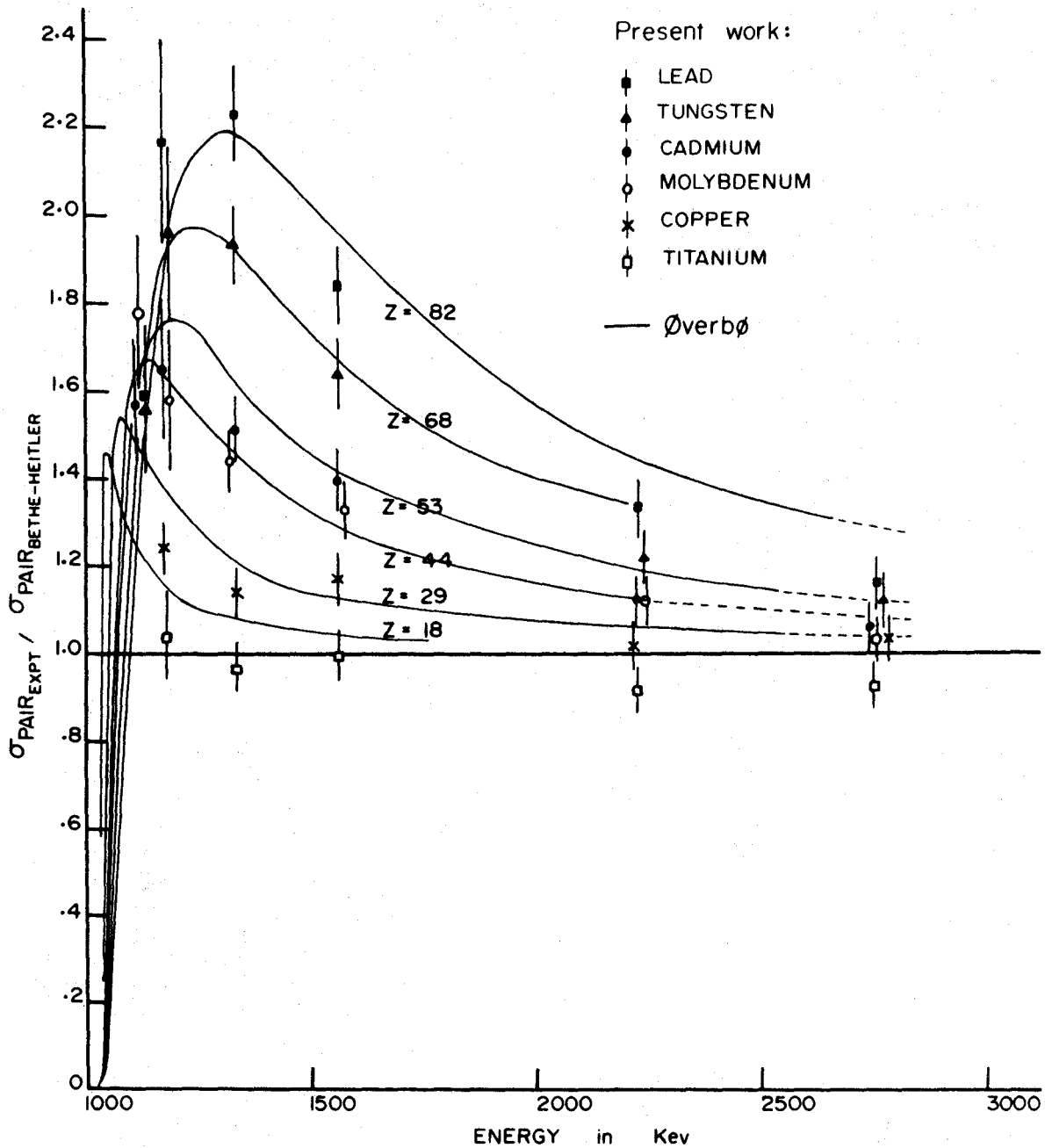

Figure 5-7: Results obtained on the pair cross section compared to the exact calculations of Øverbø, Mork, and Olsen[42]. The curves shown were reproduced from Fig. 3, reference 42.

to other experimental results, Øverbø et al also find agreement to be within 10%. The experimental results[43] they used for comparison appear to agree very well with the results obtained in this present measurement.

5.4 Summary

Measurement of the interaction cross sections for photons with energies ranging from a few keV to 2754 keV has, in the past, received considerable attention. Consequently, the various theoretical predictions, particularly in the 1-3 MeV region, have been well tested and have been improved to a point of considerable reliability. Above 2754 keV, however, difficulties experienced in obtaining adequate photon sources for good accuracy cross section studies have limited measurements to only a few isolated energies.

In the intermediate energy region from 3-15 MeV, the inelastic (Compton) scattering cross section is expected to remain well within that given by the Klein-Nishina formula. The elastic (Rayleigh) scattering cross section becomes negligible in this region. At 3 and 10 MeV and Z = 92, the total cross sections are approximately 17 and 20 barns/atom respectively whereas the Rayleigh cross sections are approximately 0.1 and 0.01 barns/atom respectively. Although the photoelectric cross section represents a greater contribution to the total effect (approximately 1.5 and 0.3 barns/atom under the conditions above) it falls off rapidly with energy and represents only a 1 1/2% effect at 10 MeV and Z = 92. Further, since the photoelectric effect has a Z^5 dependence, its contribution to the total will fall off very rapidly with decreasing

atomic number. Interest in the intermediate energy region must then be focussed on the pair production cross section which increases rapidly with energy above the 1.02 MeV threshold. At 10 MeV and Z = 92, pair production represents a contribution of 75% of the total interaction probability.

Total cross sections for 29 well distributed photon energies from 121 keV to 10.8 MeV in 9 target elements from carbon to uranium have been realized with an estimated error of approximately 1% or better. In the region of 1-3 MeV where the cross section has been previously well established, agreement with the present results is excellent. Since the 3-11 MeV data were obtained in the same measurement as the lower energy data, they would necessarily suffer from the same degree of systematic error and, therefore, with considerable certainty, can be assumed to be just as valid.

In the region from 6-11 MeV, particularly for large Z materials, the measured total cross section was observed to be high compared to the values proposed by Storm and Israel[30] and by Grodstein[21]. Deviations were found to be approximately Z^2 dependent and to be exponentially dependent on energy. In view of the magnitude and E_γ, Z dependencies of these deviations, they could clearly be related to the theoretical pair production cross section.

From approximately 2 to 10.8 MeV, pair cross sections were deduced from the total cross sections by subtracting the proposed values (Storm and Israel) for the competing processes. Above 6 MeV the results were observed to differ from the pair cross sections proposed by Storm

and Israel, the difference amounting to as much as 8% at 10 MeV and Z = 92. Previous experimental results substantiate this discrepancy. Wyckoff and Koch[44] show the carbon and aluminium total cross sections to be high at energies above about 12 MeV. Their reported values are shown in figure 5-8 where they are seen as a smooth continuation of the present results. Rosenblum, Shrader, and Warner[40] also reported high values for 10.3 MeV photons in lead and uranium; however, their reported 5.3 MeV results appear to be too high and that, to some degree, may have reduced the credibility of their 10.3 MeV results. Their results for 5.3 and 10.3 MeV photons in a uranium target are shown in figure 5-9 along with the present results on σ_T and σ_{PAIR}.

The present pair production cross section results from 1120 to 2754 keV are in good agreement with the results of an exact calculation (from threshold to about 2.5 MeV) by Øverbø, Mork, and Olsen[42]. Pair cross sections above 3 MeV calculated from their modification of Grodsteins[21] semi-empirical formula were in excellent agreement with the results of this study.

A discrepancy in the measured and proposed cross sections has been observed in the region above 5-6 MeV, particularly in high Z target materials. The nature of the discrepancy is consistent with an argument that the effects of atomic electron screening have been over estimated and perhaps, a re-evaluation of the screening effect is in order. Hopefully, the results of this study are sufficiently significant and comprehensive to facilitate a closer examination of the pair production interaction in the intermediate energy region.

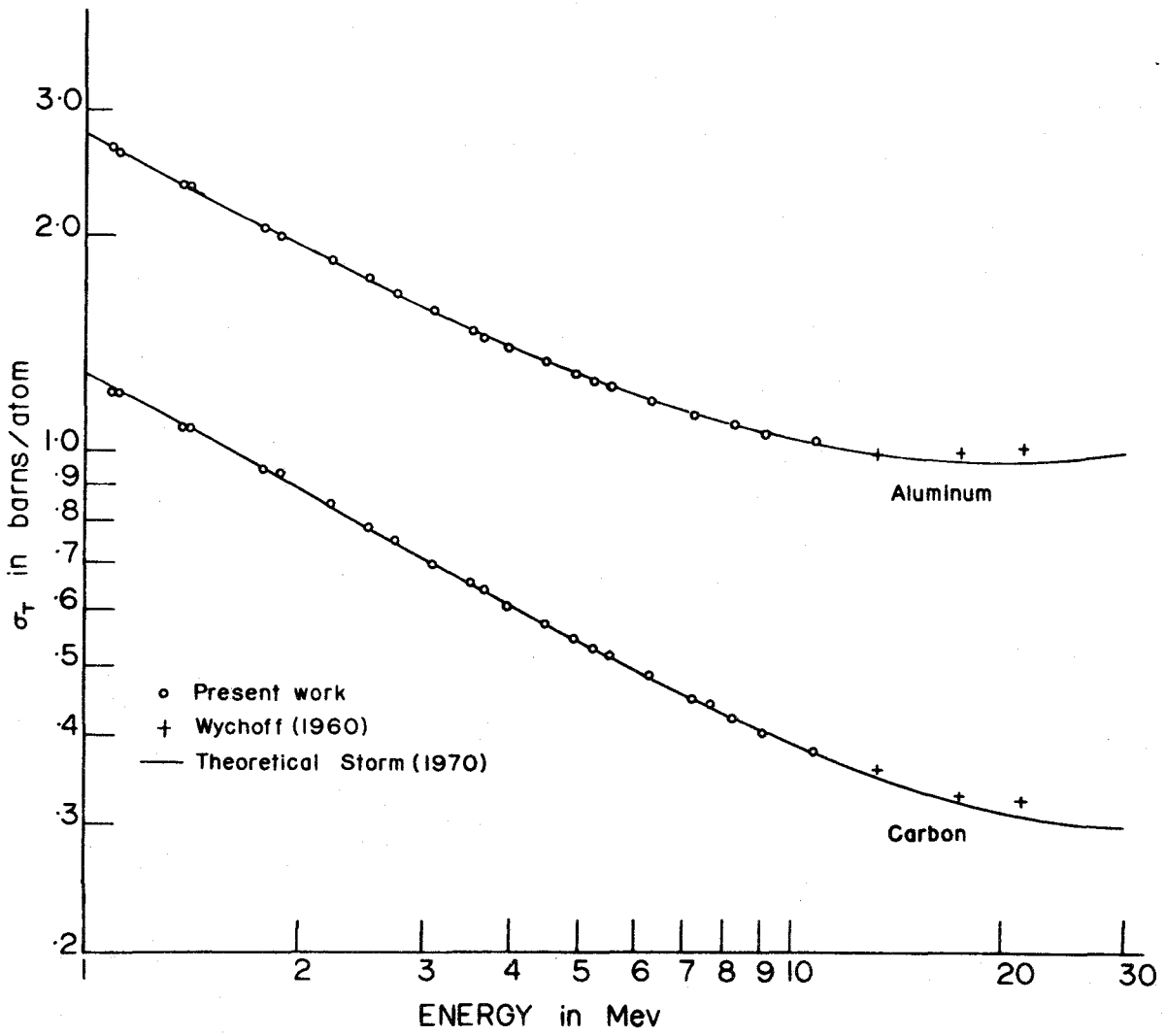

Figure 5-8: Total cross sections σ_T for carbon and aluminium target elements. Although the experimental results for these low Z materials do not differ significantly from the cross sections proposed by Storm and Israel[30], deviation appears to exist for higher energy values.

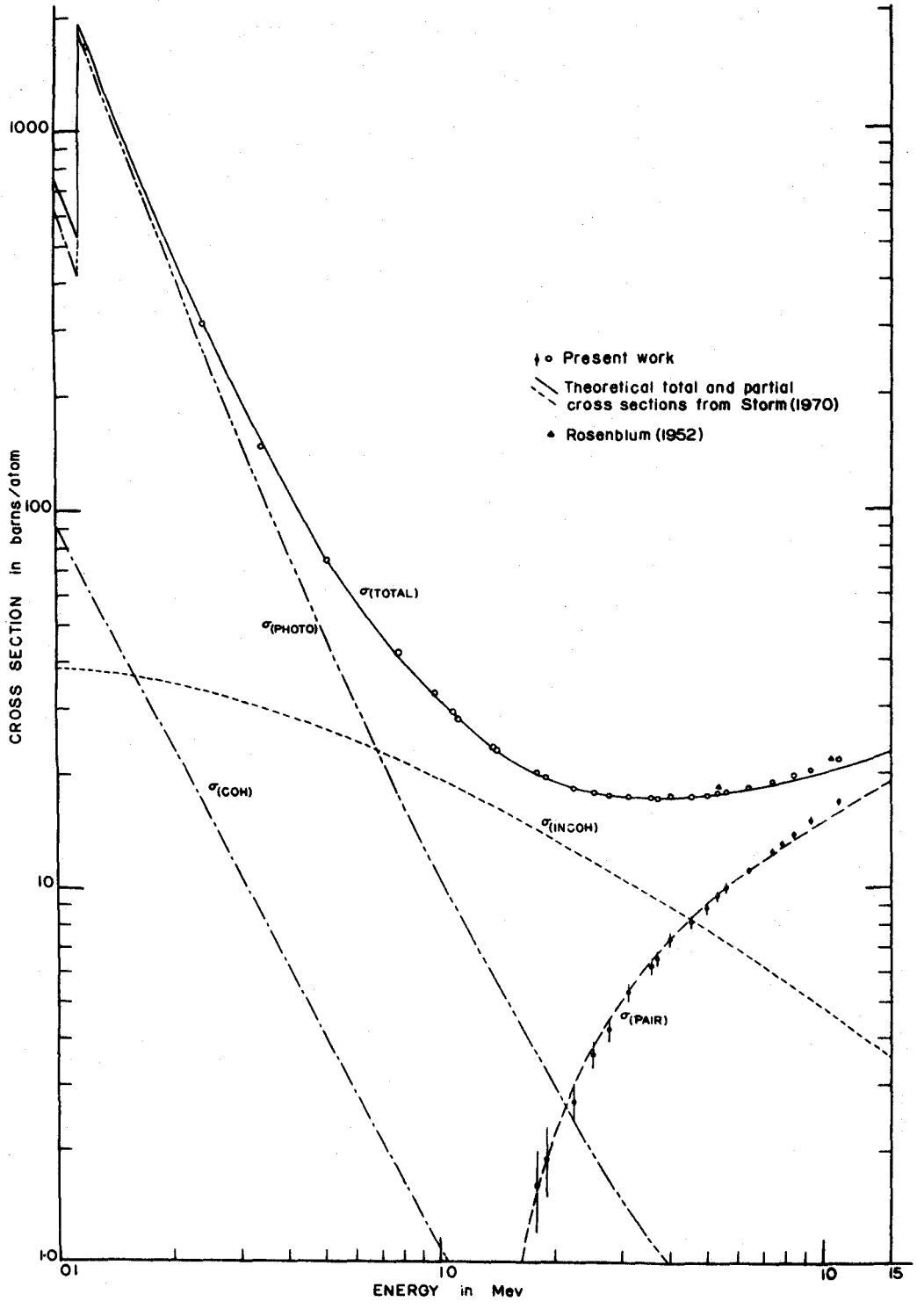

Figure 5-9: Experimental and theoretical results on the photon interaction cross sections in a uranium target.

REFERENCES

1. W. Heitler, The Quantum Theory of Radiation, Introduction, p. xii (Clarendon Press, Oxford, 1954).

2. H. M. Foley and P. Kusch, Phys. Rev. 72, 1256 (1947); 73, 412 (1948); 74, 250 (1948).
W. Heitler, The Quantum Theory of Radiation, Chapter VI, p. 311 (Clarendon Press, Oxford, 1954).
J. Schwinger, Phys. Rev. 76, 790 (1949).

3. W. E. Lamb and R. C. Retherford, Phys. Rev. 72, 241 (1947); 75, 1325, 1332 (1949); 79, 549 (1950); 81, 222 (1951).
W. E. Lamb and M. Skinner, Phys. Rev. 78, 539 (1950).

4. H. E. Jackson and K. J. Wetzel, Argonne National Laboratory Phys. Div. Summary Report ANL-7570, 3 (1969); Phys. Rev. Letters 22, 1008 (1969).

5. W. Heitler, The Quantum Theory of Radiation, Chapter V, p. 258 (Clarendon Press, Oxford, 1954).

6. H. A. Bethe and W. Heitler, Proc. Roy. Soc. (London) A146, 83 (1934).

7. H. Davies, H. A. Bethe and L. C. Maximon, Phys. Rev. 93, 788 (1954).

8. A. T. Nelms and I. Oppenheim, J. of Research of the National Bureau of Standards 55, No. 1, 53 (1955).
E. Fermi, Z. Physik 48, 73 (1928).
L. H. Thomas, Proc. Cambridge Phil. Soc. 23, 542 (1926).

9. J. W. Motz, H. Olsen and H. W. Koch, Rev. Mod. Phys. 36, 881 (1969).

10. U. Fano, Nucleonics 11(8), 8 (1953); 11(9), 55 (1953).
R. D. Evans, The Atomic Nucleus, Chapter 23 (McGraw-Hill Book Co., New York, 1955).

11. R. D. Evans, The Atomic Nucleus, Appendix A, p. 821 (McGraw-Hill Book Co., New York, 1955).

12. K. Siegbahn, Alpha-Beta-and Gamma-Ray Spectroscopy, Vol. 1, Chapter II (North-Holland Publishing Co., Amsterdam, 1968).

13. W. Heitler, The Quantum Theory of Radiation, Chapter VI (Clarendon Press, Oxford, 1954).

14. P. A. M. Dirac, Proc. Roy. Soc. (London) A117, 610 (1928).

15. G. E. Uhlenbeck and S. Goudsmit, Nature 117, 264 (1926).

16. W. Heitler, The Quantum Theory of Radiation, Chapter III, p. 107 (Clarendon Press, Oxford, 1954).

17. W. Heitler, The Quantum Theory of Radiation, Chapter V, p. 215 (Clarendon Press, Oxford, 1954).

18. L. Nichol, A. Lopez, A. Robertson, W. V. Prestwich and T. J. Kennett, Nucl. Instr. and Methods 81, 263 (1970).

19. N.C. Rasmussen, Y. Hukai, T. Inonye and V. J. Orphan, Massachusetts Inst. of Tech. Dept. Nucl. Eng., pre-publication copy of MITNE-85 (19).

20. T. J. Kennett, W. V. Prestwich and G. L. Keech, Nucl. Instr. and Methods 29, 325 (1964).

21. G. W. Grodstein, National Bureau of Standards circular 583, 55 (1957).

22. B. W. Dzhelepov, N. N. Zhukovskii and A. G. Maloyan, J. Nucl. Phys. (U.S.S.R.) 3, 785 (1966).

23. M. G. Strauss, L. L. Sifter, F. R. Lenkszus and R. Brenner, presented at the 11th scintillation and semiconductor counter symposium, March 1968, Washington D.C.

24. D. Wilkinson, Proc. Cambridge Phil. Soc. 46, part 3, 508 (1950).

25. W. Heitler, The Quantum Theory of Radiation, Chapter V, p. 268 (Clarendon Press, Oxford, 1954).

26. W. Heitler, The Quantum Theory of Radiation, Chapter V, p. 272 (Clarendon Press, Oxford, 1954).

27. K. G. Standing and J. V. Jovanovich, Can. J. Phys. 40, 622 (1962).

28. R. D. Evans, The Atomic Nucleus, Chapter 21 (McGraw-Hill Book Co., New York, 1955).

29. R. L. Heath, Scintillation Spectrometry Gamma-Ray Spectrum Catalogue, Atomic Energy Commission R & D Report TID-4500 (1957).

30. E. Storm and H. I. Israel, Nuclear Data Tables A7, 565 (1970).

31. I. Øverbø, K. J. Mork and H. A. Olsen, Phys. Rev. 175, 1978 (1968).

32. D. T. Cromer, 1971 - To be published in Acta Crystallogr.

33. H. P. Hanson, F. Herman, J. D. Lea and S. Skillman, Acta Crystallogr. 17, 1040 (1964).

34. G. Rakavy and A. Ron, Phys. Rev. 159, 50 (1967).

35. R. D. Schmickley and R. H. Pratt, Phys. Rev. 164, 104 (1967).

36. F. Kirchner, Handbuch der Experimentalphysik 24: 1, p. 256 (ed. W. Wien and F. Harms; Akademische Verlagsgesellschaft, Leipzig, 1930).

37. R. H. Pratt, Phys. Rev. 117, 1017 (1960).

38. J. H. Hubbell, National Standard Reference Data System, Rep. No. NSRDS-NBS 29 (1969).
J. H. Hubbell and M. J. Berger, NBS Report 8681 (1966)
J. H. Hubbell and M. J. Berger, Engineering compendium on radiation shielding, Vol. 1, Chapter 4 (Springer-Verlag, Berlin, 1968).

39. R. D. Evans, The Atomic Nucleus, Chapter 24 (McGraw-Hill Book Co., New York, 1955).

40. E. S. Rosenblum, E. F. Shrader and R. M. Warner, Jr., Phys. Rev. 88, 612 (1952).

41. K. J. Mork, Phys. Rev. 160, 1065 (1967).

42. I. Øverbø, K. J. Mork and H. Olsen, Phys. Rev. 175, 1978 (1968).

43. H. I. West, Phys. Rev. 101, 915 (1956).
I. E. Dayton, Phys. Rev. 89, 544 (1953).
P. Schmid and P. Huber, Helv. Phys. Acta. 27, 152 (1954).
B. Hahn, E. Baldinger and P. Huber, Helv. Phys. Acta. 25, 505 (1952).
F. Titus and A. J. Levy, Nucl. Phys. 80, 588 (1966).

44. J. M. Wyckoff and H. W. Koch, Phys. Rev. 117, 1261 (1960).